論文 / 著書情報
Article / Book Information

題目(和文)	流体及び弾性体の電気粘性効果の最適な材料特性の研究
Title(English)	Optimal material properties for the electrorheological effect in fluids and elastomers
著者(和文)	櫻井良
Author(English)	
出典(和文)	学位:博士(工学), 学位授与機関:東京工業大学, 報告番号:甲第4193号, 授与年月日:1999年9月30日, 学位の種別:課程博士, 審査員:
Citation(English)	Degree:Doctor (Engineering), Conferring organization: Tokyo Institute of Technology, Report number:甲第4193号, Conferred date:1999/9/30, Degree Type:Course doctor, Examiner:
学位種別(和文)	博士論文
Type(English)	Doctoral Thesis

DOCTORAL DISSERTATION

Optimal Material Properties for the Electrorheological Effect in Fluids and Elastomers

by

Ryo SAKURAI

1999

Adviser : Professor Masao SUMITA, Dr. Eng.

Associtate Professor Shigeo ASAI, Dr. Eng.

Department of Organic and Polymeric Materials

Tokyo Institute of Technology

1-12-1 Ookayama, Meguro-ku, Tokyo, 152-0033 JAPAN

Abstract

Composite materials are the focus of much attention in recent years, since they present an efficient way to add more functionality to conventional materials, from the point of view of cost as well as the range of mechanical and other properties attainable. Very often, it is found that various material requirements which can't be satisfied with homogeneous materials can be achieved by the judicious composition of materials with different performances.

An Electro Rheological Fluid (usually abbreviated to ERF), the subject of this thesis, can be considered a type of composite materials. ERF has the very specific property of an increasing viscosity when an electric field is applied to the material. A particle dispersed ERF consists of solid particles in an insulating carrier oil, and displays a dramatic but reversible increase in viscosity upon application of an electric field. The large change in flow resistance coupled with the short response time make ERFs ideal for use in many electrically controlled mechanical devices, and they have received considerable attention in recent years. In particular, the compactness of electrorheological devices make them suitable for a variety of automobile applications.

While there has been much recent work investigating the mechanisms of ERF and their possible applications, as yet there are no fluids widely in use. In order to realize use in many devices, ERFs must satisfy the two conditions of large shear stress increase (the so-called ER effect) and low electric power consumption under electric fields.

Since the electrorheological performance strongly depends on the nature of the particles dispersed in the suspension, the production of particles with the optimum electrical properties becomes a key issue. In spite of its importance, there have not been many reports about material properties of ERF and the detailed relationship between the electrorheological performance and its material properties remains unclear. Therefore, the objective of this thesis is to gain some

understanding of the ideal electrical properties of particles in ERF with a view to the optimization of electorheological performance.

In Chapter 1, the background of Electro Rheological Fluids is reviewed, including the basic mechanism of electro-rheological behavior and possible applications. The remaining issues that need to be resolved before ERFs can be more widely used are discussed and the objectives of this thesis are summarized.

In Chapter 2, there is a description of the materials of particle dispersed ERF systems and the measuring methods used in this thesis. Methods to estimate the electrical properties of dispersed particles by dielectric measurements are described.

In Chapter 3, we have investigated the optimum structure of ER particles. We showed that a high performance particle, with large increment in viscosity at small electric consumption, can be achieved with a particle with a layered structure.

In Chapter 4, we have investigated the effect of non-uniformity of particulate conductivity on electrorheological properties by blending particles with different conductivity. We also propose dielectric measurement as an effective method to estimate conductive uniformity of dispersed particles in suspension.

In Chapter 5, we carry out some theoretical calculations based on our model of the effect of conductive uniformity in Chapter 4.

In Chapter 6, we investigate the effect of conductive fragments on electrorheological properties, which models the effect of high conductive impurities that can be inadvertently mixed in during the fluid preparation process.

In Chapter 7, we apply the knowledge of improving electrorheological properties gained in Chapters 3 and 4 to the process of particle preparation in order to optimize electrorheological performance.

In Chapter 8, we have investigated the electrorheological properties of dispersions of ER particles in elastomers. We are able to verify the practical possibility of ER elastomers.

Lastly, the conclusions of this thesis are summarized in Chapter 9.

Contents

Chapter 1.

Introduction

An Electrorheological Fluid(ERF) consists of micron-sized highly conductive particles with insulating layer or highly polarizable particles, dispersed in a nearly insulating solvent. It shows a rapid and reversible change in suspension viscosity upon application of an electric field. ERFs have attracted considerable attention in recent years because of potential applications as well as interest in unsolved scientific questions since the first extensive study of Winslow (1949) [81].

These days, materials used for ERF are developed to the practical level and much effort continues to be put into achieving further improvement (e.g. low temperature dependence of ER effect, high durability and so on).

In this chapter, general features of ERFs are reviewed, and then the remaining problems for practical use are described. Lastly, we describe the purpose of this study.

1.1 General features of ERFs

1.1.1 Rheological properties of an ERF

ERF acts as a Newtonian fluid under no electric field, but it shows Bingham fluid behavior under an electric field as shown in FIG. **1.1**. Bingham fluid can be written as follows.

$$\tau = \eta_p \dot{\gamma} + \tau_y \tag{1.1}$$

Here, η_p is Bingham plastic viscosity, $\dot{\gamma}$ is shear rate, and τ_y is Bingham yield stress. The most important property of ERF is τ_y, and the key technical issue is obtaining maximum τ_y with the

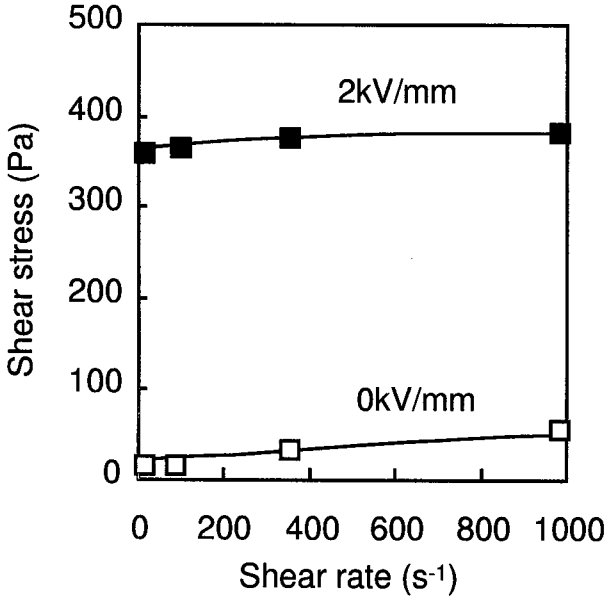

FIG. 1.1: Variation of shear stress with shear rate under no electric field and dc electric field of $2kV/mm$.

lowest possible electric consumption.

Recently, there has also been some interest shown in Magnetorheological (MR) fluids which are a similar type of fluid whereby the rheological properties can be controlled by an external magnetic fluid [15, 67]. However, despite the fact that MR fluids have been around longer, have been studied intensely and show stronger stress than ERF, they have not been developed well because of their inherent complexity. In comparison, the devices of ERF can be very simple. It can be said that this is one of the advantageous points of ERF from the point of view of development for practical applications.

1.1.2 Materials used in ERFs

Particle dispersed ERFs consist of insulating solvent and micron-sized solid particles. Here, we briefly summarize the types of particles used in ERFs. We divide particle types into two classes : hydrous particle systems and anhydrous particle systems.

Hydrous particle systems

The hydrous particles were the first to show high ER performance at a practical level. They typically contain some amount of moisture (usually about 10% by weight). The role of the water is still not completely understood, but it is clear that the ER effect depends strongly on the amount of water present.

There have been types of materials reported in the literature. For example, hydrous silica particles [43, 52, 68], cellulose particles [75], hydrated poly(methacrylate) particles [13, 50], soda lime glass beads and so on. These are usually dispersed in a nearly insulating solvent, such as silicone oil. But the one very serious problem of hydrous particle systems is that they have a large temperature dependence of the ER effect, since the water will boil off from the particles at high temperatures and tend to freeze at lower temperatures.

Anhydrous particle systems

Since the discovery of anhydrous particles for ERFs in the late 1980's, many studies have been carried out on these systems. These show less temperature dependence of ER performance and can be used at over 100 ℃. Many materials with appropriate electrical properties can be used and have been reported recently. For example, semi-conducting acenequinone radical polymers [60], polyaniline [35], polyurethane particles [11], complex strontium titanate particle [85], carbonaceous particle [41], layered particle [40] and so on. Of course durability and cost are important factors for commercial use as well as the magnitude of the ER effect (yield stress under an electric field), and studies have been done on these aspects as well (e.g. [1, 41, 53]).

In our study, we used anhydrous carbonaceous particles developed at Bridgestone Corporation [41]. The details of this type of particles are described in Chapter 2.

1.1.3 Mechanism of ER effect

The best qualitative picture of the origin of the ER response suggests that particles in an ER suspension are polarized by the external electric field and the interaction between the resulting dipoles causes the particles to form fibrinated structures aligned with the electric field. We begin

with a single particle of radius a, conductivity σ_p and relative dielectric permittivity ϵ_p, suspended in a solvent of conductivity σ_s and relative dielectric permittivity ϵ_s.

Now we consider a coordinate system centered on the sphere of interest under a uniform dc electric field in the z direction (FIG. **1.2**). Gauss's Law for this system with no free charges can

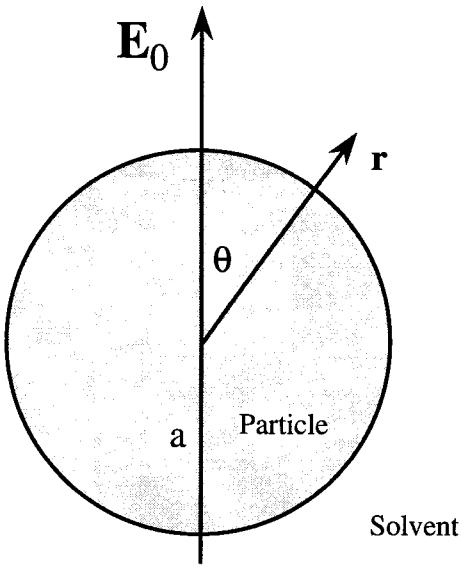

FIG. 1.2: Schematic diagram of a sphere under an electric field E_0.

be written in terms of Laplace's equation.

$$\Delta\phi_p = 0 \quad (r < a) \tag{1.2}$$

$$\Delta\phi_s = 0 \quad (r > a) \tag{1.3}$$

where Δ is the Laplacian operator, ϕ_s is the electrical potential of solvent and ϕ_p is the electrical potential of particle respectively. The Maxwell-Wagner's approach is commonly used to describe particle and solvent polarization in the presence of free charge carriers. The complex dielectric permittivity is generally written as

$$\epsilon^* = \epsilon - \frac{4\pi\sigma i}{\omega} \tag{1.4}$$

where ϵ is the dielectric permittivity, σ is the conductivity and ω is the angular frequency. At the particle interfaces, the following boundary conditions apply.

- The normal component of the current must be continuous.

$$\epsilon_s^* \left(\frac{\partial \phi_s}{\partial r}\right)_{r=a} = \epsilon_p^* \left(\frac{\partial \phi_p}{\partial r}\right)_{r=a} \tag{1.5}$$

- The tangential component of E_0 must be continuous.

$$\left(\frac{\partial \phi_s}{\partial \theta}\right)_{r=a} = \left(\frac{\partial \phi_p}{\partial \theta}\right)_{r=a} \tag{1.6}$$

We consider the dc electric field system ($\omega \approx 0$) in our argument, so eq. (1.5) can be written as follows;

$$\sigma_s \left(\frac{\partial \phi_s}{\partial r}\right)_{r=a} = \sigma_p \left(\frac{\partial \phi_p}{\partial r}\right)_{r=a} \tag{1.7}$$

The electric field can be thought as E_0 at $r = \infty$, giving us the following condition

$$-\left(\frac{\partial \phi_s}{\partial r}\right)_{r=\infty} = E_0 \cos\theta \tag{1.8}$$

The electrical potential ϕ_s is given by solution to eq. (1.3) with boundary conditions eqs. (1.6), (1.7) and (1.8) [2] and written

$$\phi_s = -\left(r + \frac{\sigma_s - \sigma_p}{2\sigma_s + \sigma_p}\frac{a^3}{r^2}\right) E_0 \cos\theta \tag{1.9}$$

And dipole moment p can be obtained [3] from the potential of eq. (1.9) by

$$p = 4\pi\epsilon_s\epsilon_0 \left(\frac{\sigma_p - \sigma_s}{\sigma_p + 2\sigma_s}\right) a^3 E_0 \tag{1.10}$$

here, ϵ_0 is the permittivity of free space.

We now consider the forces acting between particles. For simple consideration, we use here the "point dipole approximation", where it is assumed that each sphere has an electric dipole p equal to that induced in an isolated sphere.

Assuming that the spheres interact through dipoles of constant size as in eq. (1.10) (i.e. ignoring multibody effects), the force between two spheres i and j ($F^{ij}_{electro}$) can be written as :

$$F^{ij}_{electro} = 3\epsilon_s\epsilon_0 \left(\frac{\sigma_p - \sigma_s}{\sigma_p + 2\sigma_s}\right)^2 a^2 E_0^2 \frac{a^4}{\mid r_j - r_i \mid^4} \times [(3\cos^2\theta_{ij} - 1)e_r^{ij} + (\sin 2\theta_{ij})e_\theta^{ij}] \tag{1.11}$$

where e_r^{ij} and e_θ^{ij} are unit vectors defined in FIG. **1.3**. For two contacting particles aligned with the electric field, this force has the magnitude of:

$$F_{electro} = \frac{3\pi p^2}{8\epsilon_s\epsilon_0 a^4} \tag{1.12}$$

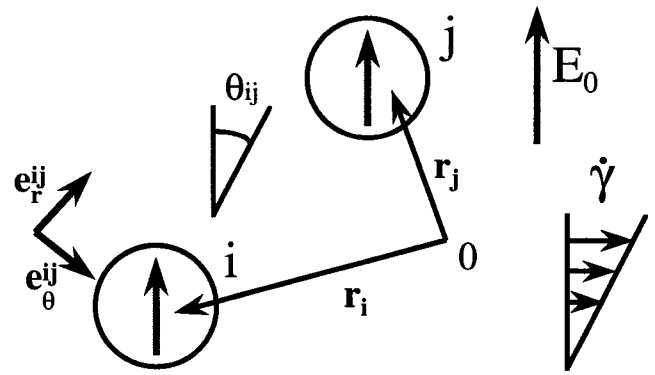

FIG. 1.3: Sketch showing two particles under an electric field E_0 and shear flow of shear rate $\dot{\gamma}$.

The induced electrostatic force $F_{electro}$ makes chain-like structure under an electric field. And the shearing or rupture of the chain-like structure is considered to be an important factor in the high shear resistance of ERFs [43] as shown in FIG. **1.4**. The chain-like structure as shown in FIG. **1.4** is observed by many optical microscopic experiments and has been reported [17, 22, 33, 74].

With this chain structure model and "point dipole approximation", there have been many works establishing the theoretical basis of the ER effect. Simulation of ER properties under steady shear at various shear rates and shear strains (e.g. [7, 12, 46, 57, 58]) and studies of ER properties under dynamic shear (e.g. [32, 45, 49, 78]) have been done by many researchers.

Apart from this chain model, other possible mechanisms of the ER effect have been reported. Block *et al.* [10] showed that the influence of a delay in the polarization of a spinning particle under shear flow is an important factor of increment of viscosity and Takimoto [71] used a model of particle aggregates suspended in the fluid which cause increased viscosity. Further, See and Saito [64] used a layered model under higher shear flow to explain the ER effect.

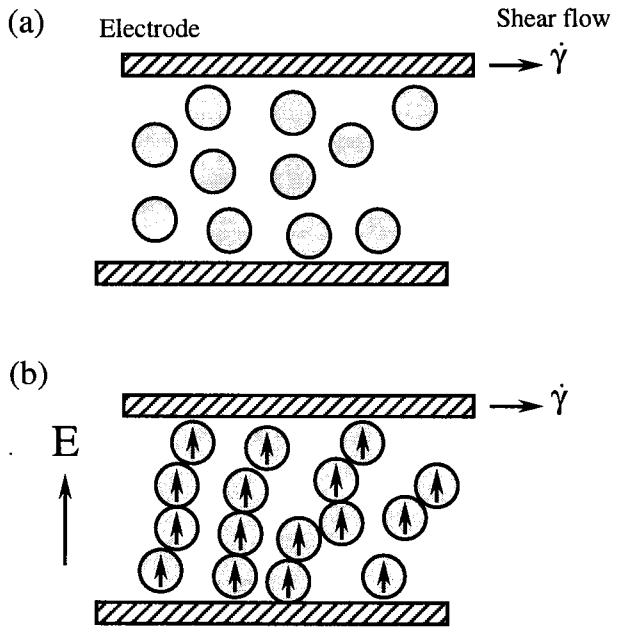

FIG. 1.4: (a) An ERF suspension under no electric field. (b) An ERF suspension after an electric field E has been applied across the electrodes at top and bottom.

1.2 Possible applications of ERFs

1.2.1 Applications for automobiles

The large change of apparent viscosity coupled with the quick response (of the order of ms) of ERFs makes them very promising, interesting and advantageous materials to be applied to many electrically controlled mechanical applications. The viscosity is continuously adjustable through selection of an applied voltage at very small electrical consumption (FIG. **1.5**). One of the most attractive ER applications are those for automobiles. First of all, we take ER engine mounts for one example of ER applications (FIG. **1.6**). Hydraulic mounts have recently been used more frequently particularly for engine mounts to improve anti-noise and vibration performance of vehicles, and now the development of higher performance mounts like ER engine mounts are required. Generally, engine mounts are required different transmissibility for different situations (e.g. $5 \sim 15Hz$ large amplitude vibration from engine shake and $100 \sim 200Hz$ small amplitude

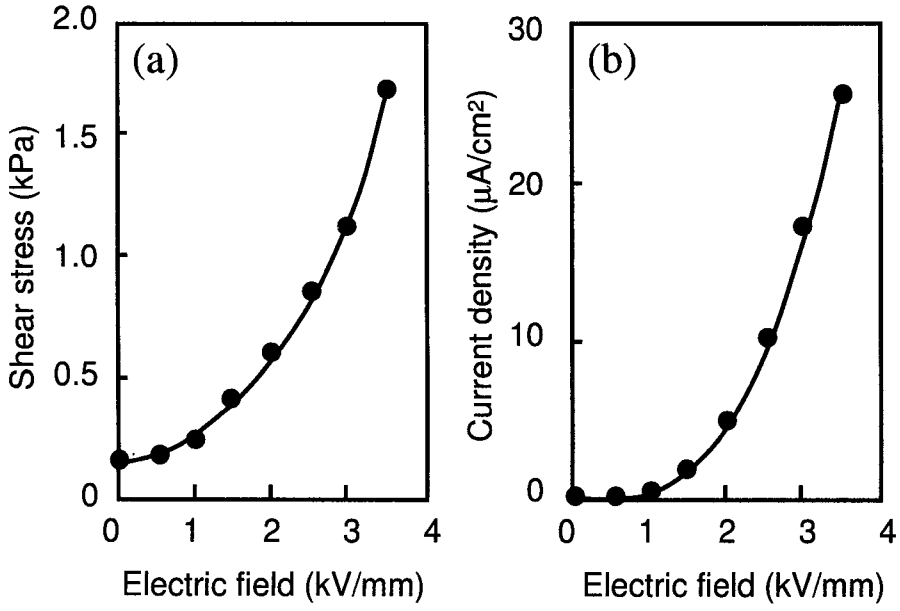

FIG. 1.5: (a) Variation of shear stress with applied dc electric field. (b) Variation of electric current density with applied dc electric field.

vibration or booming noise with a decoupler component). The transmissibility of the ER engine mounts can be controlled easily by electric field [76]. The orifices are made up of electrodes to which high voltage can be applied.

FIG. **1.7** shows construction of semi-active ER shock absorbers for automobile. Those are one of the most anticipated ER applications. Shock absorbers are required two different performance. Their damping force should be smaller for comfort drive, but it should be larger for driving stability (e.g. driving at high speed, maneuvering). ER shock absorbers can control its damper stiffness by applied electric field. Their damping force is small under no electric field and is large under an electric field and can be controlled semi-actively with feed back systems [42, 55].

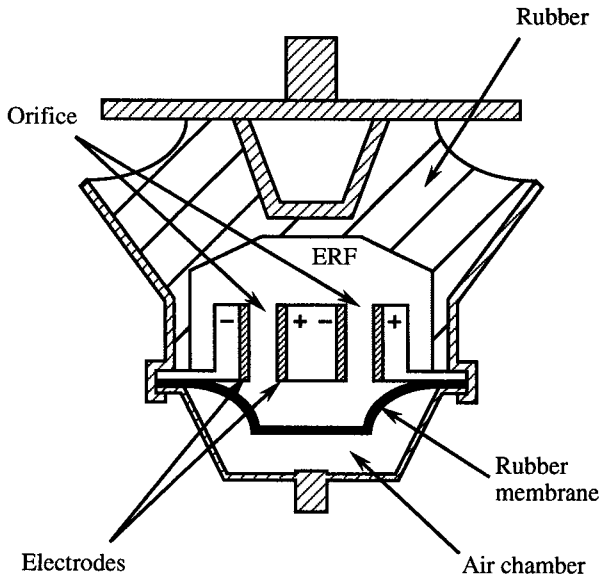

FIG. 1.6: Construction of ER fluid filled tunable engine mount.

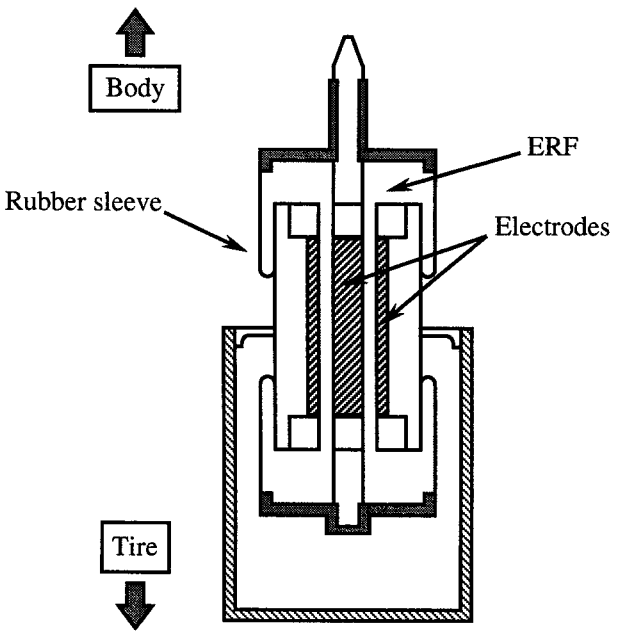

FIG. 1.7: Construction of ER dampers. Possible to damp vibrations over a wide range of external conditions (road bumpiness, maneuvering,..).

1.2.2 Other applications

FIG. **1.8** shows the composite ER beam. It can change its stiffness by applying electric field [18]. And it can be controlled semi-actively with feed back sensors.

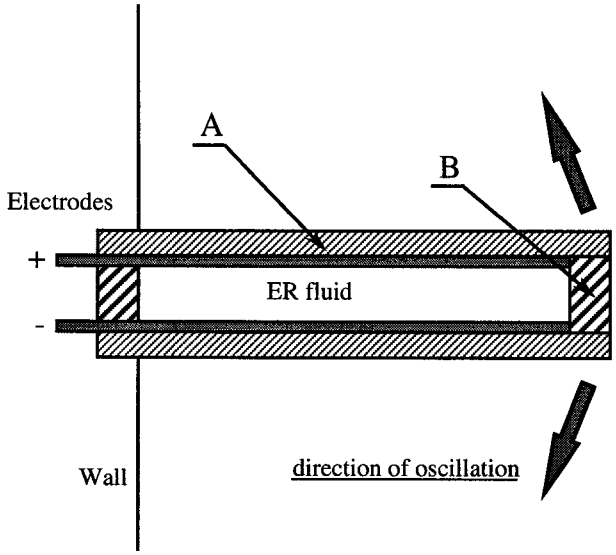

FIG. 1.8: Composite ER fluid beam construction. A : Polystyrene outer strips ($0.5mm$ thick). Lined with Al foil electrodes. B : Silicone rubber sealant.

As we described above, many advantageous and smart devices can be developed by applying ERF. But there remains a few requirements that the fluids must satisfy before practical ER devices can be developed. Increasing the yield stress under an electric field is desirable because many applications (especially automobile applications) require larger shear yield strengths than are currently available. The need for stronger ER effect in automotive applications has been discussed by Hartsock *et al.* [37]. And sedimentation of particles must be prevented over long periods of time with or without electric fields.

1.3 Objectives of this study

FIG. **1.9** shows schematically the required ER performance. ER effect (yield stress under an electric field) must be as large as possible and the electric consumption should be as little as

possible. The electric consumption is crucial problem for automobile applications because of the restriction of electric power supplying system. It is expected to obtain large ER effect by using particles with high conductivity. But it is not practical because its electric consumption may be too large. We can say that the balance of the both properties (yield stress and electric consumption) is one of the most important performance requirements of ERFs.

Particle dispersed ERF consists of particles in a nearly insulating solvent and its electro-rheological properties are dominated by the performance of dispersed particles. So we can say that the most important technical issue is how to obtain ideal and high performance particles for ERF. However there are many reports about mechanisms of ER effect and applications of ERF, there is not so many reports concerning about ER materials. So the relationship between the ER performance and material properties has not been discussed enough and many black boxes still exist. The purpose of this study is , therefore, the clarification of relationship between electrical

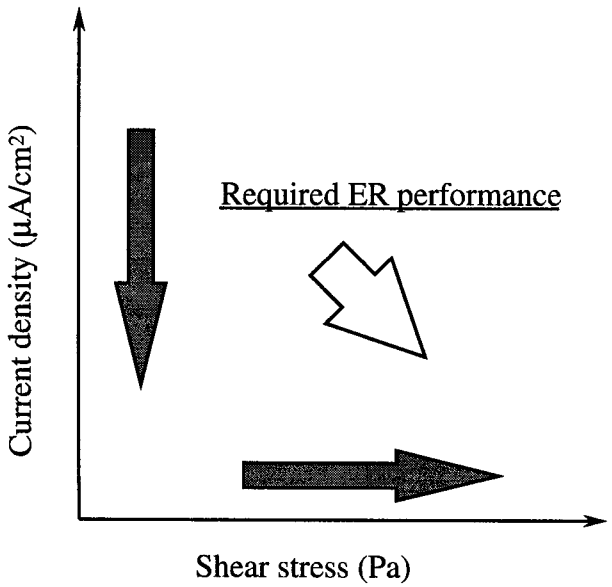

FIG. 1.9: Required ER performance. Shear stress under an electric field should be as high as possible and the current density should be as low as possible.

properties of dispersed particles and ER performance and the realization of improvement of ER performance for practical use.

The purpose of this study is summarized as follows;

1. **Realization of ideal structure of particle that shows higher ER effect than that conventional particle does.**
2. **Clarification the relationship between the electrical properties of particle and ER properties and realization of improvement of ER properties.**
3. **Clarification of the possibility of ER elastomer by dispersing ER particles in solid elastomers as one of the possible solutions to sedimentation problem of ERFs.**

Chapter 2.

Preparation of Materials and Measuring Methods for Electrorheological Fluids

In this chapter, there is a description of the materials of particle dispersed ERF systems and the measuring methods used in this thesis. Methods to estimate the electrical properties of dispersed particles by dielectric measurements are described.

2.1 Introduction

As described in Chapter 1, there are many kinds of particles for ERF reported recently. In this work, we used anhydrous carbonaceous particle that shows less temperature dependence of ER performance than that of hydrous ERF system for dispersed particle. We used silicone oil for the solvent. These materials will be described in detail in Section 2.2.

The study of anhydrous ERF has only been carried out in detail since the late 1980's , so we cannot say that the evaluation methods applicable to these materials are fully established. The most important aspects of ERFs are viscosity change and electric consumption under an electric field. We have done rheological experiments to evaluate this property by using cylinder rheometer, described in Section 2.3.

On the other hand, though techniques that combine material properties and ER performance are essential in order to achieve higher ER performance by optimizing material properties, there are few reports of these issues. Especially for the particles, whose properties govern ER performance, there are few studies on the relationship between property of particle and ER effect. So there are many unknowns in these relationships. In this thesis, we try to relate the properties of particle

to ER performance. We apply and propose dielectric measuring methods in order to evaluate electrical properties of dispersed particles and optimize particle properties in order to obtain higher ER performance. There will be a description of the measuring and estimating methods by dielectric measurements in Section 2.4.

On the other hand, there are some reports about the analytical method with microscopic observations (e.g. [17, 22]). We can say that combining microscopy and our evaluation methods would be useful in proving the appropriateness of the many approximations that have been used in recent simulations and theories appearing in the literature, as well as in clarifying the relationship between ER performance and material properties (e.g. [44, 46]).

2.2 Materials used in this thesis

2.2.1 Particles: Anhydrous-carbonaceous particle

In our studies, as base ERF particles, we used the anhydrous homogeneous carbonaceous particles developed at Bridgestone [41]. However there are several type of carbonaceous materials, we used carbonized resol type phenol resin in this thesis. We think ERF systems of carbonaceous particle are one of the most practical ones those available now. It shows less temperature dependence of ER effect, producing process is not complex and not expensive. These have a mean size of $6.0\mu m$ and have been processed so that there is a high degree of uniformity in the electrical conductivity σ_b, which is of the order of $10^{-8}S/m$. We controlled the conductivity of particle by the degree of carbonization. When we heat-treat particles at higher temperature, their conductivity goes higher since the degree of carbonization increases [30]. In Chapter 7, we optimized the particle carbonizing process and showed the description of heat treating process and the equipment used. ERF made by suspending these particles in a carrier oil shows a large increase in shear stress under the application of an electric field (see FIG. **1.5**), and the electronic nature of the polarization gives the fluid a wide range of operating temperature.

FIG. **2.1** shows the SEM (Scanning Electron Microscope) image of the raw particulate materials. We can see that they have spherical shape and narrow size distribution. We carbonize these particles with electric furnace and control the conductivities of particles. After carbonization,

the shape won't change and is still spherical. FIG. **2.2** shows the structural change of ERF by

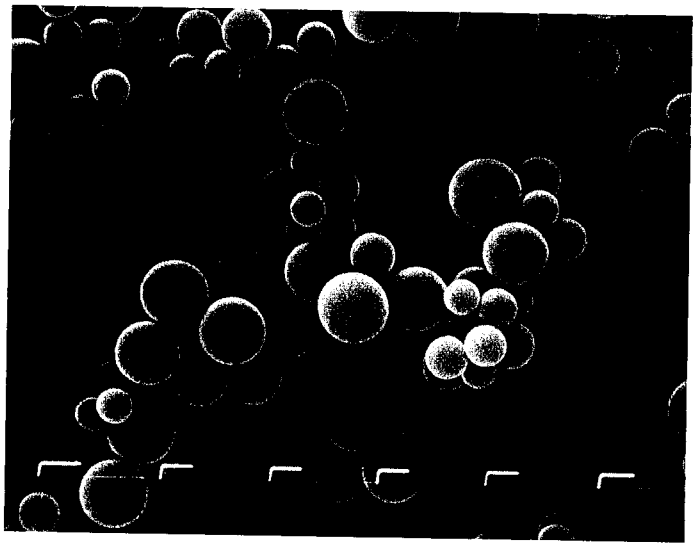

FIG. 2.1: SEM image of the particulate phenolic resin.

applying a electric field. Upon application of the electric field, the static suspension (FIG. **2.2**(a)) rapidly formed a fibrous structure (**2.2**(b)) by an essentially instantaneous formation of the fibrous skeleton, followed by slight rearrangement within the fibers on a time scale of minutes.

2.2.2 Solvent

There are many kind of solvents those can be used for ERFs. In this thesis, we used silicone oil as solvent of suspension. Silicone oil has many aspects different from mineral oils and vegetable oils. We chose silicone oil for following reasons;

- Wide range of available viscosities
- Little viscosity dependence of temperature
- 100% synthesized chemically and involves little impurities
- Not expensive and already mass produced
- High chemical stability

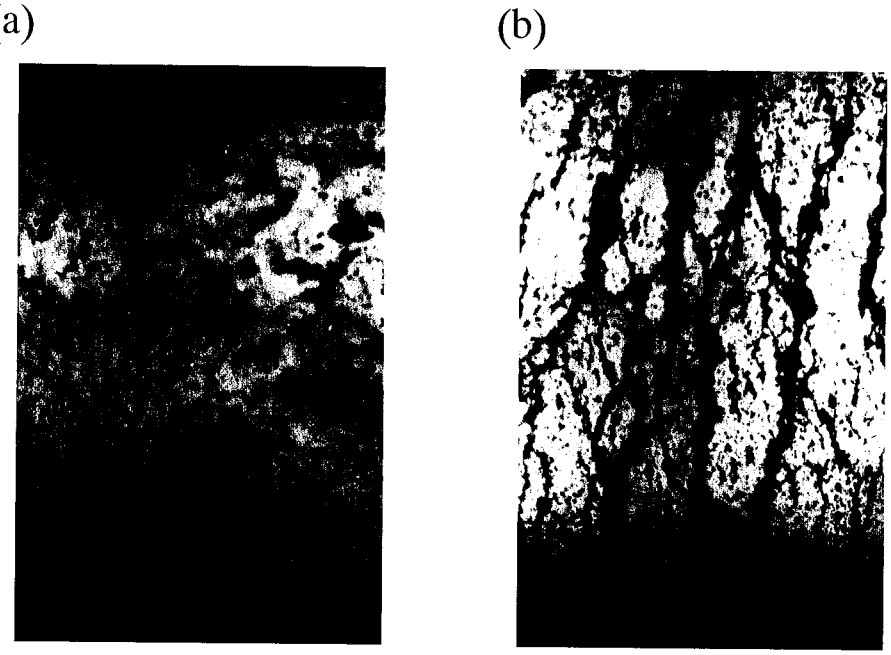

FIG. 2.2: (a) Static suspension with no electric field. (b) Static fibrous structure formed by application of the dc electric field.

FIG. **2.3** shows constitutional formula of dimethyl silicone oil. Its viscosities can be controlled by the value of n in FIG. **2.3** (n = polymerization degree). And Table **2.1** showed some aspects of typical grades used in this thesis [4]. The viscosity-temperature coefficient VTC shown in Table

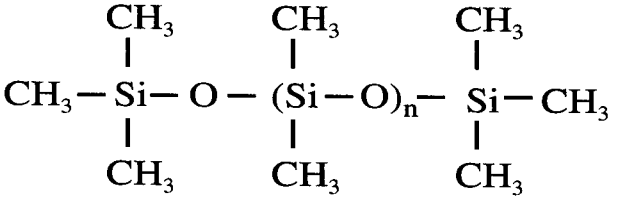

FIG. 2.3: Constitutional formula of dimethyl silicone oil.

2.1, is an index of temperature dependence of the viscosity of the oil. It is defined as follows:

$$VTC = 1 - \frac{\eta_{98.9}}{\eta_{37.8}} \tag{2.1}$$

Here, $\eta_{98.9}$ is the viscosity of oil at 98.9 ℃ and $\eta_{37.8}$ is viscosity at 37.8 ℃. From Table **2.1**, we see that silicone oils have lower viscosity-temperature coefficient than other mineral and vegetable

oils, meaning that there is a smaller variation of viscosity with temperature and hence smaller temperature dependence of the rheological properties of the ERF (under no electric fields and electric fields). This is considered as an important character of oils when we chose them as a solvent.

Table. 2.1: Typical properties of dimethyl silicone oil.

Viscosity ($mPa \cdot s$)	9.4	9.7×10	9.7×10^2
Specific gravity (g/cm^3)	0.940	0.968	0.974
Viscosity-Temperature coefficient	0.57	0.60	0.61
Relative dielectric permittivity	2.60	2.75	2.75

2.3 Rheological measurement

2.3.1 Steady shear measurement

Shear stress measurements were made using a Couette-type rheometer, manufactured by Rheometrics Inc. The bob has a radius of $25mm$ and a height of $20mm$. The surrounding cup has a radius of $26mm$ (FIG. **2.4**). The $1mm$ gap was filled with the fluid to be measured, and a constant shear flow was applied. The range of shear rate $\dot{\gamma}$ can be varied from 0.01 to $400s^{-1}$. The bottom parallel surfaces of bob and pot are made of insulation film (*Polyester*) in order not to influence the change of viscosity under electric fields. This rheometer has been modified so that a dc electric field E of $3kV/mm$ can be applied across the gap during shearing measurements. And all measurements were made at 25 ℃. The steady state torque measurements were converted to values for the shear stress. The electric current passing through the ERF is measured by a Digital Multimeter (PR 6846) manufactured by Advantest.

2.4 Dielectric measurement

Measurement of dielectric permittivity is a simple and efficient way to characterize the electrical properties of particles in an ERF [86]. The technique is used here to investigate the electrical properties of ER particles.

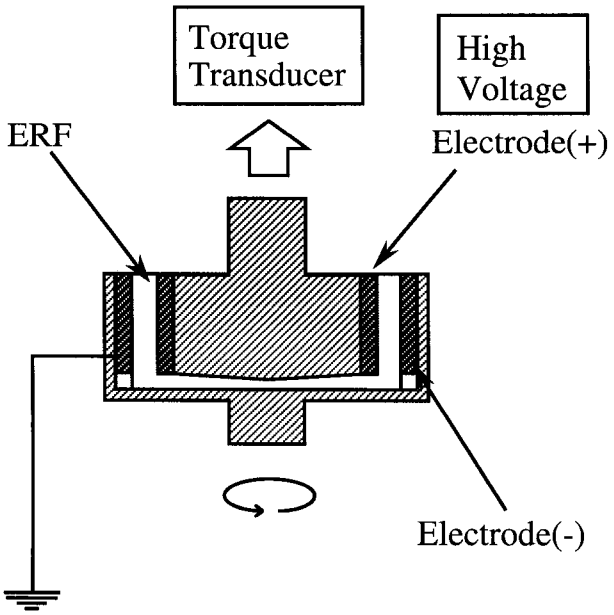

FIG. 2.4: Schematic of the ERF test fixture (rheological properties).

The results of the permittivity measurements are highly reproducible, which is an advantage over other techniques such as electrical measurement using a bed of packed particles (which is known to be very sensitive to conditions such as packing pressure, distribution of particle size and so on).

The dielectric permittivity of the ERF suspensions under quiescent conditions is measured with a Schlumberger Corp. Impedance/Gain phase analyzer (Model SI1260) at 25 ℃, under a low ac electric field $\sim 1V/mm$, which is too weak to cause any particle chaining. The sweep of frequencies f is from $10Hz$ to $100,000Hz$. From these measurements, we obtain the frequency dependence of the real and imaginary relative dielectric permittivities, $\epsilon^{'}$ and $\epsilon^{''}$. The curves for $\epsilon^{''}(f)$ typically show a maximum value which occurs at a frequency we will write as f_{max}.

ERF samples were placed into a concentric cylinders (FIG. **2.5**). $\epsilon^{'}$ and $\epsilon^{"}$ are calculated from the real and imaginary elements of the impedance.

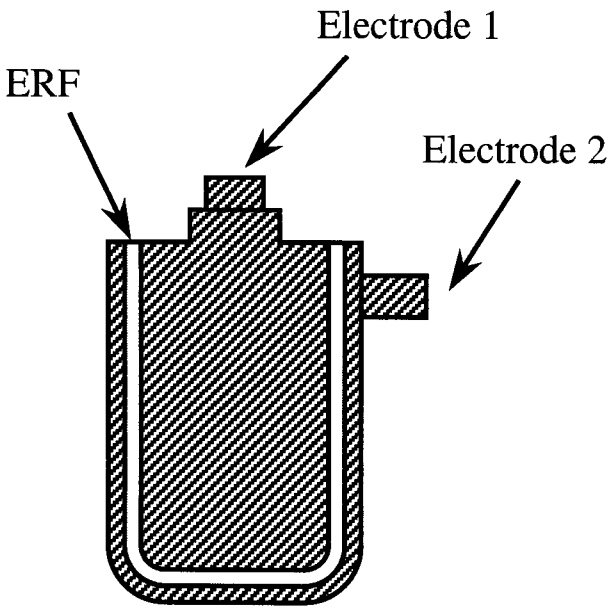

FIG. 2.5: Schematic of the ERF sample test fixture (dielectric permittivity).

2.4.1 Maxwell-Wagner approach for particle dispersed system

Particle dispersed systems like as particle dispersed ERFs can be modeled by the Maxwell-Wagner approach [23]. The complex relative dielectric permittivity ϵ^* can be written as

$$\epsilon^* = \epsilon_\infty + (\epsilon_{st} - \epsilon_\infty)\frac{1}{1 + i\omega\tau} \tag{2.2}$$

where ω is angular frequency. The real numbers ϵ_{st}, ϵ_∞ are the limits of the dielectric response at low and high frequencies as indicated in FIG. **2.6**. τ is the relaxation time, and can be estimated if we assume that the dielectric response of this system can be modeled by the Maxwell-Wagner approach, where there is a buildup of charge at the interfaces due to the mismatch in conductivities [23]. The real part ($\epsilon^{'}$) and the imaginary part ($\epsilon^{''}$) of eq. (2.2) are written as

$$\epsilon^{'} = \epsilon_\infty + (\epsilon_{st} - \epsilon_\infty)\frac{1}{1 + \omega^2\tau^2} \tag{2.3}$$

$$\epsilon^{''} = (\epsilon_{st} - \epsilon_\infty)\frac{\omega\tau}{1 + \omega^2\tau^2} \tag{2.4}$$

The relaxation time τ_{MW} of suspension can be written by Maxwell-Wagner approach as [77]

$$\tau_{MW} = \frac{2\epsilon_s\epsilon_0 + \epsilon_p\epsilon_0}{4\pi(2\sigma_s + \sigma_p)} \tag{2.5}$$

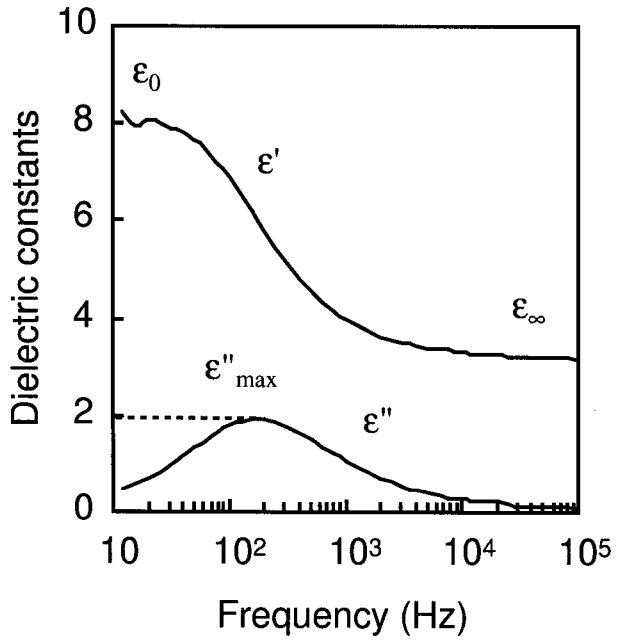

FIG. 2.6: Variation of relative dielectric permittivities $\epsilon^{'}$ and $\epsilon^{''}$ as a function of frequency (Ideal case of the single relaxation time).

where ϵ_s, σ_s are relative dielectric permittivity and conductivity of solvent and ϵ_p, σ_p are relative dielectric permittivity and conductivity of dispersed particle respectively.

2.4.2 Evaluating inter-particle conductive uniformity by Cole-Cole method

In this thesis, we take "inter-particle conductive uniformity" as one of the most crucial properties that dominates ER performance. Many systems do not show pure Debye relaxation behavior (FIG. **2.6**) and this means the materials used for measurements have broadening of the relaxation time. ϵ_s and σ_s are assumed to have a single relaxation time, so the broadening of the relaxation time derives from ϵ_p and σ_p as indicated in eq. (2.5). The Cole-Cole analysis technique is often applied where the above equations are modified by another empirical parameter α associated with a spread of relaxation times [21]:

$$\epsilon^*_{cole} = \epsilon_\infty + (\epsilon_{st} - \epsilon_\infty)\frac{1}{1 + (i\omega\tau)^{(1-\alpha)}} \tag{2.6}$$

The empirical parameter α appearing in eq. (2.6) varies between 0 and 1, and describes the broadening of the relaxation region. $\alpha = 0$ corresponds to the ideal case of the single relaxation

time Debye-type response for dilute suspensions of uniform conduction spheres shown in FIG. **2.6**. In general, eq. (2.6) can be solved for α, giving the following formula:

$$\alpha = 1 - \frac{4}{\pi} \tan^{-1} \left(\frac{2\epsilon''_{max}}{\epsilon_{st} - \epsilon_{\infty}} \right) \tag{2.7}$$

where ϵ''_{max} is the maximum value of the curve ϵ'' (see FIG. **2.6**). Thus α can be easily determined from the experimental measurements of dielectric permittivity. In these experiments particle conductivity is varied, so α provides a measure of the broadness of the conductivity distribution.

2.5 Conclusion

We summarize the description of materials we used in this thesis. We take a ERF system of carbonaceous particle and silicone oil because this is one of the most practical fluids available now.

We propose a analytical technique of dielectric measurement as a new method to evaluate the relationship between the ER effects and particulate properties. We will apply Maxwell-Wagner approach to particle dispersed ERF systems to evaluate electrical properties of particles. And we take a inter-particle conductive uniformity as a factor that affect its ER performance and apply the Cole-Cole approach in order to estimate the conductive uniformity with dielectric measurements. In the following chapters, we use these techniques, and from the parameters obtained, we suggest ways to achieve higher ER performance by optimizing material properties.

Chapter 3.

Optimization of Particle Structure to Improve its Electrorheological Effect

In this chapter, we have investigated the optimum structure of ER particles. We showed that a high performance particle, with large increment in viscosity at small electric consumption, can be achieved with a particle with a layered structure. We propose that layered particle as one of the ideal particles for ERF.

3.1 Introduction

The large change in flow resistance coupled with the short response time (of the order of *ms*) make ERFs ideal for use in many electrically controlled mechanical devices, and they have received considerable attention in recent years. In particular, the compactness of electrorheological devices make them suitable for a variety of automobile applications, such as active suspension systems (see Chapter 1).

There are some outstanding technical issues that need to be resolved before ERFs can be used in many of the mechanical devices under consideration. Some proposed automotive applications require a larger ER effect than is currently achieveable, as discussed by Hartsock *et al.* [37]. Another important design issue is minimal power consumption during operation, which is a crucial problem for automotive applications because of the restricted supply of electricity. Further, considerations of simplicity, cost, size and weight mean that dc power is often the preferred mode in an automobile. Thus, achieving a balance between maximum ER effect and minimum electric current under dc electric fields is an important problem in the development of ERFs.

Since the electrorheological performance strongly depends on the nature of the particles dispersed in the suspension, the production of particles with the optimum electrical properties becomes a key issue. In this chapter we will focus on solid-state particles, which do not use liquid additives to modify the electrical properties, and which are attractive for their potentially wide range of operating temperatures. With homogeneous solid-state particles, it has been reported that the ER effect under a dc field will increase with particle conductivity, but this has the limitation that electric current also increases. The ideal situation is to have a large induced polarization in each particle leading to strong interparticle interactions and high ER effect, but with a minimal passage of electric current. One way to achieve this would be to design particles with a layered structure, where there is a transition in the electrical properties from the surface region to the core.

Several articles dealing with the problem of the ideal structure and electrical properties of ERF particles have now appeared (e.g. [26, 40, 82, 83]). Inoue [40] reported experiments using metal particles coated with a thin insulating oxide layer, but found that a suspension of these particles in silicone oil did not show a large yield stress under dc and low frequency ac electric fields. Davis [26] was able to theoretically explain this behavior by calculating the forces in a chain of such particles, using the Maxwell-Wagner polarization model. Wu and Conrad [82, 83] investigated the forces between conducting spheres coated with a weakly conducting thin surface film, but they focussed on the effect of the non-ohmic conductivity of the oil under high fields.

In this chapter we show that a high performance solid-state ER particle for dc electric fields can be achieved with a layered structure consisting of a semi-conducting core surrounded by an outer layer of slightly lower conductivity. We compare the ER properties of this system with those for a suspension made from conventional electrically homogeneous particles. Our experiments show that the layered particle system can achieve an excellent balance of low electric current and high ER effect under a dc electric field. We verify the chemical structure of the layered particle by X-ray spectroscopic analysis, and we also estimate its electrical properties by measurements of dielectric permittivity under a weak ac electric field.

This chapter is organized as follows. The experimental procedures are described in Section

3.2. In Section 3.3, results of the rheological measurements are presented, together with the chemical composition and dielectric permittivity analyses from which the structure of the particle is verified. Conclusions are given in the final section.

3.2 Experiments

3.2.1 Sample preparation

Our aim is to produce a semi-conducting solid-state particle, comprising of a core surrounded by an outer layer of lower conductivity. To achieve this, we use resol-type phenolic resin particles as the raw material, and SiO_x to control the conductivity of the surface layer. FIG. **2.1** shows SEM (Scanning Electrron Microscope) image of raw material. The original particle is nearly spherical with a mean diameter of 6μm, and is porous. The particles are stirred for 10 hours at $100rpm$ and 25 ℃ in ortho silicate ester, which has the constitutional formula shown in FIG. **3.1**. The viscosity

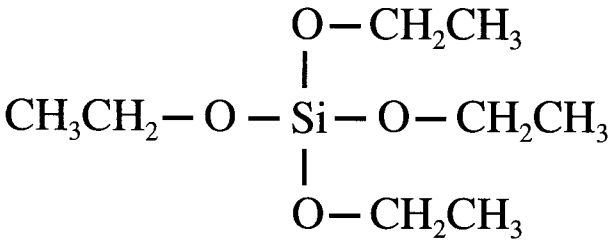

FIG. 3.1: Constitutional formula of Ortho Silicate Ester.

of ortho silicate ester is very low ($7.0 \times 10^{-4} Pa \cdot s$ at 25 ℃) and so it can easily be impregnated into the porous phenolic resin. After impregnation, the particles are filtered and washed with water to remove excess ortho silicate ester, otherwise the conductivity of the outer surface will become too low. The particles are then dispersed in water with an acidic catalyst and stirred for 2 hours at 80 ℃. During this process, the impregnated ortho silicate ester in the outer region of the particles hydrolyzes into SiO_x. After a filtration and drying stage, the particles are carbonized at 580 ℃ in Ar atmosphere using an electric furnace. By altering the carbonization conditions, the degree of conductivity of the layered particles can be closely controlled. The particles obtained

from this process have a structure shown in FIG. **3.2**, with an outer layer of SiO_x distributed in the carbonized phenol resin and a core of carbonized phenol resin.

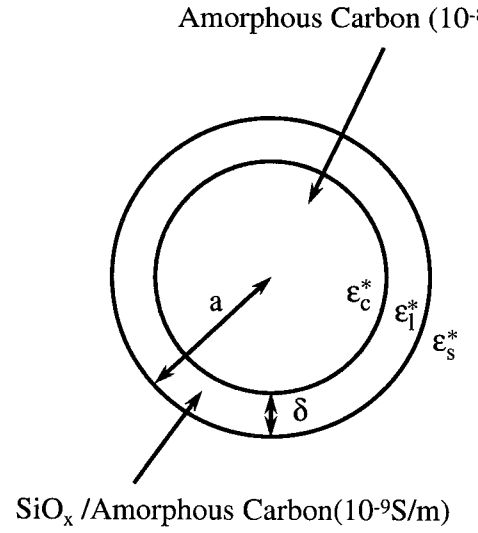

FIG. 3.2: Schematic diagram of structure of the layered particle for ERF. The parameters a, δ, ϵ_c^*, ϵ_l^*, ϵ_s^* are used in the analysis in Section 3.3.

For comparison, we also use ERFs made with conventional homogeneous particles. These homogeneous particles are made from the same phenol resin particles used above, and so have a similar size and shape. To produce the ERF particles, a similar carbonization process to the layered particle system is performed. If the same carbonization conditions are used, the conductivity of these homogeneous particles will be the same as the core of the layered particles. Both the layered and homogeneous particles have a density of $1.21 g/cm^3$.

To produce the ERF suspension, we disperse the particles in a high-insulation silicone oil manufactured by Toshiba Silicone Co. Ltd(Japan) which has a viscosity of 9.4 $mPa \cdot s$ at room temperature (see Chapter 2). The relative dielectric permittivity ϵ_s and conductivity σ_s of the oil will be determined from the dielectric measurements. The volume fraction of the particles is 30% in all experiments. An automatic mortar grinder is used to ensure that the particles are well dispersed in the oil. There appear to be minimal sedimentation effects.

3.2.2 X-ray spectroscopic analysis

To analyse the structure of the composite particles we use a Philips Model CM30 Energy Dispersive X-ray Spectroscopy (EDX) instrument. The particles are embedded in epoxy resin and cured at room temperature. The surface of the bulk epoxy resin is then carefully polished and the exposed cross section of the particle is analysed chemically to determine the distribution of SiO_x from the surface to the core.

3.2.3 Shear stress and current density measurements

Details of rheological measurements are described in Chapter 2. All measurements are performed at 25 ℃.

3.2.4 Dielectric permittivity measurements

The technique of dielectric permittivity measurements is used here to investigate the electrical properties of the layered particles, and to make a comparison with the homogeneous particles.

Details of dielectric permittivity measurements are described in Chapter 2.

3.3 Results and discussion

3.3.1 X-ray spectroscopy

FIG. **3.3** shows the AEM (Analytical Electron Microscope) image of cross section of carbonized layered particle. The blue points indicate the existence of Si. And FIG. **3.4** shows the result obtained from EDX analysis of the layered particle. As expected, we see that there is a significant amount of SiO_x in the surface region, leading to a reduction in the electrical conductivity there. We can also see that SiO_x does not exist at depths greater than $1\mu m$ from the surface (recall that the mean particle size is $6\mu m$). Note that FIG. **3.4** shows there is no Si beyond $1\mu m$ from the surface, indicating that there is little difference in the chemical constitution between the homogeneous particle and the core of the layered particle.

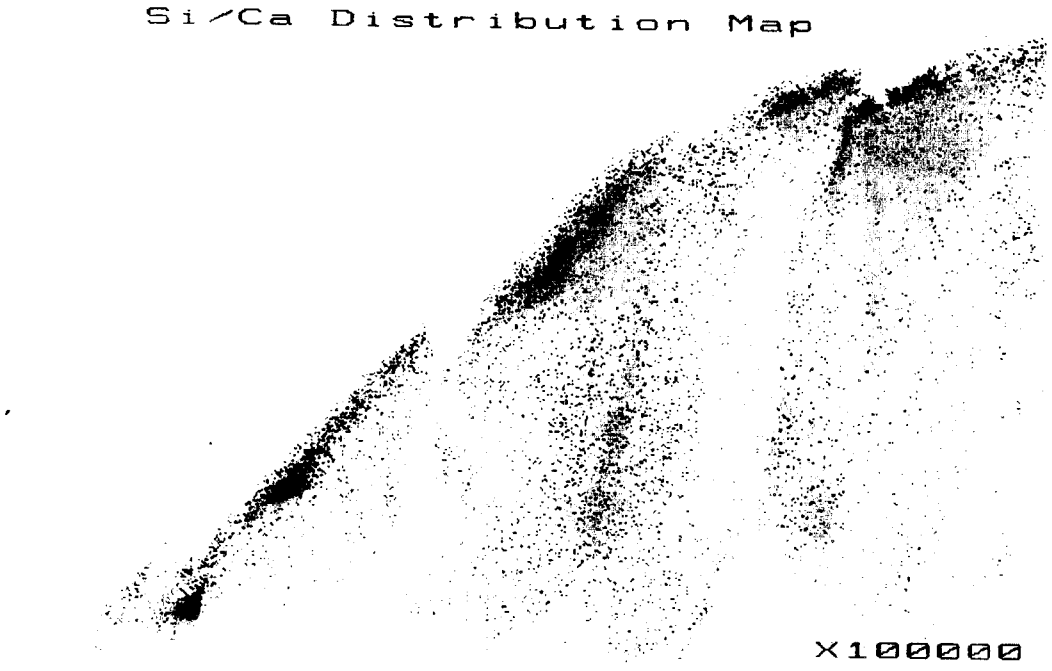

FIG. 3.3: AEM image of cross section of carbonized layered particle.

3.3.2 Rheological measurements

FIG. **3.5** shows that ERF made from the layered particles has a Bingham fluid behavior under a $2kV/mm$ dc electric field and shear rate of $366s^{-1}$, similar to ERF made with the homogeneous particles. FIG. **3.6** compares the ER effect and electric current density of the layered particle and homogeneous particle systems. When we compare the two systems at the same level of power consumption, it is clear that we can obtain a considerably higher ER effect with layered particles than with homogeneous particles. This can be attributed to the layered structure of the particle, since in other respects the two suspensions are almost identical.

Table **3.1** highlights the results for a pair of homogeneous and layered particle systems, which were both carbonized at 580 ℃ under identical conditions. We see that while the ER effect is very similar for the two systems, the layered particle system has a substantially reduced electric

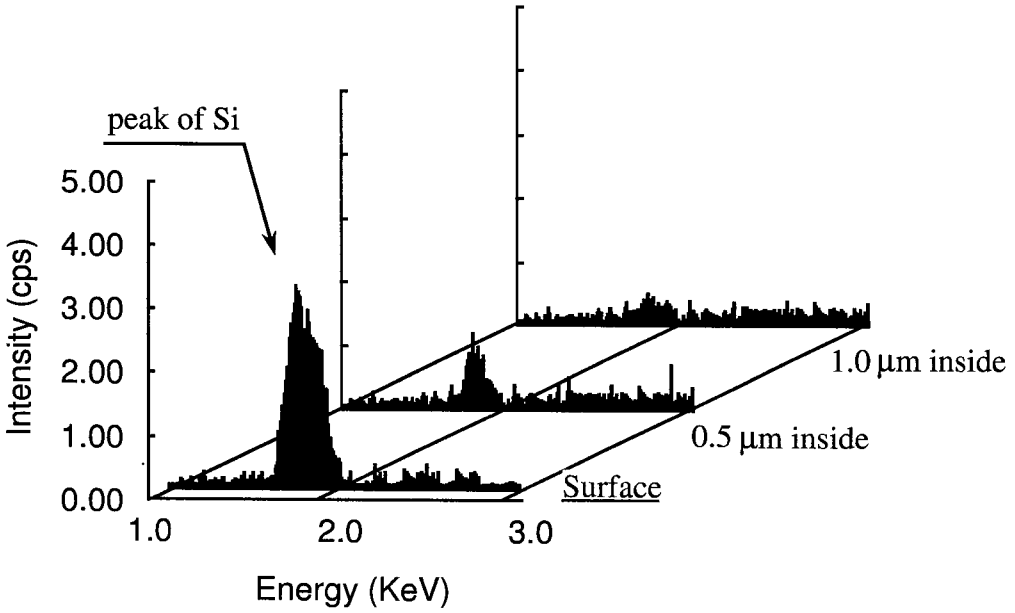

FIG. 3.4: Distribution of Si as a function of depth from particle surface, obtained by X-ray spectroscopic analysis.

current. A possible reason for the observed behavior is that the ER effect is governed by the

Table. 3.1: Comparison between homogeneous particle and layered suspensions at $2kV/mm$ and $366s^{-1}$. These particles were produced under identical carbonization conditions.

Particle	ER effect	Current density	$\epsilon_p(Hz)$
Homogeneous	$384(Pa)$	$8.6(\mu A/cm^2)$	316
Layered	$394(Pa)$	$1.6(\mu A/cm^2)$	100

degree of polarization of the particle's volume, and so will not be strongly affected by a slight decrease in the surface conductivity. To illustrate this, we note that the dipole p for an isolated layered sphere of radius a under a dc electric field E_0 is given by

$$p = 4\pi\epsilon_s\epsilon_0 a^3 \left(\frac{\bar{\sigma} - \sigma_s}{2\sigma_s + \bar{\sigma}}\right) E_0 \tag{3.1}$$

where $\bar{\sigma}$ is expressed in terms of the conductivities of the core (σ_c) and outer layer (σ_l) by the

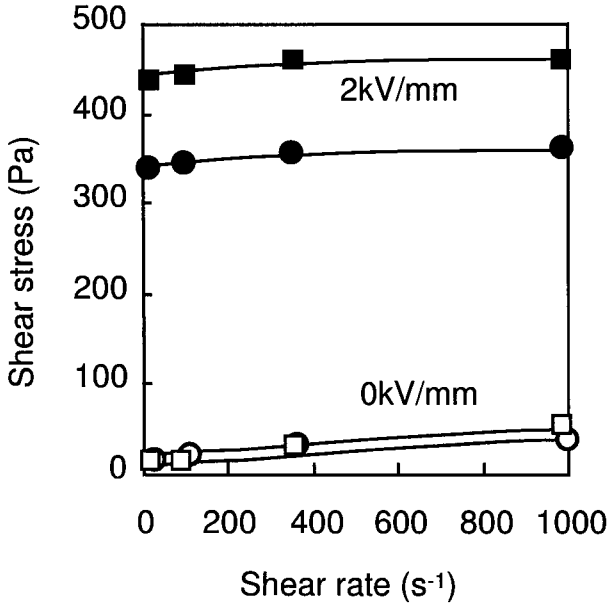

FIG. 3.5: Variation of shear stress with shear rate for layered particle suspension (square) and homogeneous particle suspension (circle), under no electric field and dc electric field of $2kV/mm$.

following

$$\bar{\sigma} = \frac{(2\sigma_l + \sigma_c)a^3 + 2(\sigma_c - \sigma_l)(a-\delta)^3}{(2\sigma_l + \sigma_c)a^3 - (\sigma_c - \sigma_l)(a-\delta)^3}\sigma_l \tag{3.2}$$

Here δ is the thickness of the outer layer (FIG. **3.2**). From eqs. (3.1) and (3.2) we see that provided the conductivities in the particle σ_c, σ_l are much larger than the oil conductivity σ_s, the polarization of the particle volume will not be significantly changed from a homogeneous particle of conductivity σ_c.

On the other hand, we would expect that the dc electric current would be significantly modified by the presence of an outer layer of lower conductivity. A simple approach would be to observe that, since the current must pass across the layer and flow into the core region, the system is analogous to a series of resistors in an electrical circuit. More sophisticated models are available which consider in detail the conduction mechanism between the particles (e.g. [82, 83]), where there is a strong dependence on the physical properties of the surface including its conductivity, but these detailed analyses are beyond the scope of the present work.

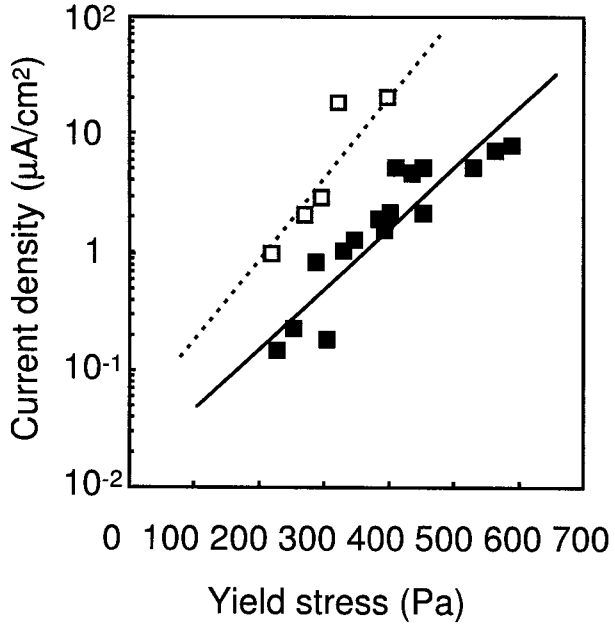

FIG. 3.6: Electric current density vs ER effect (yield stress) for various homogeneous particle suspensions (white square) and layered particle suspensions (black square) under dc electric field of $2kV/mm$ and shear rate of $366s^{-1}$.

3.3.3 Dielectric measurements

Here we use dielectric measurements to estimate the electrical properties of the core and surface of the layered particles. We will proceed in two steps: (1) We find the electrical properties of the homogeneous particle, which will equal those of the core since the carbonization conditions are identical; (2) We estimate the electrical properties of the surface of the layered particle using the shift in the polarization relaxation time from the homogeneous case. For definiteness, we will focus on the homogeneous and layered particle systems described in Table **3.1**. Following other workers, we will base our analysis on the Maxwell-Wagner model of polarization [26].

We apply a weak ac electric field $E(t) = Re(E_1 e^{i2\pi ft})$ to the suspension. For the homogeneous particles, we obtain the conductivity (σ_p) and the relative dielectric permittivity (ϵ_p) from

measurements of the complex relative dielectric permittivity ϵ^* (see Chapter 2)

$$\epsilon^* = \epsilon_\infty + (\epsilon_{st} - \epsilon_\infty)\frac{1}{1 + (i2\pi f\tau)} \tag{3.3}$$

where the real numbers ϵ_{st}, ϵ_∞ are the limits of the dielectric response at low and high frequencies, and τ is the relaxation time of polarization. For spherical particles with complex relative permittivity ϵ_p^* dispersed in an oil of complex relative permittivity ϵ_s^*, the overall complex relative permittivity ϵ^* in eq. (3.3) can be written as

$$\epsilon^* = \epsilon_s^* \frac{2\epsilon_s^* + \epsilon_p^* + 2\phi(\epsilon_p^* - \epsilon_s^*)}{2\epsilon_s^* + \epsilon_p^* - \phi(\epsilon_p^* - \epsilon_s^*)} \tag{3.4}$$

where ϕ is the volume fraction of the particles. Generally, the complex permittivity ϵ_j^* of species j can be written using the dielectric permittivity ϵ_j and conductivity σ_j as follows

$$\epsilon_j^* = \epsilon_j - i\frac{2\sigma_j}{f} \tag{3.5}$$

In the limit of $f \to \infty$, we obtain from eqs. (3.4) and (3.5)

$$\epsilon_\infty = \epsilon_s \frac{(2\epsilon_s + \epsilon_p) + 2\phi(\epsilon_p - \epsilon_s)}{(2\epsilon_s + \epsilon_p) - \phi(\epsilon_p - \epsilon_s)} \tag{3.6}$$

Thus by measuring ϵ_∞ for the ERF, we can obtain ϵ_p from eq. (3.6). Dielectric measurements of the oil alone give us $\sigma_s = 5.26 \times 10^{-13} S/m$ and $\epsilon_s = 2.5$. Measurements using the ERF made from homogeneous particles give $\epsilon_{st} = 12.01$ and $\epsilon_\infty = 3.36$, so from eq. (3.6) with $\phi = 0.3$ we obtain $\epsilon_p = 6.41$. Since the carbonization conditions are identical, we assume that this is the value of the core relative permittivity (ϵ_c) of the layered particle.

We turn now to the determination of the conductivity σ_p for the homogeneous particles (and the core of the layered particles). As we showed in Chapter 2, in the Maxwell-Wagner model the relaxation time τ of a system of monodisperse spheres can be written as

$$\tau = \frac{2\epsilon_s\epsilon_0 + \epsilon_p\epsilon_0}{2\sigma_s + \sigma_p} \tag{3.7}$$

The relaxation time τ can also be expressed in terms of the frequency f_{max} corresponding to the peak of the $\epsilon''(f)$ curve (see FIG **2.6**)

$$\tau = \frac{1}{2\pi f_{max}} \tag{3.8}$$

For the ERF made with homogeneous particles, it is found that $f_{max} = 316Hz$, which when substituted into eqs. (3.7) and (3.8) along with the result $\epsilon_p = 6.41$ gives us $\sigma_p = 1.60 \times 10^{-8} S/m$. We will use this value for the conductivity of the core of the layered particle σ_c, since the carbonization conditions are identical.

We now move on to the second step, where we consider the dielectric response of the layered particle system, and use this to estimate the electrical properties of the outer layer. To simplify the calculation, we assume that the outer layer is uniform and has a thickness δ of $0.5\mu m$ as indicated by the results from the EDX (see FIG. **3.4**). Let ϵ_l^* and ϵ_c^* be the complex relative dielectric permittivities of the outer layer and the core respectively (refer to eq. (3.5)).

An isolated layered particle of radius a in the ac electric field $E(t) = Re(E_1 e^{i2\pi ft})$ will have an induced dipole $p(t)$ given by

$$p(t) = Re\left(4\pi\epsilon_s\epsilon_0 a^3 \left(\frac{\bar{\epsilon} - \epsilon_s^*}{2\epsilon_s^* + \bar{\epsilon}}\right) E_1 e^{i2\pi ft}\right) \tag{3.9}$$

where $\bar{\epsilon}$ is the effective complex relative permittivity of the layered particle

$$\bar{\epsilon} = \frac{(2\epsilon_l^* + \epsilon_c^*)a^3 + 2(\epsilon_c^* - \epsilon_l^*)(a-\delta)^3}{(2\epsilon_l^* + \epsilon_c^*)a^3 - (\epsilon_c^* - \epsilon_l^*)(a-\delta)^3}\epsilon_l^* \tag{3.10}$$

As before, we firstly consider the limit of high frequency, so that the contribution from the conductivity terms becomes small. We still use eq. (3.6), but now replace the ϵ_p with $\bar{\epsilon}_\infty$ given by

$$\bar{\epsilon}_\infty = \frac{(2\epsilon_l + \epsilon_c)a^3 + 2(\epsilon_c - \epsilon_l)(a-\delta)^3}{(2\epsilon_l + \epsilon_c)a^3 - (\epsilon_c - \epsilon_l)(a-\delta)^3}\epsilon_l \tag{3.11}$$

Measurements of the layered particle system give $\epsilon_\infty = 3.35$. Using the values of ϵ_s and ϵ_c obtained previously, eqs. (3.6) and (3.11) yield $\epsilon_l = 1.42$.

We next use the polarization relaxation time to estimate the conductivity of the outer layer, similar to the homogeneous particle case. Because this system has three components (s, l and c), there will be two Maxwell- Wagner relaxation times τ_1, τ_2. From eqs. (3.9), (3.10) and (3.5), a straightforward but long calculation gives

$$\tau_{1,2} = \frac{A}{2C}\left(1 \pm \sqrt{1 - \frac{4BC}{A^2}}\right) \tag{3.12}$$

where

$$A = 2\frac{(a-\delta)^3}{a^3}(\epsilon_l - \epsilon_s)\epsilon_0(\sigma_c - \sigma_l)$$

$$+ \quad 2\frac{(a-\delta)^3}{a^3}(\epsilon_c - \epsilon_l)\epsilon_0(\sigma_l - \sigma_s)$$
$$+ \quad (2\epsilon_s + \epsilon_l)\epsilon_0(\sigma_c + 2\sigma_l) + (\epsilon_c + 2\epsilon_l)\epsilon_0(2\sigma_s + \sigma_l) \tag{3.13}$$

$$B = 2\frac{(a-\delta)^3}{a^3}\epsilon_0^2(\epsilon_l - \epsilon_s)(\epsilon_c - \epsilon_l) + (\epsilon_l + 2\epsilon_s)(2\epsilon_l + \epsilon_c)\epsilon_0^2 \tag{3.14}$$

$$C = 2\frac{(a-\delta)^3}{a^3}(\sigma_c - \sigma_l)(\sigma_l - \sigma_s)$$
$$+ \quad (\sigma_l + 2\sigma_s)(2\sigma_l + \sigma_c) \tag{3.15}$$

The peak observed in the $\epsilon''(f)$ curves occurs at the frequency f_{max}, which will correspond to one of the relaxation times (note that while eq. (3.12) will produce two values, by inspection clearly only one corresponds to f_{max}). In the present example, the ϵ'' peak was observed at $100Hz$, which is lower than the homogeneous case ($316Hz$) due to the presence of the outer layer. Thus, combining eq. (3.8) with eqs. (3.12), (3.13), (3.14) and (3.15), we can determine σ_l since it is the only unknown quantity. The Newton-Raphson method was used to numerically find that $\sigma_l = 9.93 \times 10^{-9} S/m$. Thus we have verified that the outer layer indeed has a lower conductivity than the core.

3.4 Conclusion

We have performed a set of experiments comparing the electrorheological behavior of suspensions of conventional homogeneous semi-conducting particles and suspensions of layered particles, which have a semi-conducting core and an outer layer with lower conductivity. The results show that under a dc electric field, the layered particle system retains a substantial ER effect but with much reduced power consumption. We thus propose that suspensions using layered particles may lead to an optimal ERF for devices with a dc power source, such as in automotive applications.

Chemical analysis using X-ray spectroscopy confirms the presence of SiO_x in the outer region of the carbonized phenol resin particle, which is the cause of the reduced surface conductivity. Measurements of dielectric permittivity enable us to estimate the dielectric permittivities and

conductivities of the core and surface of the layered particle, and we are able to verify that the surface does indeed have a reduced level of conductivity.

A detailed microstructural investigation of the optimum type of layered particle would require more elaborate tools of chemical and electronic analysis, and will be the object of future efforts.

Chapter 4.

Investigation of the Effect of Conductive Uniformity of Particles by Blending Particles with Different Conductivity

In this chapter, we have investigated the effect of non-uniformity of particulate conductivity on electrorheological properties by blending particles with different conductivity. We find that there is a significant dip in the shear stress under an electric field as the concentration of higher conductivity particles is increased, showing that uniformity of the electrical properties among the particles is a most important factor in achieving optimum ERF performance. We also propose dielectric measurement as an effective method to estimate conductive uniformity of dispersed particles in suspension.

4.1 Introduction

An electrorheological fluid (ERF) is a suspension of solid particles in an insulating solvent, which shows a dramatic increase in shear stress upon application of an electric field. This type of reversible, controllable rheological response has potential application in tunable vibration dampers for example, and presently much work is being carried out toward device development [55].

In order to realize use in such devices, ERF's must satisfy the two conditions of large shear increase and low electric power consumption under electric fields. In this chapter we investigate the effect on these ERF properties of mixing ERF particles of different conductivity. We also present a method by which this non-uniformity can be quantified through dielectric measurements.

There has recently been much work investigating the effects of electrical conductivity on

the behavior of ERF. The calculations of Chen [16], Davis [23], and Foulc [31] show that the inter-particle forces can be well described by the mismatch in particle-solvent conductivities under steady electric fields. See and Saito [64] have applied this idea to calculations of the layered model of ERF under shear. Experimentally, Gow and Zukoski [35] have investigated the relationship between particle conductivity and ERF response. However, up to now, there have been no reports on how the performance of the ERF is affected by non-uniformity of electrical properties among the particles. One possible reason could be that it has been difficult to obtain a base system of a well-characterized, homogeneous particle suspension that shows a reasonable ERF response.

In this chapter we describe a novel set of experiments we have carried out using Bridgestone's carbonaceous ERF particles where we blend differing amounts of base particles and higher conductivity particles, and observe the effects on the electrorheological properties. In the following, we outline the samples used and the experimental techniques to measure the field-induced shear stress increment and the electrical properties. We then describe our results, and follow this with a discussion and conclusion.

4.2 Experiments

4.2.1 Materials

As base ERF particles, we used the anhydrous carbonaceous particles described in Chapter 2. ERF made by suspending these particles in a carrier oil shows a large increase in shear stress under the application of an electric field, and the electronic nature of the polarization gives the fluid a wide range of operating temperature.

In this experiment, the particles are suspended in a high-insulation silicone oil manufactured by Toshiba Silicone Co Ltd (Japan) (details are described in Chapter 2).

We blend with these base ERF particles controlled amounts of higher conductivity carbonaceous particles, which have the same size distribution and density. The ratio of conductivities is approximately 10, that is

$$\frac{\sigma_h}{\sigma_b} \sim 10 \tag{4.1}$$

Table. 4.1: Blends of base and high conductivity ERF particles.

Blend No.	Proportion of base ERF particles (%)	Proportion of high conductivity particles (%)
1	100	0
2	95	5
3	90	10
4	80	20
5	70	30
6	50	50
7	20	80
8	0	100

where σ_h refers to the high conductivity particle. ERF consisting only of these high conductivity particles shows a shear stress under an electric field larger than the base fluid, as well as an increased electric current.

During the blending process, these two types of particles are thoroughly mixed to achieve macroscopic uniformity. The volume fractions of the base particles and high conductivity particles, written as ϕ_b and ϕ_h respectively, are such that the total particle volume fraction ϕ_{tot} remains constant at 30%:

$$\phi_b + \phi_h = 0.3 \tag{4.2}$$

Therefore the no-field viscosity of the fluid should be essentially constant.

Eight blends were made as in Table **4.1**, including a suspension with only base particles and one with only high conductivity particles.

4.2.2 Dielectric permittivity measurements

In our model system we know that the ratio of the conductivities is given by eq. (4.1), but in most practical ERF systems the distribution of particle conductivities is not clear. A simple and efficient way to estimate conductivity distribution is from dielectric permittivity measurement, which is a widely used way of characterizing ERFs.

The details of methods to estimate the electrical properties of dispersed particles by dielectric measurements are described in Chapter 2.

From these measurements, we could obtain the frequency dependence of the real and imaginary components of the relative dielectric permittivity, ϵ' and ϵ''. The curves for the 100/0, 50/50 and 0/100 suspensions are plotted in FIG. **4.1** (a) - (c). Clearly, the 50/50 blended suspension has a broad distribution of dielectric response.

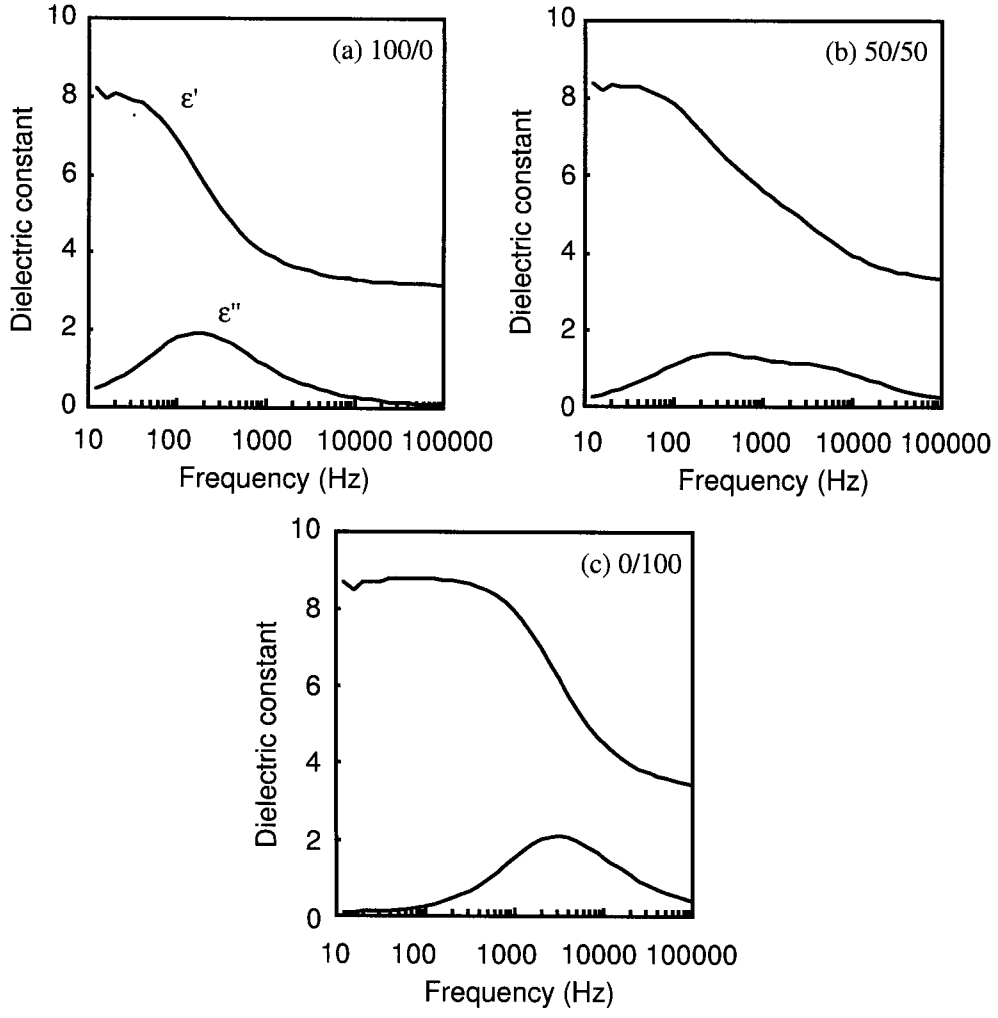

FIG. 4.1: The variation of the suspension dielectric permittivities ϵ' , ϵ'' (relative to vacuum) with the applied ac field frequency f. (a) 100% base particle suspension (100/0), (b) 50/50 blend of base and high conductivity particles, and (c) 100% high conductivity suspension (0/100).

4.2.3 Rheological measurements

The details of measuring conditions of rheological properties of ERFs are described in Chapter 2. In these experiments, a constant electric field of $2kV/mm$ was used. FIG. **4.2** shows the variation of shear stress as a function of shear rate for the 100/0 and 80/20 suspensions, under zero electric field and $2kV/mm$ field. Under the electric field, both fluids clearly show the Bingham

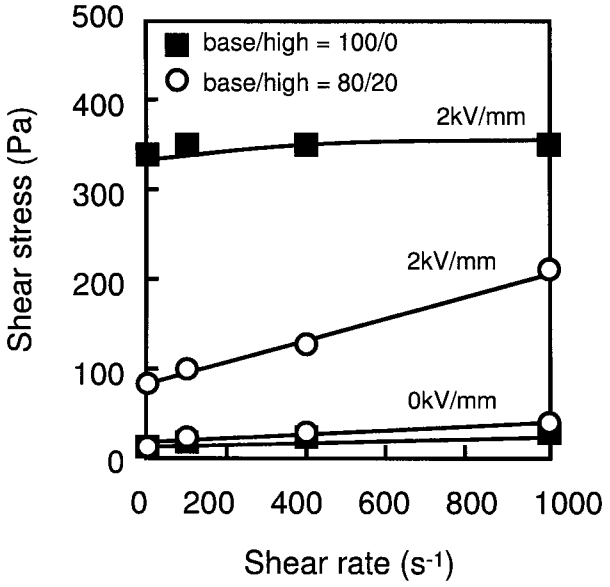

FIG. 4.2: Variation of shear stress with shear rate for 100% base particle suspension (100/0) and 80/20 blend suspension, under no electric field and dc electric field of $2kV/mm$.

fluid type behavior characteristic of ERFs. The variation of shear stress at $100s^{-1}$ shear rate for the eight suspensions is shown in FIG. **4.3**, as a function of concentration of high conductivity particles.

Simultaneously with the shear stress measurements, electric current is measured. The dependence of average electric current on the concentration of high conductivity particles is plotted in FIG. **4.4**.

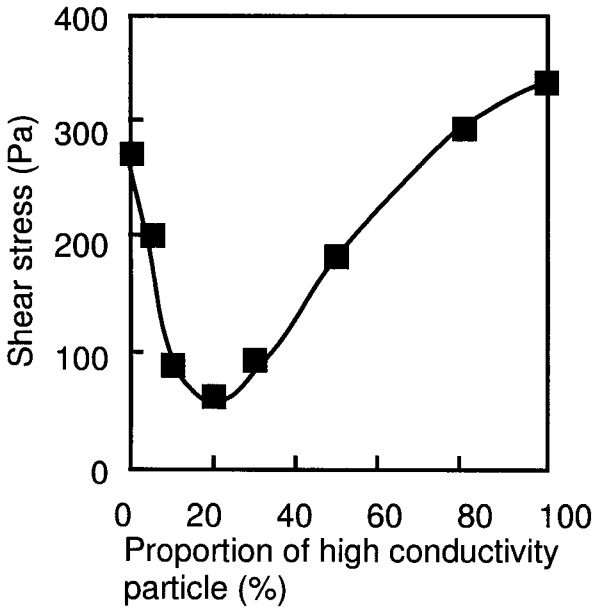

FIG. 4.3: Variation of shear stress with proportion of high conductivity particle, under constant shear rate of $100s^{-1}$ and dc electric field of $2kV/mm$.

4.3 Results and discussion

We now discuss these results of the dielectric and rheological measurements, and propose a simple model for the observed behavior.

FIG. **4.1** clearly shows that the 50/50 blended suspension has the broadest distribution of dielectric properties. To express the broadness of the distribution, we will use the approach of the Cole-Cole expression that is described in Chapter 2.

Assuming that the applied field is weak enough so we can ignore interactions between the particles, τ(relaxation time) can be written as $\tau = n_b\tau_b + n_h\tau_h$, where n_b, n_h are the volume weights of the two particle types, and $\tau_b = \frac{2\epsilon_s+\epsilon_b}{2\sigma_s+\sigma_b}$, $\tau_h = \frac{2\epsilon_s+\epsilon_h}{2\sigma_s+\sigma_h}$, with ϵ_s, σ_s the relative dielectric permittivity and conductivity of the solvent.

The empirical parameter α appearing in eq. (2.6) varies between 0 and 1, and describes the broadening of the relaxation region. $\alpha = 0$ corresponds to the ideal case of the single relaxation time Debye-type response for dilute suspensions of uniform conducting spheres (see Chapter 2).

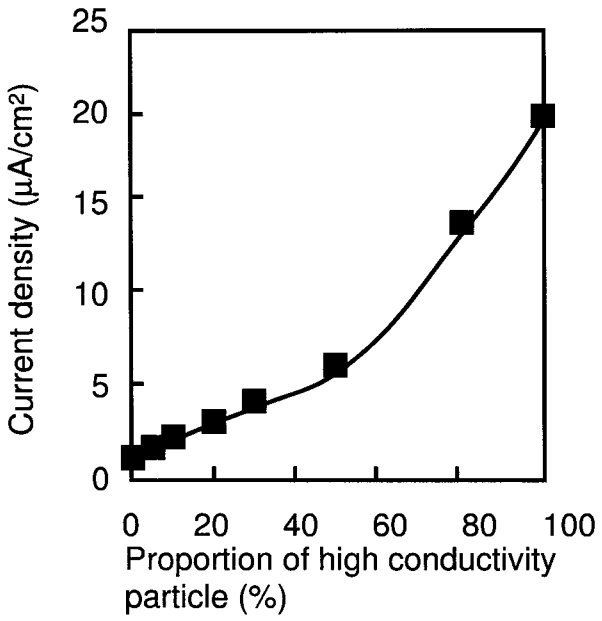

FIG. 4.4: Variation of electric current density with proportion of high conductivity particle, under constant shear rate of $100s^{-1}$ and dc electric field of $2kV/mm$.

In general, eq. (2.6) can be solved for α, giving the following formula :

$$\alpha = 1 - \frac{4}{\pi} tan^{-1} \left(\frac{2\epsilon''_{max}}{\epsilon_{st} - \epsilon_{\infty}} \right) \tag{4.3}$$

where ϵ''_{max} is the maximum value of the curve ϵ'' (see FIG. **2.6**). Thus α can be easily determined from the experimental measurements of dielectric permittivity. In the blended suspensions we are considering here it is the particle conductivity which is being varied, so α provides a measure of the broadness of the conductivity distribution.

In FIG. **4.5**, we show the dependence of α on the concentration of high conductivity particles for the eight suspensions, obtained from the dielectric measurements.

As expected, the system which has the highest degree of non-uniformity in dielectric response is the 50/50 blend, corresponding to a value of $\alpha = 0.35$. Note that both the 100/0 and 0/100 suspensions (only base ERF particles or only high conductivity particles) yield a value of $\alpha = 0.15$, indicating that a small degree of non-uniformity in the dielectric properties exist even in these systems. Clearly α is a reasonably accurate and convenient measure of the state of blending of the

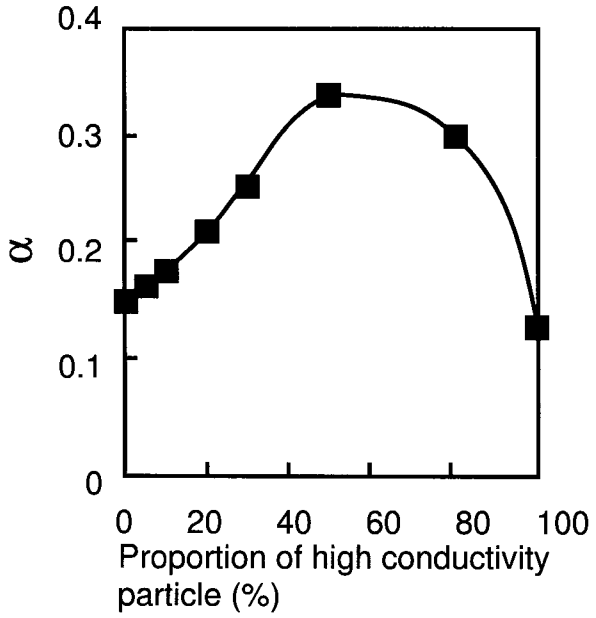

FIG. 4.5: Variation of the broadness parameter α of the dielectric response (eqs. (2.6), (4.3)) with the proportion of high conductivity particle.

suspensions.

We now turn to the measurement of shear stress in FIG. **4.3**. The curve does not follow a "linear law of mixtures" rule as we may expect, but shows a distinct dip in the field-induced shear stress, with the minimum occurring at 20% proportion of high conductivity particle.

A possible reason for this decrease in shear stress is illustrated schematically in FIG. **4.6**. We assume that the field-induced shear stress is due to thick columns of particles spanning the electrodes under the action of the electrical dipole-dipole interactions [17, 33, 36, 44]. Under the action of the shear flow, these columns perpetually undergo a process of rupture, reattachment, and rearrangement of the particle configuration within the column. Fast rearrangement of the structure is necessary to achieve a favorable column configuration which can provide a large resistance to shear. When a high conductivity particle is present, the enhanced dipole-dipole interactions mean that the electrical forces attaching it to the surrounding base particles are typically larger than the forces between the base particles [16], and so a small cluster of particles will tend to remain

attached to the high conductivity particle during the shear deformation process (FIG. **4.6**). This cluster will behave as one large entity during the deformation of the column, and will prevent the column from realizing a favorable configuration of particles for effective stress transfer. Thus there is a decrease in the measured shear stress. If the concentration ϕ_h of high conductivity particles increases so that these clusters begin to overlap with each other, this weakening effect will diminish and the shear stress will start to increase.

Notice that this model can explain why the dip occurs at lower values of ϕ_h, since only a small number of high conductivity particles would be needed to induce this effect. In the opposite case of an ERF formed from blending a small amount of base particles with high conductivity particles, we conjecture that there would be a minor weakening of the columnar structure due to the reduction in dipole-dipole interactions near the base particle. This correlates with the measured small drop in shear stress. We should add that this proposed mechanism for the dip is still very speculative, and that other explanations are possible. For example, the calculations of Bonnecaze and Brady (1992) [12] show that the Bingham yield stress is inversely proportional to the strain at which the chains rupture, and applying this result to our system it could be argued that the high conductivity particles are causing an increase in the critical breaking strain of the chains. A dip in the yield stress under small strains when particles of different size are mixed in chains has been found in the calculations of Ota and Miyamoto (1994) [56], but we do not believe that this mechanism is operative in this case, since we have taken care to ensure that the particle size distribution for all the suspensions is similar.

We carry out some theoretical calculations based on our model of the effect of conductive uniformity in order to verify our speculation in Chapter 5.

The electric current in FIG. **4.4**, on the other hand, shows a monotonic increase with ϕ_h, which merely reflects the changes in overall system conductivity. This tells us that the variation in shear stress is not due to some dramatic phenomena such as dielectric breakdown, but can be explained by a simple mechanical model like the one above, based on considerations of the interparticle forces. More information on the nature of the mechanism could perhaps be gained if experiments were to be carried out at different total volume fractions ϕ_{tot} and they should be

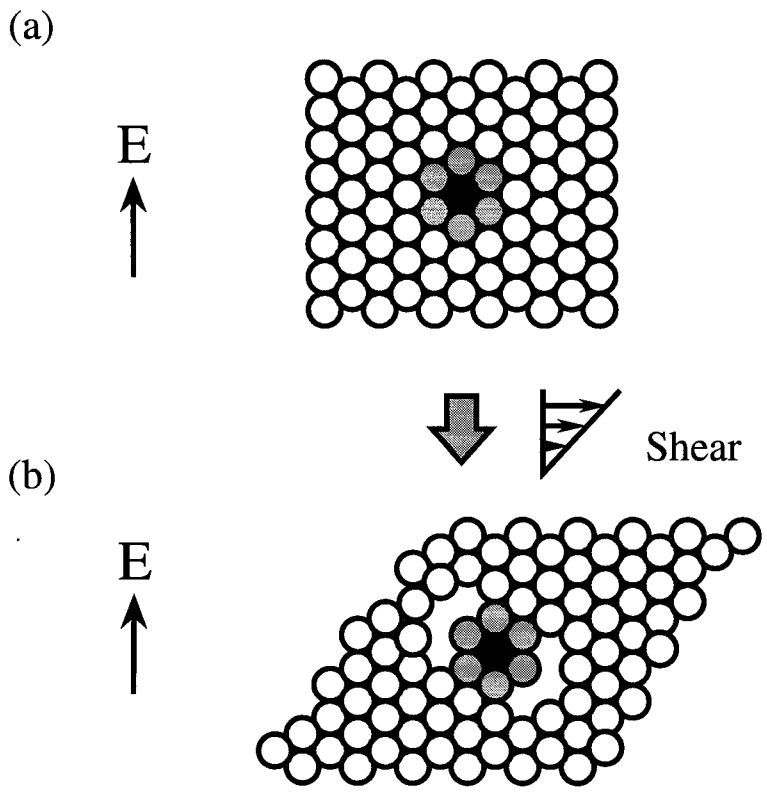

FIG. 4.6: Diagram of conjectured behavior under shear deformation when a high conductivity particle (black central particle) is present in the stress-bearing column. The enhanced dipole-dipole interaction in the vicinity of this particle creates a small "cluster" which hinders the particle re-arrangement to the optimum stress-transferring structure, leading to a reduction in measured shear stress.

done in our future works.

We thus see that it most important to have uniformity of electrical properties among ERF particles to achieve the maximum shear stress under an electric field. We also see that a clear indicator of this degree of uniformity is the α parameter of the Cole-Cole expression, which can be easily obtained from dielectric permittivity measurements on the fluid.

4.4 Conclusion

We have examined the effects of blending ERF particles of different conductivity. We have seen that the presence of a small amount of high conductivity particles leads to a dramatic decrease

in field-induced shear stress. However, as the proportion of high conductivity particles is raised, the shear stress will increase and approach the value for the pure suspension of high conductivity particles. We qualitatively explain the reduction in shear stress by a simple model that is based on the formation of particle clusters around the high conductivity particles due to the enhanced electrical forces. These clusters prevent the columns from taking the optimum configuration for stress transfer during shearing deformation.

The conclusion of this chapter is summarized as follows;

- **In order to achieve the optimum performance of ERF suspensions, it is essential to have uniformity in the particle electrical characteristics.**
- **Measurements of dielectric permittivity of these blended suspensions show that the α parameter of the Cole-Cole expression is an ideal way to express the degree of non-uniformity of the electrical properties among the particles.**

Chapter 5.

Mechanism of the Dip in Shear Stress of Blended Electrorheological Fluids

In Chapter 4, it was shown by a set of experiments that there should be minimal difference in the conductivities of the constituent particles, in order to obtain higher ER performance. Thus, the conductive uniformity of ER particles is one of the most important factors that dominate ER properties. In this chapter we carry out some theoretical calculations based on the model proposed in Chapter 4 of the effect of conductive uniformity .

5.1 Introduction

In Chapter 4, we investigated experimentally the effect on the rheological properties of blending ERF particles of different conductivity, using a suspension of carbonaceous ERF particles in silicone oil manufactured by Bridgestone Corporation, under dc electric field of $2kV/mm$ and a shear rate of $366s^{-1}$. We found that in a system of fixed overall concentration, as we increased the proportion of high conductivity particles there is a dramatic drop in the shear stress induced by the electric field. However, as we further increase the proportion of high conductivity particles, the shear stress will rise and eventually approach the value corresponding to the ERF system with only high conductivity particles. This behavior is shown schematically in FIG. **5.1**. The position of the dip ($\frac{\phi^*_h}{\phi_{tot}}$) was found to be at 20% proportion of high conductivity particle, and the magnitude of the dip ($\frac{\Delta\tau}{\tau_0}$) was 75%. These results are important because they show us that the linear law of mixtures will not hold for blended systems, even though the electrorheological effect is known to

be more pronounced with higher particle conductivities.

As a possible explanation of this behavior we postulated that there are "rigid" clusters of particles adhering to each high conductivity particle due to the strong electrostatic interactions. When the fluid is placed under shear flow this cluster will not deform affinely with the rest of the material, thus preventing the column of particles from achieving the optimum configuration for stress transfer. In Chapter 4 we propose a simple physical model of this concept, and confirm that reasonable qualitative agreement with experiment is obtained.

There have been recently many works treating the effect of particle conduction on ERF behavior, both theoretical [16, 23, 31] and experimental [35]. However, perhaps because of the lack of a suitable electrically homogeneous particle dispersion to act as a base ERF system, our study is the only work to date studying the important practical problem of blending ERF particles of different conductivity, and there have been no theoretical models presented to explain the observed behavior.

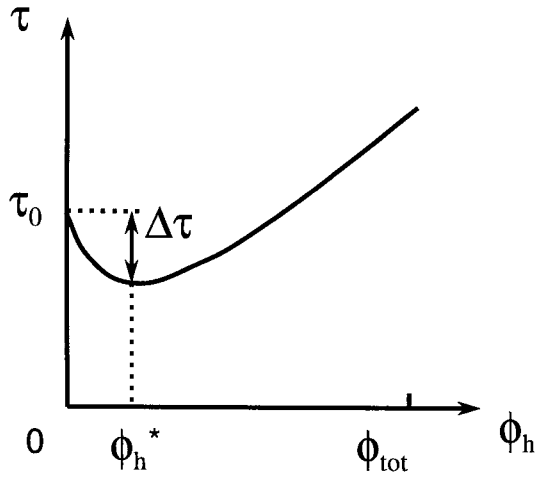

FIG. 5.1: Schematic sketch of the variation of shear stress τ of a blended electrorheological fluid under dc electric field and constant shear rate, as a function of volume fraction ϕ_h of high conductivity particle. The overall suspension volume fraction is ϕ_{tot}.

In this chapter, we present a model considering the effects that a "rigid" cluster of particles

adhering to a high conductivity particle will have on the electrorheological properties. In particular we will examine the changes in the stress transfer and deformation characteristics of the particle column spanning the electrodes. In the section of "Model", we describe the basic model we will use, and in the section of "Calculations" we consider from an electrostatic energy viewpoint the process of deforming a column of particles in which a cluster is imbedded. We find that "cavities" will tend to form in the columns and we estimate the resulting decrease in shear stress. As the concentration of high conductivity particles is increased we use the concept of a percolating chain of overlapping clusters to explain the rise in shear stress. In the section of "Discussion", we present a brief discussion of the results, and we give a conclusion in final section.

5.2 Model

5.2.1 The ERF Suspension

FIG. **5.2** is schematic sketch of the model we use for a blended system of high and low conductivity ERF particles suspended in a carrier liquid.

All the ERF particles are assumed to be spheres of radius a. The base particles have electrical conductivity σ_b and volume fraction ϕ_b. The higher conductivity particles have conductivity σ_h and volume fraction ϕ_h, and typically $\frac{\sigma_h}{\sigma_b} \approx 10$. We will ignore sedimentation effects.

As in the experiments, the total volume fraction of particles ϕ_{tot} is kept constant at 30% (see Chapter 4):

$$\phi_{tot} = \phi_b + \phi_h = 0.3 \tag{5.1}$$

ϕ_b, ϕ_h are varied from 0 to ϕ_{tot}, but always satisfying eq. (5.1) for every sample.

Regarding the carrier liquid, we assume it is a leaky dielectric (nearly insulating) with electric conductivity σ_s and relative dielectric permittivity ϵ_s, and viscosity η_s. We have of course $\sigma_b >> \sigma_s$.

To this suspension of blended ERF particles we apply an external dc electric field E_0. For simplicity, we assume that the field is uniform through electrode gap. At steady state, this electric field induces a dipole in each particle, due to the difference in conductivities between the particle

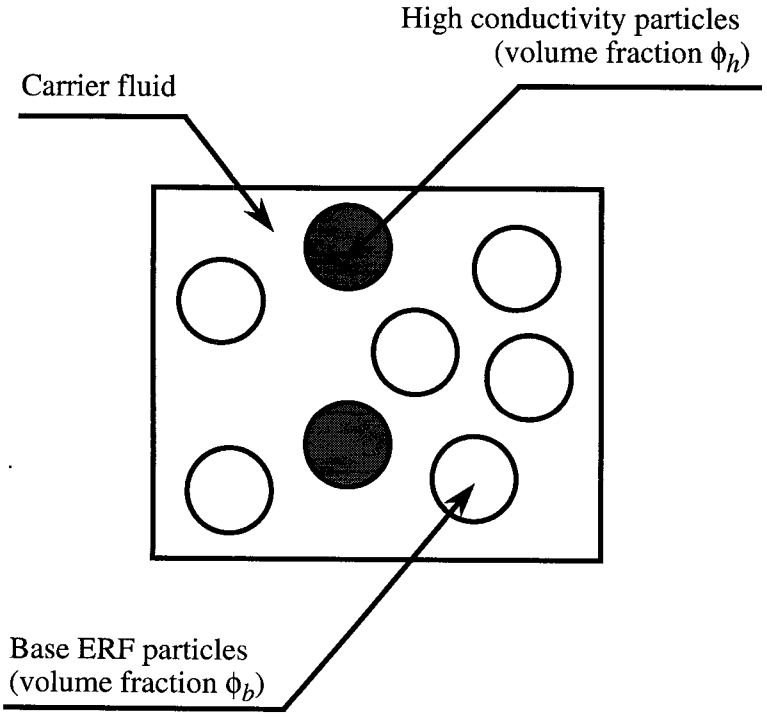

FIG. 5.2: Sketch of a blended suspension of ERF particles.

material and the carrier liquid (see Chapter 1). For the simplest case of an isolated particle, the dipole moment is parallel to the electric field and its magnitude is (for a base particle):

$$p_b = 4\pi\epsilon_s\epsilon_0\beta_{bs}a^3E_0 \tag{5.2}$$

where β_{bs} is the conductivity mismatch factor given by

$$\beta_{bs} = \frac{\sigma_b - \sigma_s}{\sigma_b + 2\sigma_s} \tag{5.3}$$

The dipole p_h induced in a high conductivity particle is given by a similar equation to eq. (5.2), but with σ_h for the particle conductivity in the expression for the conductivity mismatch factor eq. (5.3) (here β_{hs}).

The interactions between the induced electric dipoles will cause the particles to aggregate, with a preference for attachment in the direction of the electric field. To the lowest level of ap-

proximation, the dipole-dipole interaction energy U_{ij} between two particles i and j with separation vector r_{ij} is given by the following equation [80]:

$$U_{ij} = -p_i \cdot T_{ij} \cdot p_j \tag{5.4}$$

where T_{ij} is the dipole-dipole interaction tensor

$$T_{ij} = \frac{1}{4\pi\epsilon_s\epsilon_0 r_{ij}^3}\left(\frac{3r_{ij}r_{ij}}{r_{ij}^2} - I\right) \tag{5.5}$$

The interaction force F_{ij} is given by

$$F_{ij} = -\frac{\partial U_{ij}}{\partial r_{ij}} \tag{5.6}$$

Actually when particles are close there are multipole and multibody effects which significantly strengthen the interactions between the particles [12, 16, 23, 84].

Due to these dipole-dipole interactions, there will eventually form thick columns of particles between the electrodes. These are generally believed to be the reason for the increase in shear stress under shear flow [8, 17, 36]. This picture is valid for low to moderate shear rates, and for high shear rate (e.g. higher than $\sim 1000s^{-1}$), it has been proposed that a "layered" model of ERF structure is a more realistic representation [64, 84]. In this chapter we will focus on lower shear rates (e.g. $< 1000s^{-1}$), under strong electric fields and so will use the column model as our foundation.

5.2.2 The clusters around high conductivity particles

We now consider the physical reason for the "clusters" that form around the high conductivity particles.

As has been shown by several calculations which take into account the multipole and multibody effects [12, 16, 23, 84] the induced electrostatic interactions between spherical particles depend strongly on the degree of mismatch of the electrical properties between the particles and the solvent. Thus, in our present system, the attractive force between a high conductivity particle and a base particle would be much stronger than that between a pair of base particles. Therefore we

would expect that, when we externally deform a column of particles, there will appear a cluster of base particles adhering to each high conductivity particle, which will tend to behave as a single "rigid" entity while the surrounding material undergoes deformation, as illustrated in FIG. **5.3**.

This cluster will not undergo the affine deformation that that particular part of the column would have undergone in the completely uniform case.

We will take a phenomenological approach in this chapter, and will model this cluster as a sphere of radius $r_{cluster}$:

$$r_{cluster} = \alpha\beta_{bh}a \tag{5.7}$$

Here α is a dimensionless factor which would depend on the degree of conductivity mismatch β_{bh}, as well as the electric field E_0. Chen *et al.* [16] estimate the relationship between particle-particle force and particle-particle distance. They say particle-particle force becomes very small when $\alpha > 2$. So we can estimate that $\alpha \approx 2$.

Finally we note that in this chapter we will refer to this rigid entity in a column as a "cluster".

5.3 Calculations

5.3.1 Cavity formation

In this section we will show that under shear flow conditions, cavities will form around the clusters in the columns, reducing the stress transfer ability of the material. We will use an argument based on the two competing effects of the "elastic" energy cost $\Delta U_{elastic}$ of a column deforming near an imbedded cluster, and the "surface energy" energy cost ΔU_{cavity} of a cavity forming around a cluster in a column. Both of these energy concepts arise from the electrostatic energy of the system. There have been several works treating ERF from the point of view of energy, including electric field induced phase transition [72], energy changes during aggregation [48], and energy of structures under shear deformation [12, 39].

When considering these energy arguments, we should note that strictly speaking, there will also be Joule heating due to the electric current. However, the magnitude of this is estimated to

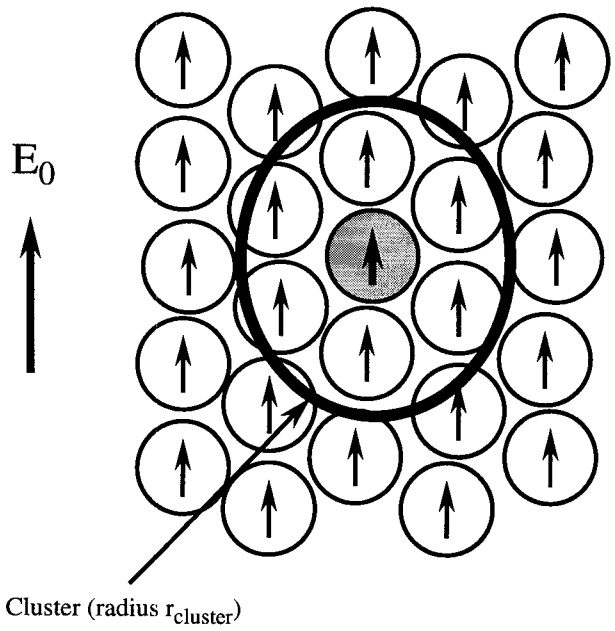

FIG. 5.3: The "rigid cluster " of particles adhering to the central high conductivity particle within a column due to the enhanced electrostatic forces under the electric field E_0. Arrows indicate magnitude of polarization.

be very small (typically the power density will be $\sim 0.01 W/cm^3$ under $2kV/mm$ field), and there is no noticeable rise in temperature of the ERF at the end of the $30s$ measurement. In this chapter we will take a continuum mechanics approach and treat the bulk of the column as a continuous medium.

Firstly, we consider the columns and the distribution of the clusters in them. Consider a system where columns have formed across the electrodes, as in FIG. **5.4** (a).

The electrode gap is written as h and the width of each column is r_{col}. The average number of clusters per column is

$$n_{clusters} \sim \frac{\phi_h}{\phi_b}\left(\frac{hr_{col}^2}{a^3}\right) \tag{5.8}$$

(In this chapter we will present mostly scaling arguments with the numerical coefficients removed, and will use the symbol $\sim$ in the equations). Assuming the clusters are uniformly distributed

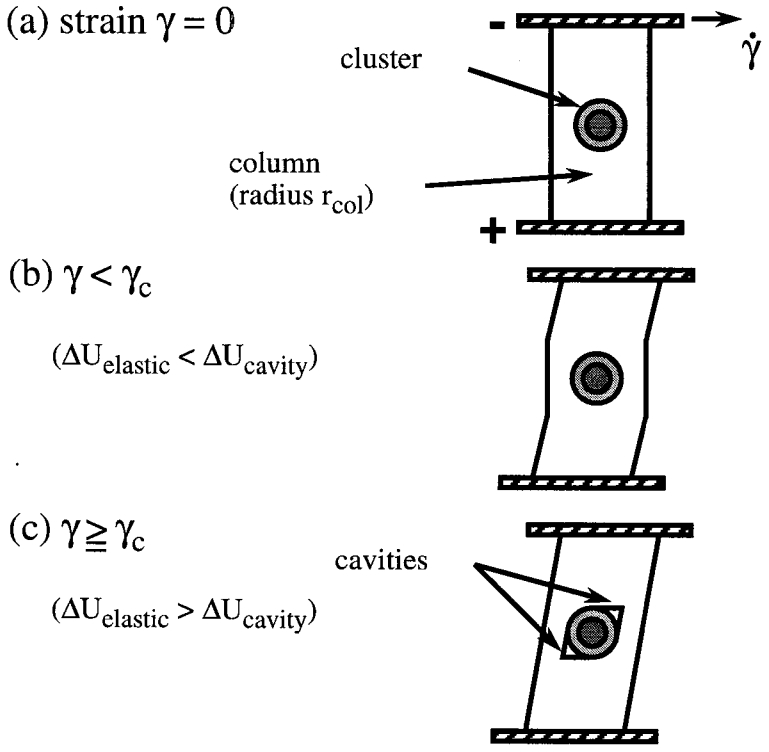

FIG. 5.4: The formation of the "cavity" around a cluster within a column under shearing deformation. Beginning with the configuration in (a), under small shear strain γ the column locally deforms around the cluster ((b)), until the cavity becomes energetically favorable at larger strains $\gamma > \gamma_c$ ((c)). After the cavity is formed the column's capacity to transfer stress is significantly reduced.

within the columns, the average distance between clusters in a column is

$$r_{av} \sim \left[\frac{hr_{col}^2}{n_{clusters}}\right]^{\frac{1}{3}} \tag{5.9}$$

Substituting eq. (5.8) into eq. (5.9) yields

$$r_{av} \sim a\left(\frac{\phi_b}{\phi_h}\right)^{\frac{1}{3}} \tag{5.10}$$

Now let us consider the "elastic" energy cost $\Delta U_{elastic}$ of a column deforming around an imbedded cluster. Let us assume that the top electrode is displaced slightly by a small strain γ

as shown in FIG. **5.4** (b). In this configuration, the column will have a base electrostatic energy which can be treated as a type of elastic energy [5, 24, 39], and we now consider the increment in the energy due to the extra deformation caused by the presence of the cluster. In the spirit of the previous calculations, we will model the column material between the electrodes as an "elastic body" with an "elastic modulus" Y determined by the interparticle forces between the base particles:

$$Y \sim \beta_{bs}^2 E_0^2 \tag{5.11}$$

However, due to the presence of the "rigid" clusters, the column must locally deform its preferred affine deformation to go around the clusters, as indicated in FIG. **5.4** (b). The extra elastic strain energy per column volume due to these local disturbances is

$$\Delta U_{elastic} \sim n_{clusters} \tau_{elastic} \Delta\gamma \tag{5.12}$$

Here $\Delta\gamma$ is the extra strain (in addition to the externally applied affine strain γ) caused by the disturbances due to the clusters. $\tau_{elastic}$ is the characteristic elastic stress in the column.

From simple geometrical considerations, $\Delta\gamma$ can be approximated by

$$\Delta\gamma \sim \frac{r_{clusters}}{r_{av}}\gamma \tag{5.13}$$

and $\tau_{elastic}$ can be estimated by

$$\tau_{elastic} = Y\gamma \sim \beta_{bs}^2 E_0^2 \gamma \tag{5.14}$$

Substituting eqs. (5.7), (5.10), (5.13) and (5.14) into eq. (5.12) gives us

$$\Delta U_{elastic} \sim \alpha\beta_{bh}\beta_{bs}^2 E_0^2 \left(\frac{\phi_h}{\phi_b}\right)^{\frac{4}{3}} \left(\frac{h r_{col}^2}{a^3}\right) \gamma^2 \tag{5.15}$$

Recall that this quantity $\Delta U_{elastic}$ is the extra energy cost of maintaining the configuration in FIG. **5.4** (b); that is, the extra elastic strain energy due to the disturbances caused by the clusters.

We now further increase the strain γ and when it exceeds a certain critical value γ_c (calculated later) a cavity will form around the cluster (FIG. **5.4** (c)), since the total energy of this configuration will become lower.

We now consider the "surface energy" energy cost ΔU_{cavity} of a cavity forming around a cluster in a column. Recalling that the column will have a base electrostatic energy, we now consider the increment in the energy due to the formation of the "cavity" and the newly created interface between the carrier liquid and the ERF particles. The modeling of ERF particle aggregate surfaces by a surface energy deriving from the electrostatics has been discussed and calculated in detail by Toor and Halsey [73], Davis [25], Toor [74] and Clercx and Bossis [19].

The magnitude of the surface energy S per surface area [24] at the interface between the carrier liquid and particle aggregate is

$$S = \beta_{bs}^2 E_0^2 a \tag{5.16}$$

The surface area A_{cavity} of the cavity formed will be approximately equal to

$$A_{cavity} \sim r_{cluster} w \tag{5.17}$$

Here w is the width of the strip of particles peeled off to form the cavity. We assume that w is of the order of several a.

Thus the extra surface energy ΔU_{cavity} due to these cavities per column volume V_{col} is

$$\Delta U_{cavity} = \frac{n_{clusters} S A_{cavity}}{V_{col}} \tag{5.18}$$

Substituting eqs. (5.8), (5.16) and (5.17) into eq. (5.18), we obtain

$$\Delta U_{cavity} = \frac{\phi_h}{\phi_b} \left(\frac{h r_{col}^2}{a^3} \right) \beta_{bs}^2 E_0^2 a r_{cluster} w \frac{1}{h r_{col}^2} \sim \frac{\phi_h}{\phi_b} \beta_{bs}^2 E_0^2 \alpha \beta_{bh} \tag{5.19}$$

Let us now compare these two competing processes, by considering the ratio of the energy costs of the two configurations (FIG. **5.4** (b) versus FIG. **5.4** (c)) :

$$\frac{\Delta U_{cavity}}{\Delta U_{elastic}} \sim \left(\frac{\phi_b}{\phi_h}\right)^{\frac{1}{3}} \left(\frac{a^3}{hr_{col}^2}\right) \frac{1}{\gamma^2} \tag{5.20}$$

We substitute the typical values $\frac{\phi_b}{\phi_h} \sim 10$ and $h \sim 100a$. We also note from the simulations of column formation reported by Toor [74] that $r_{col} \sim 10a$, indicating that we can estimate $\frac{a^3}{hr_{col}^2} \sim 10^{-4}$. If we now consider the critical state of cavity formation and set $\frac{\Delta U_{cavity}}{\Delta U_{elastic}} \approx 1$, eq. (5.20) gives us for the critical strain

$$\gamma_c \sim 10^{-\frac{11}{6}} \tag{5.21}$$

which is a very small strain indeed. So we would expect cavities to form in ERF's under steady or oscillatory shear unless the shear strain is extremely small.

Thus under constant shear conditions, we see that there will be a strong tendency for cavities to form in blended systems, and the shear transfer strength of the columns will be consequently reduced.

5.3.2 Decrease in shear stress at low ϕ_h

Here we consider the physical mechanisms for the reduction of shear stress with small amounts of high conductivity particles, due to these cavities. We model the decrease in shear stress by modifying a model often used in ceramics to estimate the effect of air pores on ceramic mechanical strength.

First of all we note that the presence of the cavities in the columns will reduce the ability of the column to transfer shear stress. There are a number of possible mechanisms for this:

(a) The maximum stress that a column will be able to transfer will be reduced since there would be a weakening of the dipole-dipole interactions through the cross section of the column containing the cavity. This is because of the reduction of the multibody reinforcing effect of the polarized particles in close proximity.

(b) Since the maximum stress of the column is reduced, there will also be a reduction of the critical strain at which the column will rupture. Thus these columns will spend less time on

average participating in stress transfer compared to columns without cavities (i.e. the uniform particle case).

As ϕ_h is increased, we would expect both of these effects to be more pronounced and consequently a larger reduction in stress transfer through the ERF.

We now quantify this reduction in shear stress with increasing ϕ_h. One approach would be to base our calculations on the theoretical microscopic model proposed by Ahlquist [6] and Gilman [34], which relates the mechanical strength of crystalline solids to the dislocation concentration. This model is also based on considerations of electrostatic energy. However here we will modify and use a different model, which has been widely used to explain the mechanical properties of ceramics. This model relates the mechanical strength of ceramics to the amount of air cavities present [9, 20, 69], the essential idea being that the cavities will accelerate crack propagation and so reduce the overall strength of the material.

We should note of course that there are significant differences between the fracture of a ceramic, and the deformation and rupture of a column of ERF particles, the most obvious difference being the brittleness of the ceramic material as opposed to the fluidic nature of the ERF aggregates. Nevertheless, we believe that the basic physical picture of a material containing cavities under mechanical stress, is still applicable when we consider the instantaneous strength of a column of ERF particles. We will also make the reasonable assumption that this reduced strength of the columns will translate directly to reduced shear stress of the ERF. Thus, using the model of the air cavities in ceramics [9, 20, 69], we can write for the reduction in shear stress $\frac{\Delta\tau}{\tau_0}$:

$$\frac{\Delta\tau}{\tau_0} = 1 - exp(-k\phi_{cavities}) \tag{5.22}$$

Here $\phi_{cavities}$ is the volume fraction of cavities in the column (with respect to volume of column). k is a numerical constant, which is approximately $k \approx 5$ from the results of Spriggs [69]. If cavities exist in ceramics of original modulus of H_0, its shear modulus H is obtained as $H = H_0 exp(-k\phi_{cavity})$ under the fabrication technique.

Using this value of k and an experimentally typical value of $\frac{\phi_h^*}{\phi_{tot}} = 0.2$, we find from eq. (5.22) after a simple calculation

$$\frac{\Delta\tau}{\tau_0} = 0.5 \tag{5.23}$$

which is of similar magnitude as the dip curve measured experimentally. We thus see that although eq. (5.22) was originally developed for modeling the effect of air cavities on ceramic mechanical properties, it also appears to provide a reasonable picture for the reduction in shear stress of the ERF due to cavities as ϕ_h is increased.

We now move on to consider what happens at the bottom of the "dip" (i.e. the minimum of shear stress). The essential idea is that when ϕ_h increases, a "slip layer" will form with most column breakages occurring in a shearing layer predominantly occupied with cavities. That is, at this value of ϕ_h, there are enough cavities to almost occupy a shearing layer at some height through the columns. Since there are mostly cavities in this slip layer, re-attachment of columns and their reformation to the optimum configuration for stress transfer will be impeded.

We will now estimate the volume fraction ϕ_h at which this slip layer will form. As shown in FIG. **5.5**, we would expect a slip layer when there is a planar region parallel to the electrodes of height of order $r_{cluster}$ in which almost all columns would have a cavity. Clearly, from simple geometrical considerations, this will occur when the distance between cluster centres r_{av} within a column is of the order $r_{cluster}$. So we set

$$r_{av} \approx r_{cluster} \tag{5.24}$$

Using eqs. (5.7), (5.10) and substituting typical values($\alpha = 2$ and $\beta_{bh} = 0.75$) gives us $\frac{\phi_h}{\phi_{tot}} \sim 0.22$ for the slip layer to form. This is of the correct order of magnitude for the dip position.

Here in FIG. **5.4** and FIG. **5.5**, only one cluster is shown for brief consideration of the effect of one cluster on the column. Actually there exist a large number of clusters in one column randomly distributed, but each cluster is expected to be in a situation as depicted in FIG. **5.4** and FIG. **5.5**.

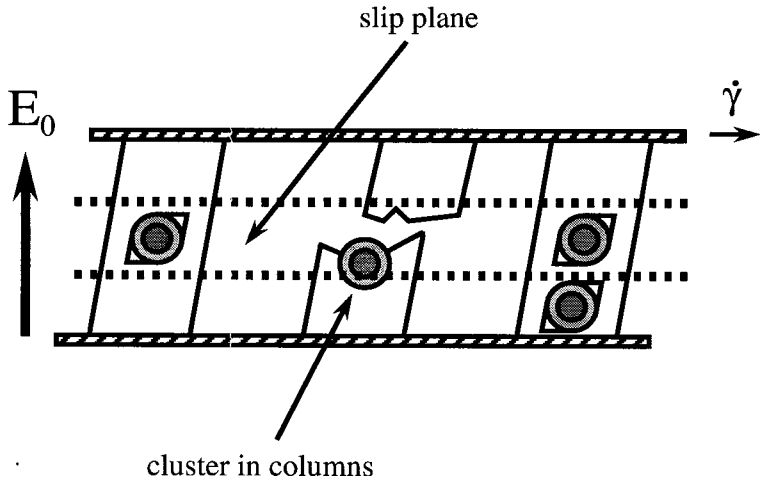

FIG. 5.5: The formation of the "slip plane" when cavities predominantly occur in one shear plane through the columns. The ability of the fluid to transfer shear stress is minimal when this occurs, and this corresponds to the volume fraction ϕ_h^* in FIG. **5.1**.

5.3.3 Increase in shear stress at higher ϕ_h : Percolation of clusters

We now propose a model for the increase in the shear stress above a certain value of ϕ_h (i.e. the reason for the dip). The basic idea is that for higher values of ϕ_h we will get percolation of clusters through a column which will lead to increasing strength (FIG. **5.6** (a)). Thus the columns achieve larger stress transfer and consequently have a larger strain at rupture, leading to increased overall shear stress. Note that this model is also able to explain the continuous increase of shear stress with larger ϕ_h.

To check that this model qualitatively agrees with experiment, we will estimate the volume fraction ϕ_h^{perc} at which the percolation of clusters will occur. It is known from percolation analysis [63] that the threshold volume fraction for percolation ϕ_{sphere}^{perc} for a system of randomly placed spheres is

$$\phi_{sphere}^{perc} \approx 0.15 \tag{5.25}$$

Although eq. (5.25) is for infinite (or near-infinite) systems, let us use this result to estimate

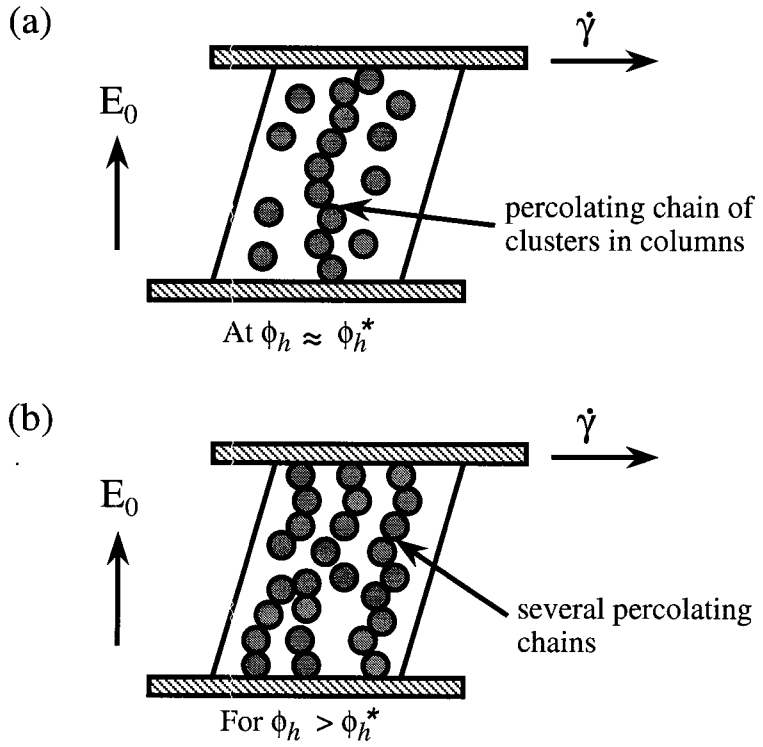

FIG. 5.6: With increasing volume fraction ϕ_h of high conductivity particles, a percolating chain of overlapping clusters will form and the shear stress transferred will rise ((a)). As ϕ_h is further increased, more percolating clusters are formed and the shear stress continuously rises to the value of the suspension with only high conductivity particles ((b)).

ϕ_h^{perc} by considering the percolation of clusters in a column. Noting that the clusters' volume fraction inside the column is given by the total volume of the clusters ($\sim n_{clusters} r_{cluster}^3$) divided by the column's total volume ($\sim h r_{col}^2$), and using eqs. (5.7), (5.8) with (5.25), we have

$$\frac{\phi_h^{perc}}{\phi_b} \alpha^3 \beta_{bh}^3 \approx 0.15 \tag{5.26}$$

This is the volume fraction at which the clusters will form a percolating chain through the column. Note that for the strengthening effect of the percolating clusters, we will require that there be some overlap between the clusters, which indicates we set $\alpha \approx 2$. Substituting other typical values into eq. (5.26) yields $\frac{\phi_h^{perc}}{\phi_{tot}} = \frac{\phi_h^*}{\phi_{tot}} \approx 0.05$. This figure is somewhat lower than the figure of $\frac{\phi_h^*}{\phi_{tot}} \approx 0.2$

measured in our experiments, but may be the best we can expect from such a crude model. Here we estimate the distribution of clusters at the dip position of ϕ_h/ϕ_b. The calculated volume fraction of clusters in the column is 68% for $\frac{\phi_h}{\phi_{tot}} = 0.2$, which is of the expected magnitude. We also should keep in mind that we are assuming only that the dip position will scale as the percolation threshold, and that there need not be precise quantitative agreement. Nevertheless, this idea of percolation of the clusters leading to stronger columns is able to neatly explain the position of the dip in shear stress at lower volume fractions ϕ_h.

As ϕ_h is further increased, more of these percolating chains of clusters will form, leading naturally to stronger columns (FIG. **5.6** (b)). Thus there will be a smooth transition to the state with all high conductivity particles.

Note that in this model the volume fraction of particles for the dip is assumed to depend on the ratio of σ_h/σ_b, since $r_{cluster}$ will vary with σ_h/σ_b. For example, when σ_h/σ_b is relatively large, $r_{cluster}$ will be larger and the volume fraction for the dip will be smaller. Thus we expect the position of the dip will not be symmetric with respect to the proportion of high and low conductivity particles. The relationship between the dip position and σ_h/σ_b will be studied in more detail in a future work.

5.4 Discussion

We have seen that this model, based on cavity formation at low ϕ_h and percolation of clusters at high ϕ_h in the columns of ERF particles, is able to explain the dip in shear stress in blended systems which has been measured experimentally. Let us now discuss the experimental conditions under which this model would be applicable.

Firstly, we should note we have been assuming strong electric fields and low to moderate shear rates. In terms of the non-dimensional quantity the Mason number ($Mn = \frac{\eta\dot{\gamma}}{2\epsilon_s\epsilon_0{\beta_{bs}}^2E_0^2}$) used by many researchers (see for example the review of Zukoski [86]), we are considering the low Mn regime. We require the electric field effects to be strong to ensure that thick columns of particles will form between the electrodes, as has been confirmed by computer simulations [74].

We now consider the effect of increasing the shear rate. If we were to keep the electric field

constant and raise the shear rate, the system will undergo a transition to a "layered " structure, with solid layers of particles adhering to the electrodes and a free-flowing layer in the center where all the flow is concentrated [44, 64]. It has been confirmed that even within the framework of this "layered " structure model, the dip in shear stress for blended suspensions can be explained. Thus the concept of columns is not essential for the understanding of this dip behavior. However, we should also keep in mind that as we increase the shear rate, we are increasing the plastic viscosity contribution of the shear stress. If we recall that the rheological response of ERF is usually modeled as a Bingham fluid, we would expect the relative magnitude of the dip to decrease with shear rate since the dip is essentially due to the induced dipole interactions between the particles, corresponding to the Bingham yield stress contribution.

5.5 Conclusion

We have proposed a simple model to explain the "dip" in electric field induced shear stress when ERF particles of differing conductivity are blended.

The essential idea is the rigid "clusters" of particles forming around each high conductivity particle, due to the enhanced electrostatic forces, which prevent affine deformation of the columns under shear deformation. At low concentrations of high conductivity particles, considerations of elastic versus surface energies (both of which arise from the electrostatic interaction forces), show that a cavity will form around each cluster, which will severely weaken the column and thus the stress transfer. We find that this effect can be quantified by modifying the model often used for the effect of air cavities in ceramics. The minimum of the shear stress dip is thought to correspond to the formation of a slip zone predominantly containing cavities in a single shearing plane.

The reason for the increase in shear stress as the concentration of high conductivity material is further raised is well explained by the formation of a percolating chain of clusters in the columns between the electrodes. These chains will increase the stress transfer capability of the columns. Further increase in concentration will cause the formation of even more percolating chains, increasing the strength even further, until it approaches the value of the ERF composed of only high conductivity particles.

The degree of uniformity of electrical properties of ERF particles is of great practical importance. This chapter has attempted to clarify the mechanism of the dip in shear stress in blended suspensions.

Chapter 6.

Effect of Conductive Fragments on Electrorheological Properties

We have shown the uniformity of particle conductivity is a most important property for the improvement of ER performance. In the particle production process, some impurities may be present and these can worsen the inter-particle conductive uniformity and lead to the deterioration of the ER properties.

In this chapter, we investigate the effect of conductive fragments on electrorheological properties, which models the effect of high conductive impurities that may be inadvertently mixed in during the fluid preparation process.

6.1 Introduction

An important problem when developing electrorheological fluids or their devices is the degradation of fluid performance when extraneous conductive fragments find their way into the fluid. Examples would include conductive materials which enter the fluid through the manufacturing process, or metallic fragments coming from excessive wear of metallic parts in devices.

In this chapter, we examine through a controlled set of experiments the effect of adding small amounts of conductive carbon black powder to an ERF. We propose a model of "bouncing motion" of the carbon black powder between the electrodes to explain the observed behavior. We also show that the results of dielectric measurements reflect the presence of the conductive fragments.

There have been recently many works treating the effect of particle conduction on ERF behavior, both theoretical [16, 23, 31] and experiments [35]. However, perhaps because of the lack

of a suitable electrically homogeneous particle dispersion to act as a base ERF system, there have been to date no controlled studies on the effect of adding conductive fragments to an ERF.

In this chapter we describe a novel set of experiments we have carried out, using a suspension of Bridgestone's carbonaceous ERF particles, into which we disperse controlled amounts of conductive carbon black powder and observe the effects on the electrorheological properties. In the section of "Experiments", we describe the samples and the experimental techniques used to measure the field-induced shear stress increment and the electrical properties. We describe and discuss our results in the section of "Discussion", and give a conclusion in the final section.

6.2 Experiments

6.2.1 Materials

For our base ERF system, we used a dispersion of anhydrous carbonaceous particles (details are described in Chapter 2). ERF made by suspending these particles in a carrier oil shows a large increase in shear stress under the application of an electric field, and the electronic nature of the polarization gives the fluid a wide range of operating temperature.

For our base ERF system, we dispersed these particles in a high-insulation silicone oil (see Chapter 2). The volume fraction of the particles was 30%. We have confirmed that the resulting ERF displays a Bingham fluid-type response under an electric field with a large increase in viscosity.

Into this base ERF system we dispersed controlled amounts of conductive carbon black powder (trade name: "Toka black"), manufactured by Tokai Carbon Co. Ltd (Japan). This carbon black powder has an average size a_{cb} of $100nm$, and an electrical conductivity σ_{cb} of $10^{-1}S/m$. An automatic mortar grinder was used to ensure that the powder was well broken-up and evenly dispersed in the ERF.

The weight fraction of the carbon black powder was varied from 0% to 1.0%. The small change in total volume fraction of particulate (i.e. ERF particles + carbon black powder) was observed not to cause a significant change in the zero-field viscosity of the fluid.

6.2.2 Measurements

Steady shear measurements were made using a concentric sylinder rheometer (see Chapter 2). In these experiments, a constant dc electric field of $2kV/mm$ and shear rate of $366s^{-1}$ are applied. The variation of shear stress as a function of concentration of carbon black powder is shown in FIG. **6.1**. The reference value (no carbon black fragments) is $425Pa$.

Simultaneously with the shear stress measurements, electric current was measured. The dependence of average electric current on the concentration of carbon black powder is also plotted in FIG. **6.1**. The reference value (no carbon black fragments) is $8.9\mu A/cm^2$.

We also carried out measurements of the dielectric permittivity of the ERF suspension under quiescent conditions (details of measurement are described in Chapter 2). The real and imaginary components of the relative dielectric permittivity were used to calculate the α parameter of the Cole-Cole parameterization, which indicates the degree of non-uniformity of the electrical properties of the particulate material [77]. We found that α increases steadily from a value of 0.216 for the ERF with no carbon black powder to 0.231 for the 1.0% concentration system. This agrees with the results of our investigation of blended ERF particles of Chapter 4.

6.3 Discussion

We now discuss the results of the rheological and electric current measurements, and propose a simple model of "bouncing motion" of the conductive carbon black powder.

First, consider the measurement of field induced shear stress in FIG. **6.1**. The curve shows a definite decrease in shear stress as the concentration of carbon black powder is increased, reaching 18% of the original value.

We note that the large reduction in shear stress is clearly different to the variation of shear stress when ERF particles with different degrees of semi-conductiveness are blended, which was investigated in Chapter 4.

As a possible explanation of this behavior, it may be considered that the carbon black powder dispersed in the oil would raise the overall conductivity of the liquid surrounding the ERF particles. The increased conductivity of the liquid would weaken the dipole-dipole interactions

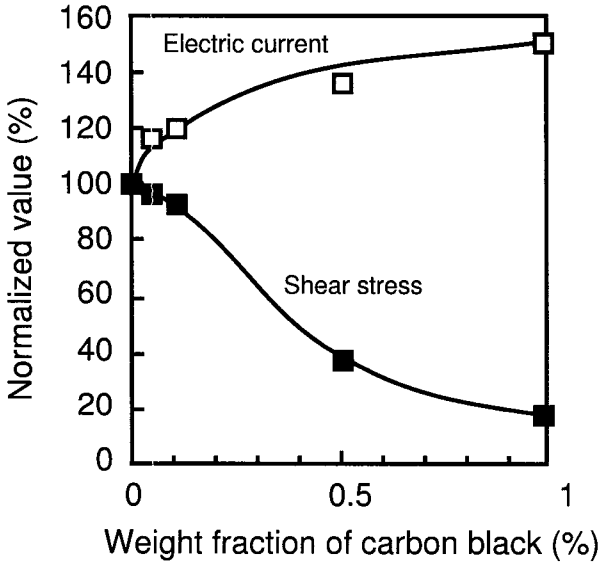

FIG. 6.1: The effect on shear stress and electric current density of adding conductive carbon black fragments to an ERF suspension. The electric field is $2kV/mm$ and the shear rate is $366s^{-1}$. The reference values for the shear stress and current density with no carbon black present are $425Pa$ and $8.9\mu A/cm^2$ respectively.

between the particles, which depend on the degree of conductivity mismatch between the particles and the oil, leading to a reduction in shear stress. However, this is essentially a static mechanism, similar to the increase in electrical conductivity of solid materials with the addition of filler particles [62]. In the present case of a liquid dispersion, we would expect a more dynamic process to be operative since the conductive particles are completely free to move under the high electric fields. We thus turn to a dynamic mechanism to explain the observed behavior.

We propose that the "bouncing motion" of the conductive carbon black powder between the electrodes gives a possible realistic picture of what is occurring in the system, and can explain many features of the changes in shear stress and electric current. We now outline this "bouncing motion" model.

A schematic diagram of "bouncing motion" is shown in FIG. **6.2**. The central concept is that a conductive fragment will become electrically charged when it comes in contact with an electrode,

and will then move under electrophoretic force across the electrode gap until it encounters the oppositely charged electrodes, where a transfer of charge takes place and the process is repeated. The result is that the conductive fragments will oscillate between the electrodes when an electric field is applied. Such behavior has been described in the literature [10, 28, 38, 47, 52, 54, 86], where rapid "oscillations" or "shuttling" of some particles have been observed microscopically. Across a $1mm$ electrode gap, the speed of this conductive particle oscillation under a $3kV/mm$ electric field was observed to be several Hz [52]. Buffman and Brignell [14] have reported similar behavior in their experiments on electrically stressed liquid dielectrics. We have also observed this behavior in the carbonaceous ERF particle systems when some conductive particulate is present. However, to date there have been no calculations of this effect or its influence on the electrorheological properties. Although very speculative, we present below a rough calculation of this phenomena. To simplify matters, we assume that a carbon black fragment can be approximated by a sphere

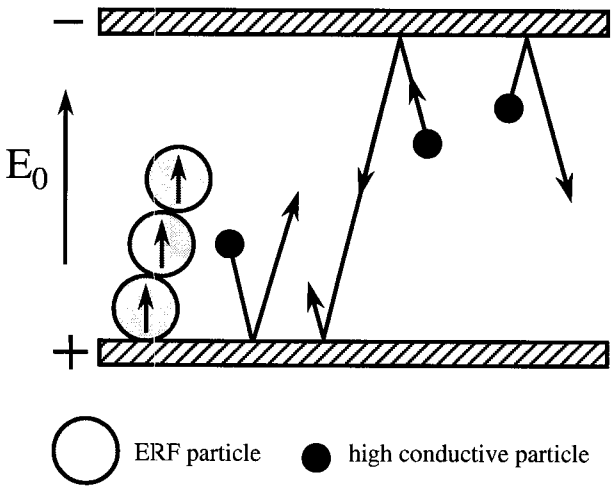

FIG. 6.2: Schematic diagram of "bouncing motion", which is the oscillatory motion of charged conductive fragments between the electrodes.

of diameter a_{cb}, and that the electrodes are planar conductors maintained at constant potential. We will also assume that the oil is an insulating liquid, and will ignore such effects as dielectric breakdown or electrochemical reactions at the electrode surface.

Now we examine the process of discharging and charging at an electrode as in FIG. **6.3**

(a) - (c). Consider a charged fragment approaching the electrode (FIG. **6.3** (a)) and making direct electrical contact with the electrode surface (FIG. **6.3** (b)). An electrical charge Q will be transferred to the fragment in order for the electrode and fragment to reach the same electrical potential:

$$Q = k_1 \epsilon_s \epsilon_0 a_{cb}^2 E_0 \tag{6.1}$$

Here the constant of proportionality $k_1 = 1.645\pi$ [29]. E_0 is the electric field in the electrode gap, and ϵ_0 is the permittivity of free space.

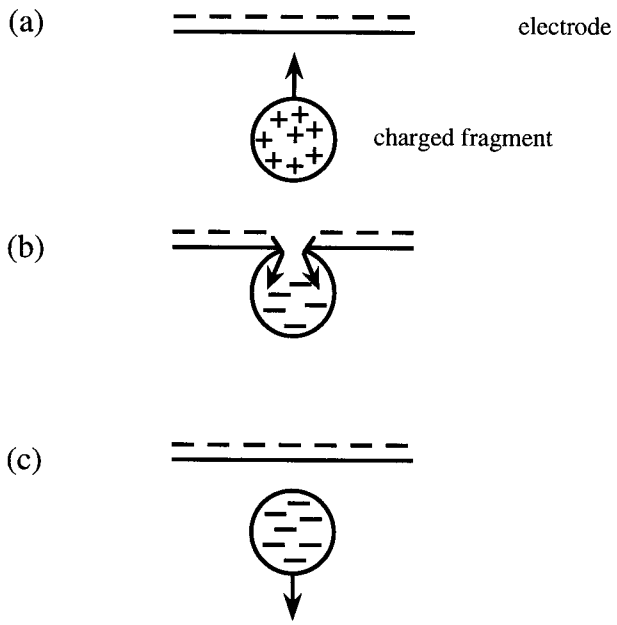

FIG. 6.3: A step-by-step account of "bouncing motion". (a) The charged conductive fragment is attracted to the oppositely charged electrode. (b) Electrical contact is made, and there is a transfer of charge until an equipotential condition is reached. (c) The particle is repelled from the electrode, moves under the electric field to the opposite electrode and the process is repeated.

Assuming that the fragment will stay attached until the charging process is completed, it will then experience a force repelling it from the electrode surface, since they both have the same

sign of charge (FIG. **6.3** (c)). The carbon black fragment will thus break away and move under the action of the electric field across the gap between the electrodes. The electrophoretic force F_{el} acting on the fragment is given by

$$F_{el} = QE_0 \tag{6.2}$$

Strictly speaking, once the fragment detaches from the electrode there will also be an electrostatic image force, acting to attract the fragment to the electrode again [64]. However, this force decreases inverse quadratically with distance from the electrode, and a simple estimate shows that the greatest magnitude of this force will be less than the constant electrophoretic force. We will therefore neglect the effects of the image force in this basic calculation.

As it moves through the oil, the fragment will also experience a drag force F_{drag}. We will use the free-draining Stoke's approximation, and assume F_{drag} is given by

$$F_{drag} = 3\pi a_{cb}\eta_s v \tag{6.3}$$

where v is the velocity of the fragment. Since the electrophoretic motion being considered is perpendicular to the shearing motion of the oil, we need not consider the effect of the shear flow in this equation of motion.

We will ignore the effects of Brownian motion of the fragments, which we justify by noting that the value of the characteristic "Brownian force" will scale as $F_{Brown} \sim kT/a_{cb}$ with k the Boltzmann constant, and T the absolute temperature [61]. Comparing this with the electrophoretic force F_{el} (eq. (6.2) with eq. (6.1)), we find by substituting $T = 300K$ and other characteristic values that $F_{Brown}/F_{el} \sim 10^{-2}$. Thus although the fragments will experience Brownian motion, their overall movement will be governed by the electrostatic force.

Thus the steady state velocity of the carbon black fragment as it moves across the electrode gap will be given by a force balance between F_{el} and F_{drag}:

$$F_{el} = F_{drag} \tag{6.4}$$

Thus from eq. (6.2) and eq. (6.3), we obtain for the velocity v:

$$v = 0.5483\frac{QE_0}{\eta_s a_{cb}} \tag{6.5}$$

Substituting eq. (6.1) into eq. (6.5) yields

$$v = k_2\frac{\epsilon_s\epsilon_0 a_{cb}}{\eta_s}E_0^2 \tag{6.6}$$

where $k_2 = 0.9020\pi$.

When the fragment reaches the opposite electrode, the process of charge transfer and subsequent movement across the electrode gap is repeated.

As a check, we can estimate from eq. (6.6) the typical time $\tau_{traverse}$ for a carbon black fragment to traverse a $1mm$ gap in the ERF system we are considering. Substituting the appropriate values from the experimental section, we find that $\tau_{traverse}$ is of the order of $0.1s$, in rough agreement with microscopic observations [52].

It is important to note that the oil also has a slight degree of conductivity and so the electric charge carried by the fragment will eventually be dissipated into the surrounding liquid. We expect the time scale for this dissipation τ_{diss} to scale as

$$\tau_{diss} \sim \frac{\epsilon_s\epsilon_0}{\sigma_s} \tag{6.7}$$

However, substituting into eq. (6.7) the same characteristic values yields $\tau_{diss} \sim 10s$, which is much longer than the characteristic "traverse time" $\tau_{traverse}$ estimated previously. Thus, we would expect the carbon black fragments to retain almost all of their electrical charge as they move across the electrode.

We thus see that this "bouncing motion" model gives a physically consistent picture of the behavior of the conductive carbon black fragments in ERF. We will now use this model to consider the effect of the fragments on electric current and shear stress of ERF systems. As a first approximation to estimate the electric current density j_{cb} due to the carbon black fragments, let us assume that all the fragments are equally participating in the "bouncing motion". Then the "electric current" i due to one particle can be written as

$$i \sim \frac{vQ}{h_0} \tag{6.8}$$

where h_0 is the electrode gap width. Here we will perform a scaling calculation, and so will drop numerical coefficients. Substituting eqs. (6.1), (6.6) into eq. (6.8) yields

$$i \sim \frac{(\epsilon_s \epsilon_0)^2 a_{cb}^3}{\eta_s h_0} E_0^3 \tag{6.9}$$

Therefore, the electric current density j_{cb} (per unit area of electrode) due to these carbon black fragments can be estimated by multiplying i (eq. (6.9)) by the average number of carbon black fragments under a unit area of electrode. A simple calculation yields

$$j_{cb} \sim \phi_{cb} \frac{(\epsilon_s \epsilon_0)^2}{\eta_s} E_0^3 \tag{6.10}$$

where ϕ_{cb} is the volume fraction of the carbon black fragments in the ERF.

As a check, letting $\phi_{cb} \sim 10^{-2}$ and substituting typical values in eq. (6.10), we find $j_{cb} \sim 0.1 \mu A/cm^2$. Although this result is somewhat smaller than the increase in current density observed in FIG. **6.1**, we should keep in mind that the average distance traversed by the fragments is much smaller than the electrode gap distance as has been assumed here, since the fragments will often oscillate between the protruding ERF particle agglomerates that have adhered to each electrode. Nevertheless, we see that the rough calculation above gives a physical picture that is not unreasonable.

An interesting feature of eq. (6.10) is that it predicts a cubic dependence on electric field for the current caused by the "bouncing motion". Further, the fact that the quantity a_{cb} does not appear in eq. (6.10) suggests that there could be only a weak dependence on fragment size of the current j_{cb}. These predictions could form the basis of future experimental investigations.

Turning to the effect of the conductive carbon black fragments on shear stress, we can speculate that the "bouncing motion" would make it more difficult for stable columns of ERF particles to form. It is thought that columns of ERF particles that span the electrodes are the main reason for the field induced shear resistance [17, 36], and so clearly "bouncing motion" would reduce the stress transfer ability of the fluid. This concept is illustrated schematically in FIG. **6.4**,

and is a possible reason for the reduction in shear stress as the concentration of carbon black is increased. This inability of columns of ERF particles to form due to "bouncing motion" could

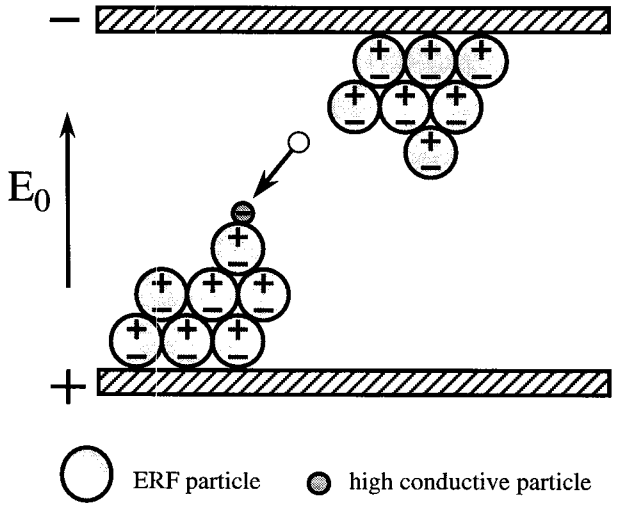

FIG. 6.4: Schematic diagram illustrating the effect on the shear stress of the ERF of conductive fragments undergoing "bouncing motion". The ERF particles will be prevented from making stable columns, leading to a reduction in the shear stress.

also explain why the stress reduction is much more than that expected from the blending of ERF particles.

Regarding the ERF particles, we would not expect these to undergo "bouncing motion" themselves for the following reasons. The ERF particles are made from semi-conducting material, so they would take more time to be charged compared to the carbon black fragments if in electrical contact with the electrodes. Their larger size means that they will be more susceptible to external flow forces detaching them from the electrode surface. Thus we would expect most ERF particles to not be significantly charged at the electrodes. Further, as has been pointed out previously [64], most operative ERF particles will possess a thin outer layer of lower conductive material. This outermost layer on the ERF particles will prevent direct contact with the electrodes, and so the requirement that the particle have the same electrical potential as the electrode, as was the case for the carbon black fragment (eq. (6.1)), is not applicable. We would expect this high resistance

gap to restrict the flow of current through the particle to a steady state, minimizing the occurrence of particle charging.

Finally we should add that recent computer simulations by Ota and Miyamoto [56] reveal that large disparities in the size of ERF particles can also cause a reduction in the yield stress of ERF. However, we feel that this mechanism would not be operative in the present case because the highly conductive nature of the carbon black fragments would prevent them from participating in stable column or chain configurations.

We thus see that this simple model based on the "bouncing motion" of conductive fragments in ERF, observations of which have been reported by several researchers, is able to explain many of the features of the increase in electric current and reduction in shear stress.

6.4 Conclusion

We have examined the effects of adding conductive carbon black powder to ERF. We observed a large reduction in the electric field-induced shear stress as the concentration of carbon black is increased to 1.0%, with an accompanying increase in the electric current. The degree of reduction in the shear stress is much larger than that due to broad distribution of particle conductivity as investigated in Chapter 4, and indicates that a different mechanism is operative.

We have thus proposed the "bouncing motion" model, where there is a transfer of charge by the carbon black fragments oscillating between the electrodes. We find that this model can explain the increase in the electric current with the addition of carbon black, as well as provide a reason for the dramatic reduction in shear stress.

The problem of degradation of ERF performance due to the introduction of extraneous conductive materials is of great practical importance. This chapter has aimed to clarify the effect of conductive fragments on electrorheological fluids.

Chapter 7.

Improvement of Electrorheological Properties by Optimizing Particle Preparing Process

In this chapter, we apply the knowledge of improving electrorheological properties gained in Chapter 3 and Chapter 4 to the process of particle preparation in order to optimize electrorheological performance.

7.1 Introduction

We have carried out a set of experiments to determine the effect of conductive uniformity on ER properties by blending particles with different conductivity in Chapter 4. These experiments showed that conductive uniformity is essential in order to achieve the optimum performance of ERF suspensions (higher ER effect at lower electric consumption). And we carried out some theoretical calculations of the effect of conductive uniformity in Chapter 5 and confirmed the importance of conductive uniformity for higher ER performance.

From these results we see that "**The conductive uniformity of ER particles is one of the most important factors that dominate ER properties and minimal difference in the inter-particle conductivity is essential for higher ER performance**".

One of the objectives of this thesis is the realization of improvement of ER properties for practical use. In this chapter, we describe attempts to obtain optimum ER particles by applying the above concepts to the particle preparing (carbonizing) process.

We clarify the problem of conventional carbonizing process from the relationship between the carbonizing conditions and ER properties and attempt to design a new process for higher ER

properties.

We have done experiments with layered particles shown in Chapter 3 for still higher ER performance.

In the section of "Experiments", we outline the used materials and experimental techniques to measure the ER properties and the electrical properties of carbonized particles. In the section of "Conventional particle carbonizing process", we discuss the property of particles obtained by conventional carbonizing process and clarify the problems of this process. In the section of "Ideal and practical particle carbonizing process", we design a heat treating process in order to carbonize particles more uniformly and evaluate the ER performance with the resulting particles. We then summarize our results in the section of "Conclusion".

7.2 Experiments

7.2.1 Materials

In this chapter we describe optimization of carbonizing process. For raw materials, we used layered particle (see Chapter 3) and we carbonized and dispersed these particles in a high-insulation silicone oil (see Chapter 2). The volume fraction of the particles was kept at 30%.

7.2.2 Steady shear measurements under an electric field

Steady shear measurements were made using a concentric sylinder rheometer. In these experiments, a constant dc electric field of $2kV/mm$ and shear rate of $366s^{-1}$ were applied. Simultaneously with the shear stress measurements, electric current was measured (measuring details are described in Chapter 2).

7.2.3 Dielectric permittivity measurements

We also carried out measurements of the dielectric permittivity of the ERF suspension under quiescent conditions (details of measurement are described in Chapter 2). The real and imaginary components of the relative dielectric permittivity were used to calculate the α parameter of the Cole-Cole parameterization, which indicates the degree of non-uniformity of the electrical

properties of the particulate material [21].

7.3 Conventional particle carbonizing process

7.3.1 Sample preparation

Conventional electric furnace for carbonizing particles is shown in FIG. **7.1**. All carbonizing experiments were performed under an inert atmosphere (we used Ar).

The amount of raw material that can be treated by this equipment is $10g$ at the most at one time, so this furnace can be considered as a small laboratory-scale equipment and is clearly unsuitable for mass production. The sample container is made of high heatproof material Al_2O_3. We set raw materials obtained by the process of Chapter 3 and carbonize them. FIG. **7.2** shows

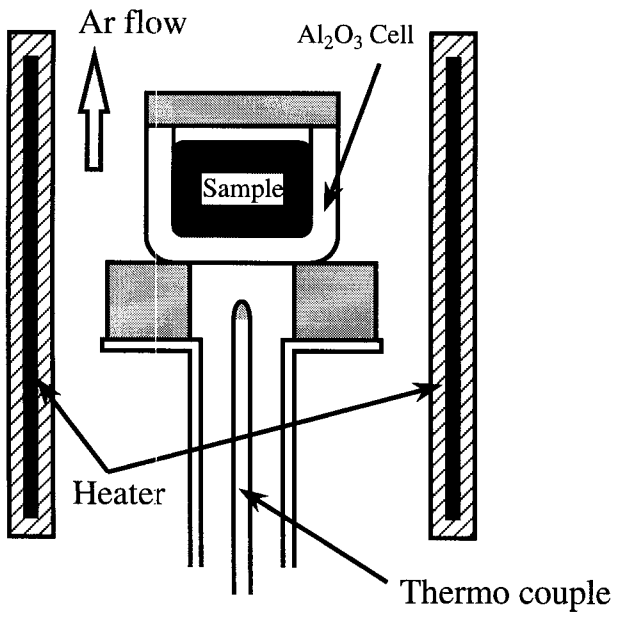

FIG. 7.1: Schematic diagram of conventional electric furnace.

the heat treatment pattern. First step; heat the container at constant rate $((T_h - R_T)/T_1)$ to the carbonizing temperature. Second step; keep the temperature for fixed carbonizing period $(T_2 - T_1)$. Third step; cool the container to the room temperature (R_T).

This laboratory-scale equipment can control the temperature very precisely and raise the

heating rate up to 20 ℃/*min* at the most.

In this chapter, we evaluate the relationship between particle preparation conditions (heating rate) and ER properties. We varied heating rate as 1, 5, 10, 15 and 20 ℃/*min*.

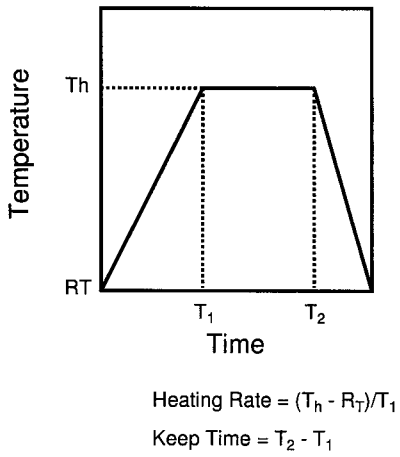

FIG. 7.2: Heat treatment pattern of electric furnace.

7.3.2 Results

FIG. **7.3** shows the variation of normalized ER properties as a function of heat treatment rate of particle preparation process. Measurements are done at $2kV/mm$ and $366s^{-1}$. This figure indicates that we can obtain higher ER performance (higher yield stress at lower electric consumption) with lower heating rate.

We can say that particle with lower heating rate is a more ideal particle.

Up to this time, there is no efficient index to clarify this kind of difference of ER performance by varying particle preparing conditions. Now we apply the technique of evaluating conductive uniformity with dielectric measurements and the consideration of effect of conductive uniformity on ER properties to this case.

That is to say, we combine the particle preparing conditions with inter-particle conductive uniformity and evaluate the relationship between the ER effect and inter-particle conductive uniformity with different preparing conditions.

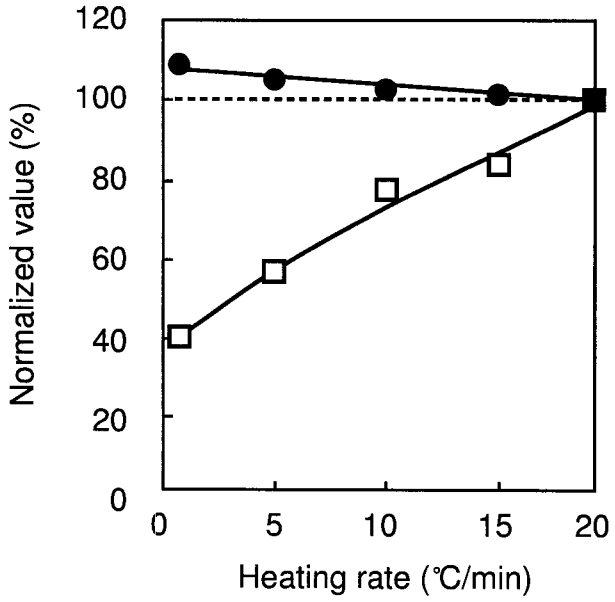

FIG. 7.3: Variation of ER properties as a function of heat treatment rate of particle preparing process: (•), relative shear stress change; (□), relative current density.

FIG. **7.4** shows the relationship between the broadness parameter α of the dielectric response and heat treatment rate of particle preparing process.

At higher heating rate, α is relatively large (i.e. it indicates that inter-particle conductivity is not uniform). We can hypothesise that this non-uniformity of particle conductivity derives from the difference of heat transmittivity between the center and the outer of the container. The temperature of the material in the central part of the container should be lower than that of the outer part, especially for the particles treated under the condition of relatively higher heating rate. On the other hand, at lower heating rate, there exists little difference in temperature between the central part and the outer part and all sample in the container treated equally. Consequently, at lower heating rate, inter-particle conductivity goes uniform and the empirical parameter α approaches to 0.

From these results with conventional carbonizing equipment, it is shown that in order to carbonize sample uniformly for higher ER performance, the heating rate should be lower for minimal

difference in the conductivities of the particles.

In the next section, we apply this knowledge to design an ideal equipment that can carbonize particles more uniformly.

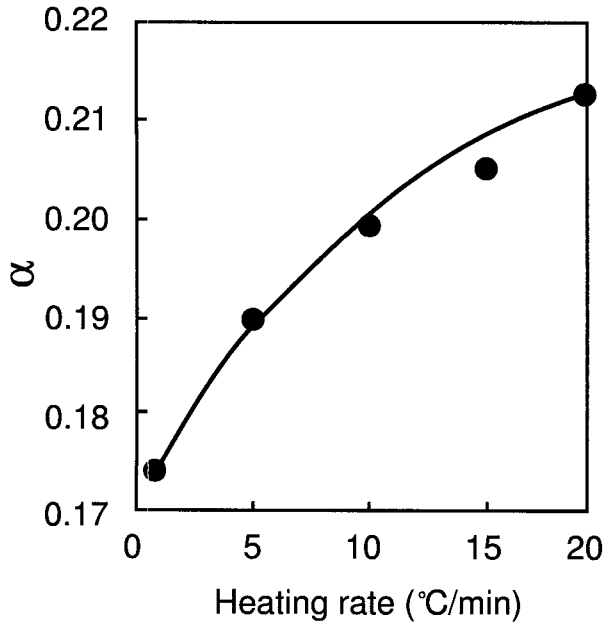

FIG. 7.4: Variation of the broadness parameter α of the dielectric response with heat treatment rate of particle preparing process.

7.4 Ideal and practical particle carbonizing process

7.4.1 Sample preparation

As we described above, we can expect higher ER performance with an equipment that can heat samples uniformly. One solution for uniform carbonization is heating at lower heating rate. But, clearly if we were to use a scaled-up version of the conventional furnace, the difference in temperature between the central and outer part of the container would be larger and the conductive uniformity of the particle is expected to become worse (the equipment we used in this thesis can treat $10g$ at the most).

Furthermore, the lower heating rate is not practical for mass production (e.g. it would take

$9hours$ to reach the carbonizing temperature of 550 ℃).

Here, we design a new type of electrical furnace for uniform carbonization and for larger scale treatment as shown in FIG. **7.5**. We can rotate the sample container and treat the sample uniformly at larger scale, and so this type of furnace we will refer to as a "Rotary Furnace".

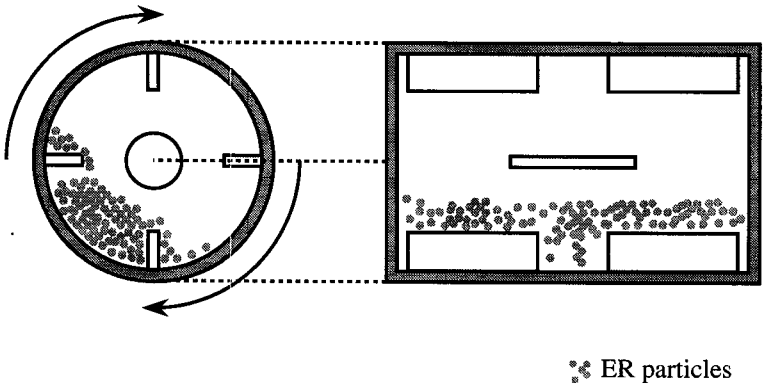

FIG. 7.5: Schematic diagram of rotary electric furnace.

The presence of the baffles in the container ensure that sample is stirred well as the container rotates and can undergo more uniform heat treatment.

7.4.2 Results

All carbonizing experiments were performed under an inert atmosphere (we used Ar). FIG. **7.6** shows the comparison of relationship between ER effect and current density with particles made by several process. It indicates that we can obtain higher ER effect at lower current density with particles made by "Rotary Furnace" than those with particles made by conventional equipment.

Now we check if the conductive uniformity of particles is improved or not with empirical parameter α obtained by dielectric measurements.

The calculated α from results of dielectric measurements are $0.11 \sim 0.12$. These values are smaller than $0.16 \sim 0.20$ obtained by conventional furnace.

From comparison of α, we can confirm that conductive uniformity of particles carbonized by rotary furnace is improved from that by conventional furnace. Consequently, ER performance

is enhanced with this improvement of inter-particle conductive uniformity.

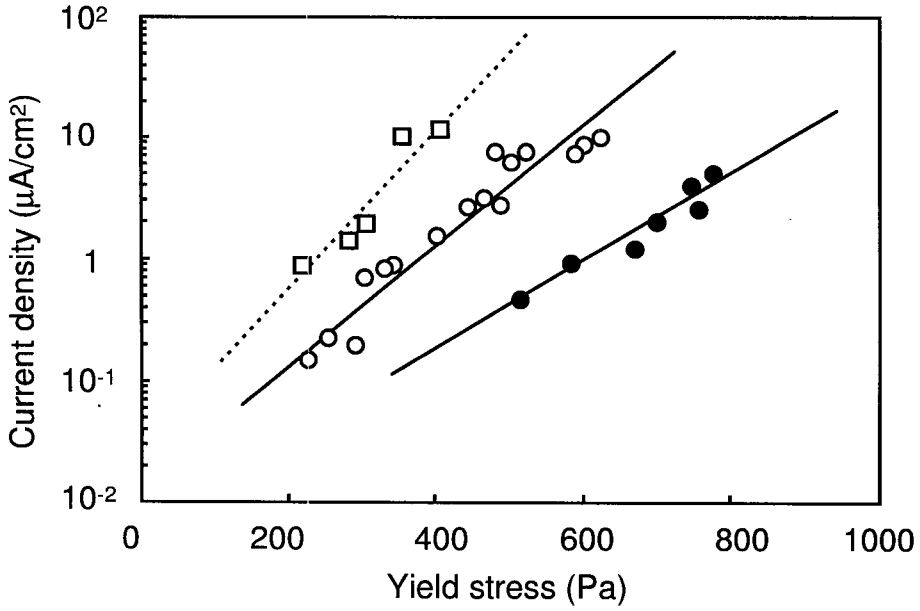

FIG. 7.6: Improvement of ER performance by optimizing heat treatment process: (□), homogeneous particle made by conventional process; (○), layered particle made by conventional process; (●), layered particle made by optimized process.

7.5 Conclusion

We optimize the particle preparation process using the knowledge obtained in previous chapters that conductive uniformity is important for higher ER performance.

It was confirmed that with conventional electrical furnace, particles obtained with conditions when heat treatment is carried out uniformly show higher ER performance, similar to the results of model experiments described in previous chapters.

From these results, we have designed a new type of rotary electrical furnace in order to heat samples uniformly, and we have confirmed that this furnace is possibly the suitable one for scaling up towards mass production.

We thus see that ERF showing performance at practical levels can be obtained by optimiza-

tion of the particle preparation process and by the use of layered particles.

Chapter 8.

Study on the Possibility of Using Elastomers as Electrorheological Material

In this chapter we have investigated the electrorheological properties of dispersions of particles in oils and elastomers. We focussed on how the dynamic mechanical properties measured under oscillatory shearing change with the viscosity of the oil or the elasticity of the elastomer. We find that there are parallels between the electrorheological behavior of particles dispersed in elastomers and the behavior of particles dispersed in oils. These results should find application in the selection of suitable matrix materials for electrorheological suspensions. We are able to verify the practical possibility of ER elastomers.

8.1 Introduction

One of the recurring problems of using ERF in devices such as active engine mounts, controllable shock absorbers, and clutches, is the sedimentation of the particles when the suspension is left undisturbed for long periods of time, leading to sluggish initial response as well as the possible formation of a solid cake-like layer of aggregated particles at the bottom of the vessel. Possible solutions to this problem include density matching of the solvent and the particulate, as well as the attachment of polymer layers on the particle surface to prevent irreversible flocculation, but both of these are only effective within a certain range of temperature. Another solution to the sedimentation problem is to disperse the particles in a elastomer (a synthetic rubber-like material). The solid-like nature of the elastomer would keep the particles suspended in place, but the particle-

particle interactions would cause changes in the overall mechanical properties of the material. The use of such an elastomer as the matrix has the additional advantage that the sealing of the material in devices is much easier to achieve, compared to liquid-state ERF. Since the elastomer is unable to flow continuously, we would expect that devices using this material would involve tuning the mechanical resistance over small displacements, such as a small stroke vibration isolation device. We will henceforth refer to this type of material as "ER Elastomer", and will use "ERF" to refer to the suspension of particles in a liquid solvent.

Despite its technological importance, there have been surprisingly few investigations of the electrorheological behavior of particles dispersed in a rubber-like matrix. Shiga *et al.* have investigated the linear viscoelasticity of dispersions of electrorheological particles in polymer gels [65, 66]. They applied very small sinusoidal deformations and focussed on the dependence of the mechanical properties on the electric field. They found that when an electric field of $5kV/mm$ was applied the storage modulus G' and loss modulus G'' increased by factors of 2.5 and 2.0 respectively, and the loss tangent decreased from 0.55 to 0.45 at $10Hz$. They also found that the minimum volume fraction required to produce this increment in G' and G'' was about 11%. This study did not investigate the effect of the elasticity of the original polymer gel used as the matrix. It also did not examine how the increment of the moduli under an electric field depended on the strain amplitude, which would be of much interest from a device development point of view.

There is thus still a practical need for an investigation of the behavior of ER elastomers. Further, a comparison of the mechanical properties of the ER elastomer with the corresponding ERF would help illuminate the basic mechanisms of the electrorheological effect and so would be of much interest from a fundamental viewpoint. In this chapter, we describe a series of experiments using similar semi-conducting particles dispersed in oils of different viscosity and elastomers of different elasticity. Particular attention was paid to how the dynamic mechanical response changed with the viscosity or elasticity of the matrix and the strain amplitude. While there have been numerous investigations of the dynamic behavior of ERF [7, 32, 45, 49, 57, 58, 78], there have been no reports, to the authors' knowledge, of experiments where one standard type of particle is dispersed in a range of elastomers and oils. We will see that we can interpret our results in terms of

the widely used particle polarization model, where the induced electric dipole-dipole interactions lead to changes in the overall mechanical properties of the material.

In the section of "Experiments", we describe the materials used and the experimental set-up. In the section of "Results and discussion", we present the results and discuss them, and show that the electric dipole interaction model is able to qualitatively explain the observed behavior of ERF and ER elastomers. Finally we will present our conclusions of this chapter.

8.2 Experiments

8.2.1 Materials

We use a system of carbonaceous electrorheological particles which have been treated to have a highly controlled level of conductivity as we described in Chapter 2. For the carrier liquid in the ERF, we used in these experiments silicone oils of viscosity $\eta = 9.4, 9.7 \times 10, 9.7 \times 10^2$ and $9.8 \times 10^3 mPa \cdot s$. The volume fraction of particles (ϕ) in the ERF was kept fixed at 30%. For the case of ERF, there are already detailed reports on the concentration dependence of the rheological properties [50], and so in this chapter we keep the volume fraction constant and focus on the effect of the oil viscosity.

For the investigations of ER elastomer, we used a high-insulation silicone elastomer manufactured by Shinetsu Silicone Co. Ltd. (Japan), which has an electrical conductivity of $10^{-14} mho/m$ at the most. The particles were mixed into the uncured elastomer material, and an automatic mortar grinder was used for at least $30 min$ to ensure that they were well dispersed in the matrix. The elastomer was then cured, with the moduli of the elastomer controlled by the curing temperature and time. This curing process is not expected to change the particle properties, in particular the electrical properties such as conductivity, since it has been shown that the particles do not undergo any permanent change if maintained for long times at temperatures of 100 ℃ [41]. Further, the particles will undergo negligible sedimentation during the curing process because the viscosity of the uncured elastomer is high ($\approx 1 Pa \cdot s$). The elastomer with the smallest shear elastic modulus used in the experiments ($= 1.0 \times 10^4 Pa$) was produced after curing at 100 ℃ for $10 min$, and the elastomer with the highest modulus ($= 1.5 \times 10^5 Pa$) was produced at 100 ℃ for $60 min$. The

volume fraction of the particles (ϕ) was 0%, 20%, 30%, 35%, 40% and 50% in the ER elastomer.

8.2.2 Steady shear stress measurements

The measurements of shear stress of ERF under shearing flow were performed in a Couette-type rheometer, manufactured by Rheometrics Inc. Details are described in Chapter 2.

8.2.3 Dynamic mechanical measurements

The dynamic mechanical measurements were performed using the same rheometer. For the ERF, the same Couette cell as the steady shear measurements was used. For the elastomer, however, a parallel plate geometry (plate radius $12.5mm$) was used since this had the advantages of easier sample loading and better adhesion between the sample and the walls. Since with parallel plates the strain varies with radius only an averaged torque response can be obtained, but this was found to adequately reflect the behavior of the material. A $1mm$ thick disc-shaped sample of the ER elastomer (radius $12.5mm$) was placed centrally between the plates as shown in FIG. **8.1**.

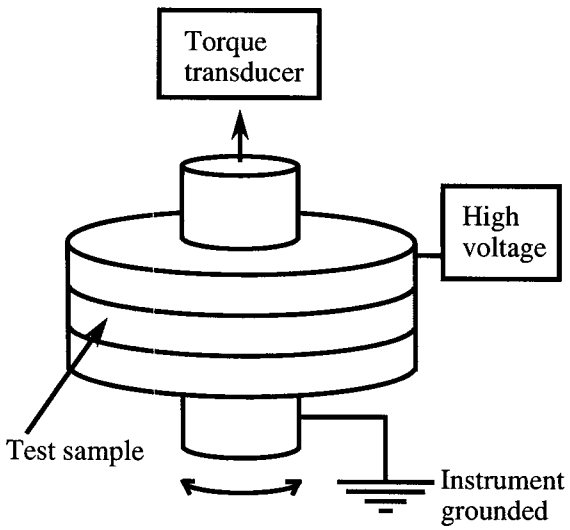

FIG. 8.1: Schematic of the ER material test fixture (Dynamic mechanical properties).

For the dynamic experiments a sinusoidal strain deformation was applied. Writing the strain as $\gamma(t) = \gamma_0 sin(\omega t)$, the stress response $\tau(t)$ was measured :

$$\tau(t) = \gamma_0 \left(G^{'}(\gamma_0) \sin(\omega t) + G^{''}(\gamma_0) \cos(\omega t) \right) \tag{8.1}$$

where $G^{'}(\gamma_0)$ and $G^{''}(\gamma_0)$ are the in-phase and 90 degree shifted components of the response. Note that in general these quantities were found to depend on the strain amplitude γ_0, so the material is not in the regime of linear viscoelasticity. For both the ERF and the ER elastomer measurements, γ_0 was varied from 0.003% to 1%. The frequency of the oscillation was kept fixed at $\omega = 100 rad/s$ (i.e. $15.9 Hz$) for all experiments, since in this chapter our main focus is on how the viscous or elastic properties of the matrix affect the response of the material at a particular frequency. The frequency $\omega = 100 rad/s$ was selected because it is typical of the vibration frequencies encountered in such applications as engine mounts for cars [76], and so has practical significance. The dependence of the behavior on the frequency introduces an extra complication since it is intricately connected with the dynamics of the electrorheological response, and the results of our investigations of this will be reported in the near future. Finally, we note that reasonable reproducibility of the results was confirmed for the dynamic measurements of both the ERF and ER elastomer systems.

8.3 Results and discussion

8.3.1 The effect of oil viscosity on yield stress and dynamic mechanical property of ERF

We first of all ascertain that the ERF used does indeed display electrorheological characteristics. FIG. **8.2** show typical flow curves of the ERF with and without the electric field. We can see that the material does follow the Bingham fluid model (eq. (1.1)), with a clear yield stress (defined here as the increment in the shear stress under an electric field, compared to the value at zero electric field).

We now focus on the effect of the oil viscosity on the yield stress. For definiteness, we will hereafter present the results for a shear rate of $100 s^{-1}$. FIG. **8.3** shows the variation of yield stress as a function of viscosity of oil, under $0.5 kV/mm$, $1.0 kV/mm$ and $2.0 kV/mm$ electric fields. We see that there is little dependence of the yield stress on oil viscosity under the higher electric fields of $1.0 kV/mm$ and $2.0 kV/mm$. However, under $0.5 kV/mm$ the yield stress shows a significant

decrease as the oil viscosity becomes large.

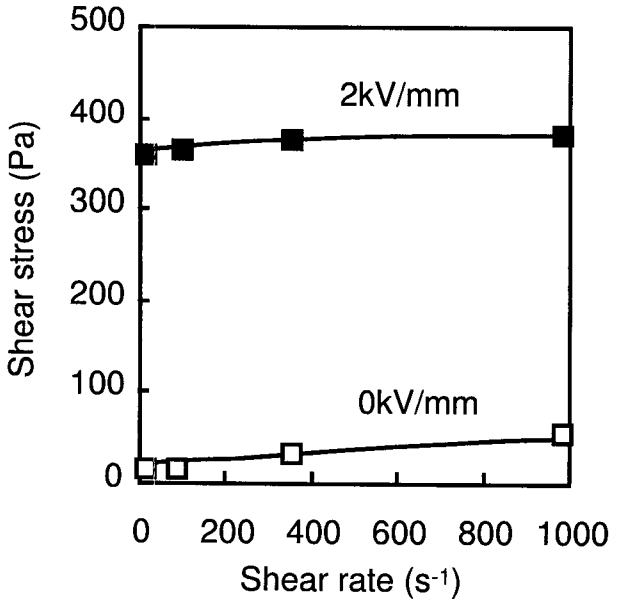

FIG. 8.2: Variation of shear stress with shear rate under no electric field (white square) and dc electric field of $2.0kV/mm$ (black square).

We can understand this behavior if we recall that the yield stress reflects the contribution to the overall stress of the electrostatic interparticle forces [44, 64]. Assuming that the particles are uniform spheres of radius a and that the polarization is of the Maxwell-Wagner type, the electric field will induce in an isolated particle a dipole of magnitude p (see Chapter 1):

$$p = 4\pi\epsilon_s\epsilon_0 \left(\frac{\sigma_p - \sigma_s}{\sigma_p + 2\sigma_s}\right) a^3 E_0 \tag{8.2}$$

where E_0 is the electric field strength, and σ_p, σ_s are the electrical conductivities of the particle and matrix respectively. These dipoles will result in electrostatic forces between particles [16, 23, 27]. At the lowest level of approximation (the "point dipole" model), the magnitude of the force between two particles aligned with the electric field and with a center-center separation of r is

$$F_{elec} = \frac{3\pi p^2}{8\epsilon_s\epsilon_0 r^4} \tag{8.3}$$

There is also a hydrodynamic force F_{shear} experienced by the particles due to the flow field. This is

often modeled by the Stokes equation, where we assume the force is proportional to the difference between the velocity of the particle and the ambient solvent velocity:

$$F_{shear} = 6\pi\eta a(v_{solvent} - v_{particle}) \tag{8.4}$$

If the electric field is large F_{elec} will dominate the particle interactions, and particle aggregates will form leading to increased flow resistance and thus the yield stress. There have been many works that model the steady shear response of ERF based on these ideas [12, 44]. See and Saito [64] have used this approach to estimate the stress due to aggregated structures, and find that the yield stress can be expressed as

$$\tau_y \approx \epsilon_s \epsilon_0 \left(\frac{\sigma_p - \sigma_s}{\sigma_p + 2\sigma_s}\right)^2 {E_0}^2 \frac{\eta_0}{\eta} \tag{8.5}$$

where η_0 is the viscosity of suspension at $0kV/mm$ and η is the solvent viscosity. η_0 is a function of volume fraction of particles and typically will be proportional to η . Thus this equation tells us that under strong electric fields there is not a strong dependence of τ_y on oil viscosity, and the results of our experiments are consistent with this.

On the other hand, if the electric field is weak and the viscosity large so that the F_{shear} will dominate over F_{elec}, we would expect that the yield stress will decrease as the viscosity is further increased since the relatively weaker electrostatic interactions will be unable to form aggregates of any size. It should be noted that these ideas can also be expressed by considering the Mason number, the non-dimensional ratio of hydrodynamic to electrostatic forces : Marshall *et al.* observed that at large Mason numbers the electrorheological response becomes very small [50]. In their work however, the shear rate and electric field were altered but the oil was of fixed viscosity.

8.3.2 The effect of oil viscosity on dynamic mechanical properties of ERF

Now we consider the relationship between the dynamic mechanical response of the ERF and the oil viscosity, and we will confirm that the observed behavior is also consistent with the

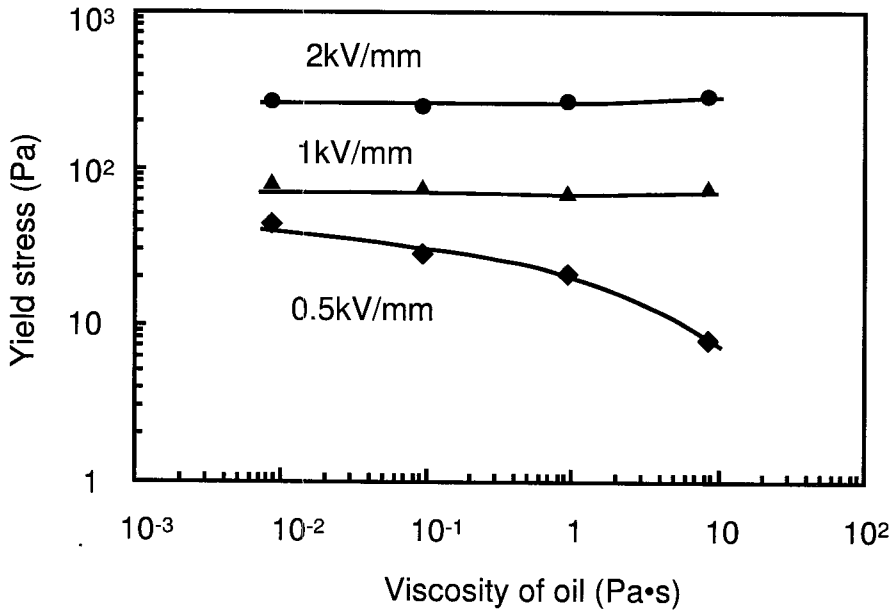

FIG. 8.3: Yield stress as a function of viscosity of oil, under dc electric fields of $0.5kV/mm$ (lozenge), $1.0kV/mm$ (triangle) and $2.0kV/mm$ (circle), for shear rate of $\dot{\gamma} = 100s^{-1}$

dipole-dipole interaction model.

FIG. **8.4**(a) - (c) show the relationship between viscosity of oil and $G'(\gamma_0)$ at strain amplitudes of 0.1%, 0.5% and 1.0% at a frequency $\omega = 100rad/s$. These figures show that the strongest dependency of $G'(\gamma_0)$ on the oil viscosity occurs at large strain amplitude (1%) under weak electric field ($0.5kV/mm$) - see FIG. **8.4** (c). The curves for the higher electric fields seem to be almost independent of oil viscosity at all strain amplitudes. Somewhat surprising however is the fact there is no significant difference of $G'(\gamma_0)$ between electric fields of $1.0kV/mm$ and $2.0kV/mm$ at the low strain amplitude (FIG. **8.4** (a)). For the case of the large electric fields ($1.0kV/mm$ and $2.0kV/mm$) at 0.5% and 1.0% strain amplitude, the increase in $G'(\gamma_0)$ with E is expected since there will be a larger contribution from the interparticle electrostatic forces. This has been predicted by theoretical calculations based on the dipole-dipole interaction model (eq. (8.3)) [49], and also confirmed experimentally [32]. However, at present we have no explanation of the closeness of the curves for 1.0, $2.0kV/mm$ at the 0.1% strain.

Turning now to the $0.5kV/mm$ curves in FIG. **8.4** (a) - (c), we note the following two

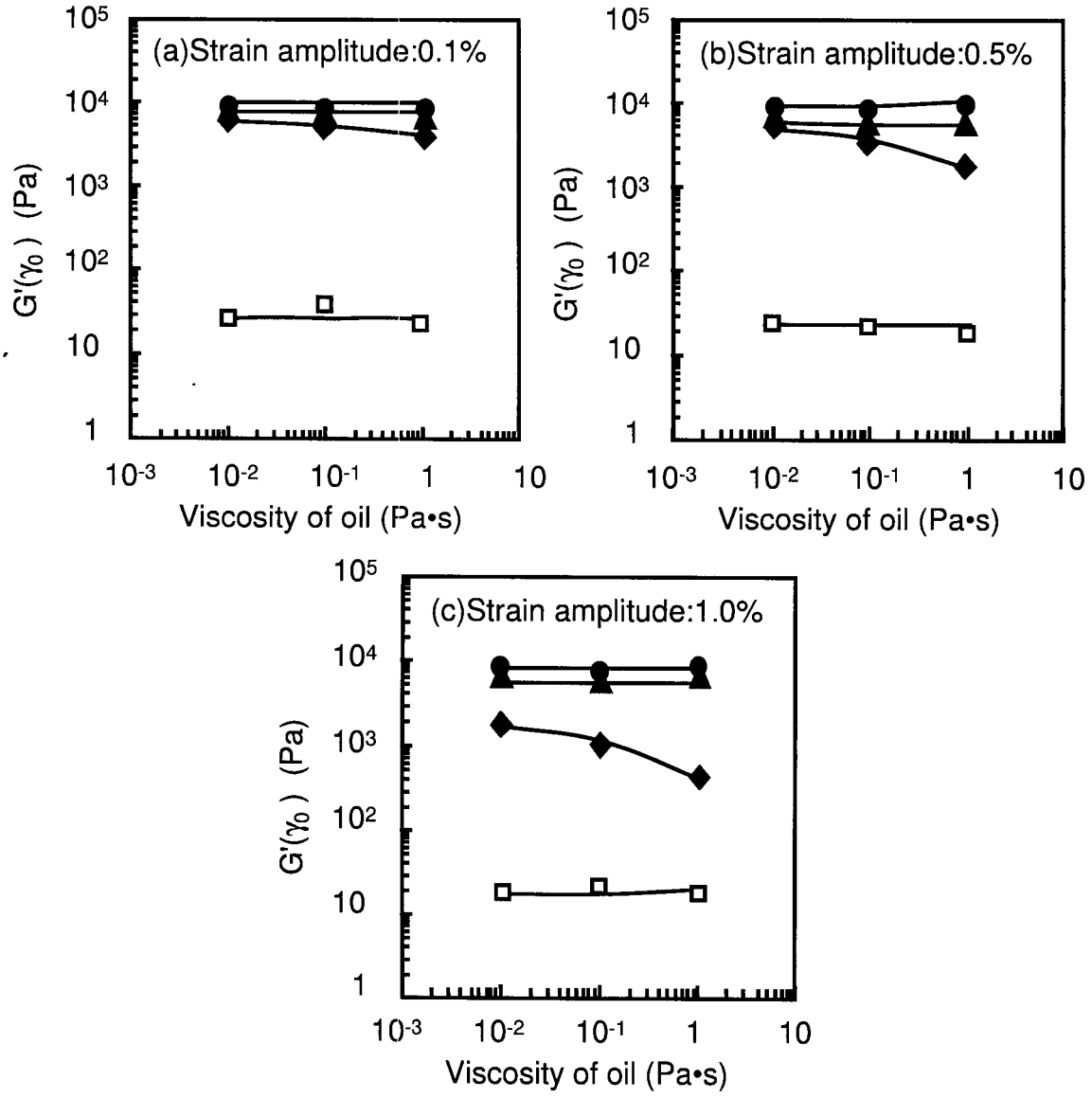

FIG. 8.4: $G'(\gamma_0)$ for ERF as a function of viscosity of oil, under dc electric field of $0kV/mm$ (square), $0.5kV/mm$ (lozenge), $1.0kV/mm$ (triangle) and $2.0kV/mm$ (circle). The strain amplitudes γ_0 are (a) 0.1%, (b) 0.5% and (c) 1.0%.

features:

(i) For a fixed oil viscosity, the $0.5kV/mm$ curves are close to those for $1.0kV/mm$ and $2.0kV/mm$ at small strain amplitude, but shift to significantly lower values as strain amplitude is increased.

(ii) At each amplitude, the $0.5kV/mm$ curves show a strong decrease in $G^{'}(\gamma_0)$ as oil viscosity is increased.

This behavior of the $0.5kV/mm$ curves can be qualitatively explained as follows. As before, we consider the hydrodynamic and electrostatic forces, and examine the rupturing process of the particle chains or columns spanning the electrodes. For simplicity, we consider two adjacent particles aligned in the electric field direction, and determine the minimum electric field E_{crit} required for these particles to remain adhered under the oscillatory shear. In this case, the maximum value of hydrodynamic force acting to pull the two particles apart is

$$F_{shear} = 6\pi\omega\gamma_0\eta a^2 \tag{8.6}$$

Balancing this with the magnitude of the electrostatic force F_{elec} ((eq. (8.3)) with $r \approx 2a$), $F_{elec} = F_{shear}$, gives us

$$E_{crit} = \frac{4}{\pi}\sqrt{\frac{\omega\gamma_0\eta}{\epsilon_s\epsilon_0\beta^2}} \tag{8.7}$$

Eq. (8.7) shows that if strain amplitude γ_0 is increased, E_{crit} will increase. Also, if we increase the oil viscosity η, E_{crit} will increase. Both of these results agree with the trends (i) and (ii) described above. Further, substituting typical values $\omega = 100rad/s$, $\gamma_0 = 1.0\%$ and $\eta = 9.7 \times 10mPa \cdot s$ gives us $E_{crit} \approx 123V/mm$, which is of the correct order.

We now consider the 90 degree shifted component $G^{''}(\gamma_0)$. In FIG. **8.5** (a) - (c), $G^{''}(\gamma_0)$ is plotted against oil viscosity at frequency $\omega = 100rad/s$ at strain amplitude of 0.1%, 0.5% and 1.0%. These results also support the above interpretation of the ERF mechanism. Firstly, we notice that at all amplitudes for the suspension using the lowest oil viscosity ($9.4mPa \cdot s$), the values of $G^{''}(\gamma_0)$ under electric fields $0.5, 1.0, 2.0kV/mm$ are roughly an order of magnitude smaller than the corresponding values for $G^{'}(\gamma_0)$. This is as expected, since the electrostatic forces dominate when low viscosity oils are used, and these forces will contribute to the in-phase component of

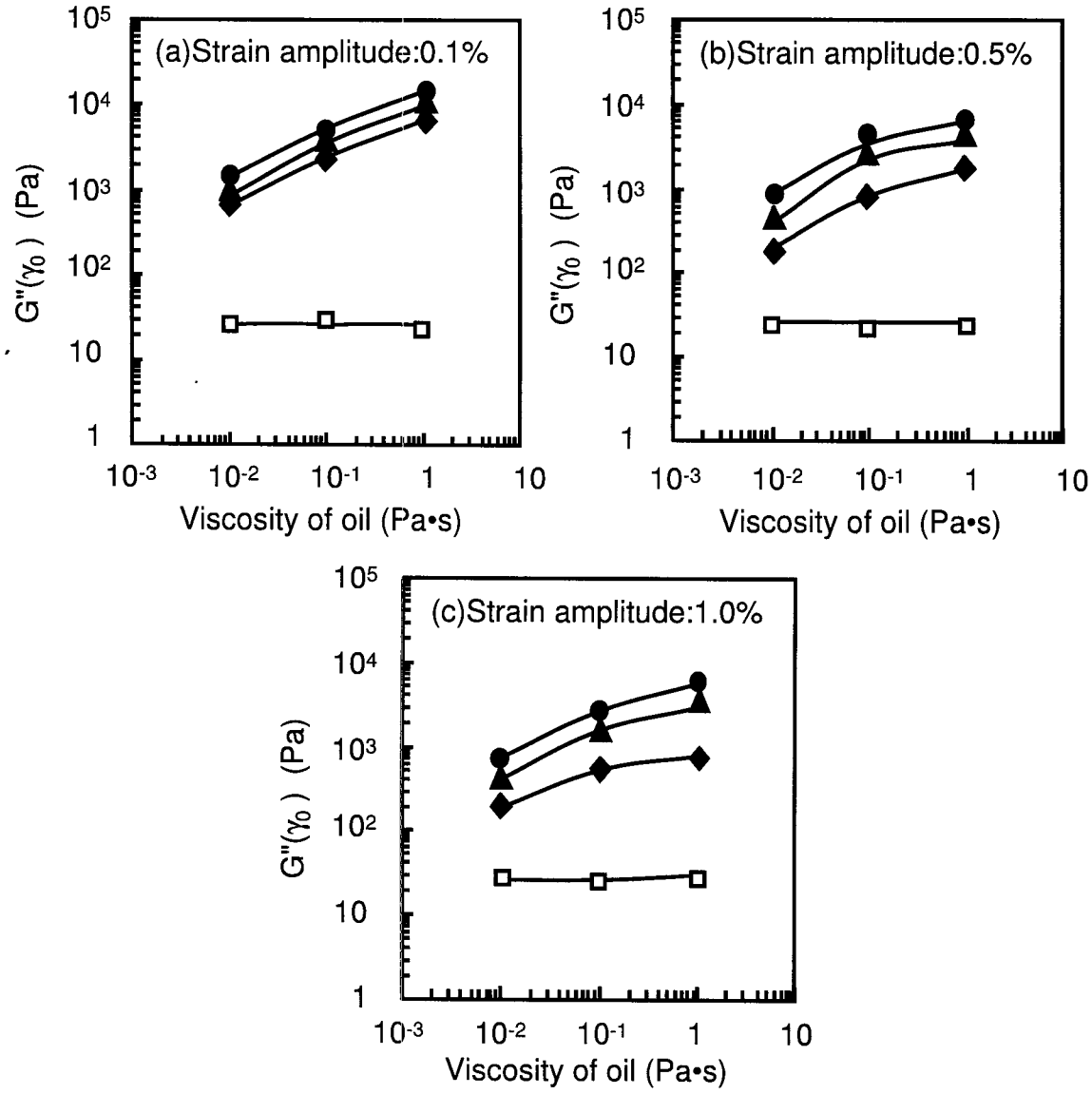

FIG. 8.5: $G''(\gamma_0)$ for ERF as a function of viscosity of oil, under dc electric field of $0kV/mm$ (square), $0.5kV/mm$ (lozenge), $1.0kV/mm$ (triangle) and $2.0kV/mm$ (circle). The strain amplitudes γ_0 are (a) 0.1%, (b) 0.5% and (c) 1.0%.

the stress response (i.e. they contribute to $G^{'}(\gamma_0)$). However, as the oil viscosity is increased, the viscous response from the oil begins to dominate (as discussed above), and so the value of $G^{''}(\gamma_0)$ increases, eventually reaching values that are comparable with the corresponding in-phase value ($G^{'}(\gamma_0)$). For example, for the case of oil of viscosity $1Pa{\cdot}s$ under strain amplitude of 1% and field of $2.0kV/mm$, the values for $G_0^{'}(\gamma_0)$ and $G_0^{''}(\gamma_0)$ are $1.0 \times 10^4 Pa$ and $9.0 \times 10^3 Pa$ respectively. Thus the behavior of the curves in FIG. **8.5** (a) - (c) supports our basic picture that the response under oscillatory shear and electric field is determined by the competition between the electrostatic forces and the hydrodynamic forces.

It is appropriate to compare these results with those found from molecular dynamics computer simulations of ERF under oscillatory shear. Klingenberg investigated the dynamic response of single and multiple particle chains spanning the electrodes under small amplitudes (no rupture of columns), and found that the moduli (scaled by the electrostatic interaction strength) were only functions of the dimensionless frequency $\omega^* = (16\eta\omega)/(\epsilon_s\epsilon_0\beta^2E_0^2)$ [45]. The results imply that if the electric field, oscillation frequency and amplitude are held constant, $G^{'}$ will increase with increasing oil viscosity since the hydrodynamic forces are larger and the chains undergo larger deformations. This would appear to contradict the decrease in the $0.5kV/mm$ curves with oil viscosity seen in FIG. **8.4** (c) of this chapter, but it must be kept in mind that this simulation was carried out at very small deformations ($\gamma_0 = 10^{-4}$), where there was no rupture of the chains. Parthasarathy and Klingenberg found in their simulations at larger strain amplitudes that if γ_0 exceeded some critical value (0.1 in their simulation), rupturing begins to occur in the percolating structures across the electrodes [58]. Thus we would expect at these amplitudes to see a decrease in $G^{'}$ as oil viscosity is increased (particularly under weaker electric fields), since larger hydrodynamic forces would accelerate the rupturing of the stress-bearing structures. This is indeed what we observe in FIG. **8.4** (c), and the simple calculation given above based on chain rupture would appear to be quite reasonable. A similar molecular dynamics simulation in 3 dimensions has been recently reported by Wang *et al.* [78], who investigated both small strain amplitudes and larger strain amplitudes with chain rupture. In the latter case, they too found that $G^{'}$ is significantly reduced as chain rupturing commences, supporting our observations (FIG. **8.4** (c)).

Thus, our experiments with ERF using oils of different viscosity have shown that the oil viscosity has a large effect on the field-induced mechanical response, and we are able to explain the observed behavior in terms of the dipole-dipole interaction model. In the next section we will consider the case of ER elastomers, and will see the effect of elasticity of the matrix on the electric-field induced properties. Analogous to the ERF case, we find that a higher elastic modulus of the matrix tends to reduce the electrorheological response, showing that low modulus materials would be the best for achieving large changes in mechanical properties.

8.3.3 The electrorheological property of ER elastomer

Firstly, we consider for reference the dynamic mechanical behavior of an elastomer containing no particles. In FIG. **8.6**, we plot the storage and loss moduli against frequency for a typical elastomer. The frequency was varied from $1 rad/s$ to $100 rad/s$ and the strain amplitude was 1.0%.

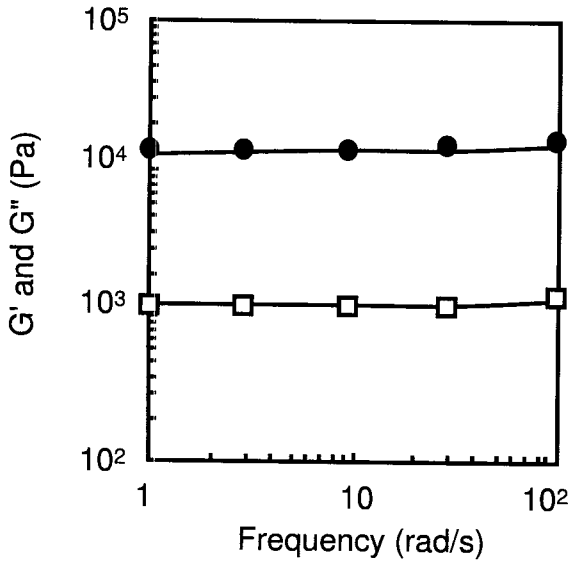

FIG. 8.6: Variation of storage modulus (•) and loss modulus (□) with frequency for elastomer with no particle.

This material showed linear viscoelastic behavior, and FIG. **8.6** shows the dynamic properties expected of a polymeric elastomer. We note that the material shows strongly elastic behavior, since G' is over an order of magnitude larger than G'' over the entire range of frequencies covered.

We now consider the response of ER elastomers under an electric field. In FIG. **8.7** we

show the effect of volume fraction of particles on the response under a $2.0kV/mm$ electric field at strain amplitude of 1.0% and frequency $\omega = 100rad/s$, using the elastomer with $1.5 \times 10^4 Pa$

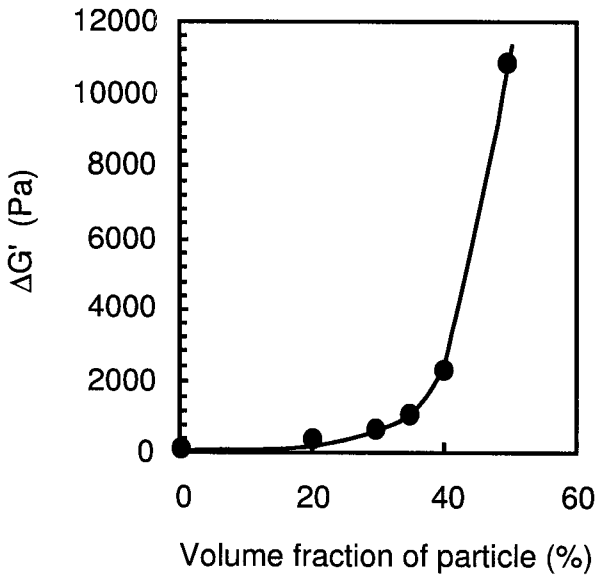

FIG. 8.7: Variation of increment in storage modulus ($\Delta G^{'}$) with volume fraction of particle under $2.0kV/mm$ electric field at strain amplitude of 1.0% and at frequency of $100rad/s$.

modulus as the matrix. For the vertical axis we take the increment in the modulus due to the $2.0kV/mm$ electric field $\Delta G^{'} = G^{'}(\gamma_0, 2kV/mm) - G^{'}(\gamma_0, 0kV/mm)$. We see that at the larger volume fractions, the electric field produces a significant change in the mechanical properties. Thus, even though the particles are embedded in the elastomer and are restricted in their movement, the interaction between the induced electric dipoles (eqs. (8.2), (8.3)) will cause changes in the overall mechanical properties. We see that when the volume fraction ϕ is small, $\Delta G^{'}$ is very small but shows a dramatic increase with volume fraction. This can be explained by noting that the electrostatic interactions will be stronger when the average distance between particles is small (i.e. higher volume fraction), since these forces are short-range by nature (i.e. the $1/r^4$ dependence of the dipole-dipole force (eq. (8.3)). From now on, we will focus attention on the high volume fraction case 50% since this is the one showing the clearest electrorheological effect.

Of particular interest to us in this chapter is the effect of the elastomer elasticity. In FIG. **8.8**, the normalised increment in the modulus $\Delta G^{'}/G^{'}(\gamma_0, 0kV/mm)$ is plotted against the elastic

modulus of the matrix material (at strain amplitude $\gamma_0 = 1\%$ and frequency $\omega = 100 rad/s$). The

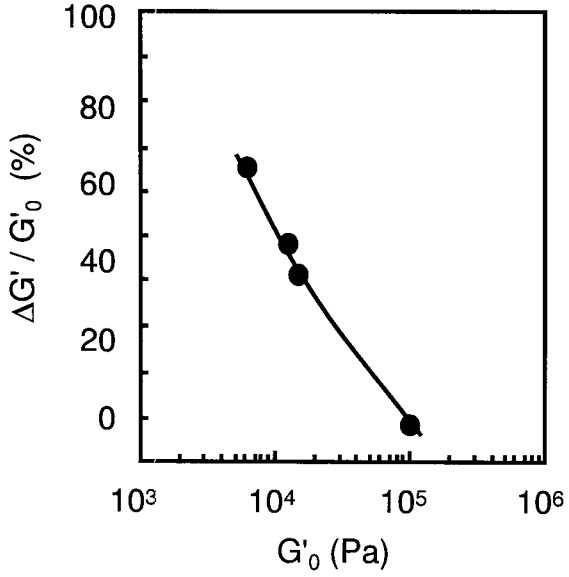

FIG. 8.8: Normalised increment in the modulus $\Delta G^{'}/G^{'}(\gamma_0, 0kV/mm)$ as a function of original modulus of elastomer $G_0^{'}$, at strain amplitude of 1.0% and at frequency of $100 rad/s$.

reason for plotting the quantity $\Delta G^{'}/G^{'}(\gamma_0, 0kV/mm)$ is that it shows the increase in modulus of the ER elastomer due to the $2.0kV/mm$ electric field as a fraction of the modulus in the absence of a field, and this fractional increase would be of much interest from a practical engineering viewpoint. From FIG. **8.8** we see that the electric field causes a large increment in the value of $\Delta G^{'}/G^{'}(\gamma_0, 0kV/mm)$, with the largest fractional increase in the ER elastomer using the matrix of lowest elasticity. So from the viewpoint of producing large relative changes in mechanical properties under the electric field, we have verified that it is advantageous to use for the matrix an elastomer with a low elastic modulus.

We now examine in more detail the relationship between the electrorheological response and the elasticity of the matrix. In FIG. **8.9** (a) - (c) we have plotted $G^{'}(\gamma_0)$ against elastic modulus of the original elastomer under electric fields of $0, 0.5, 1.0, 2.0kV/mm$, for strain amplitudes of 0.05%, 0.1% and 1%, with deformation frequency held constant at $\omega = 100 rad/s$.

In FIG. **8.10** (a) - (c) $G^{''}(\gamma_0)$ is plotted against elastic modulus of the original elastomer, under the same set of conditions. Note that the values for $G^{'}(\gamma_0)$ were consistently an order

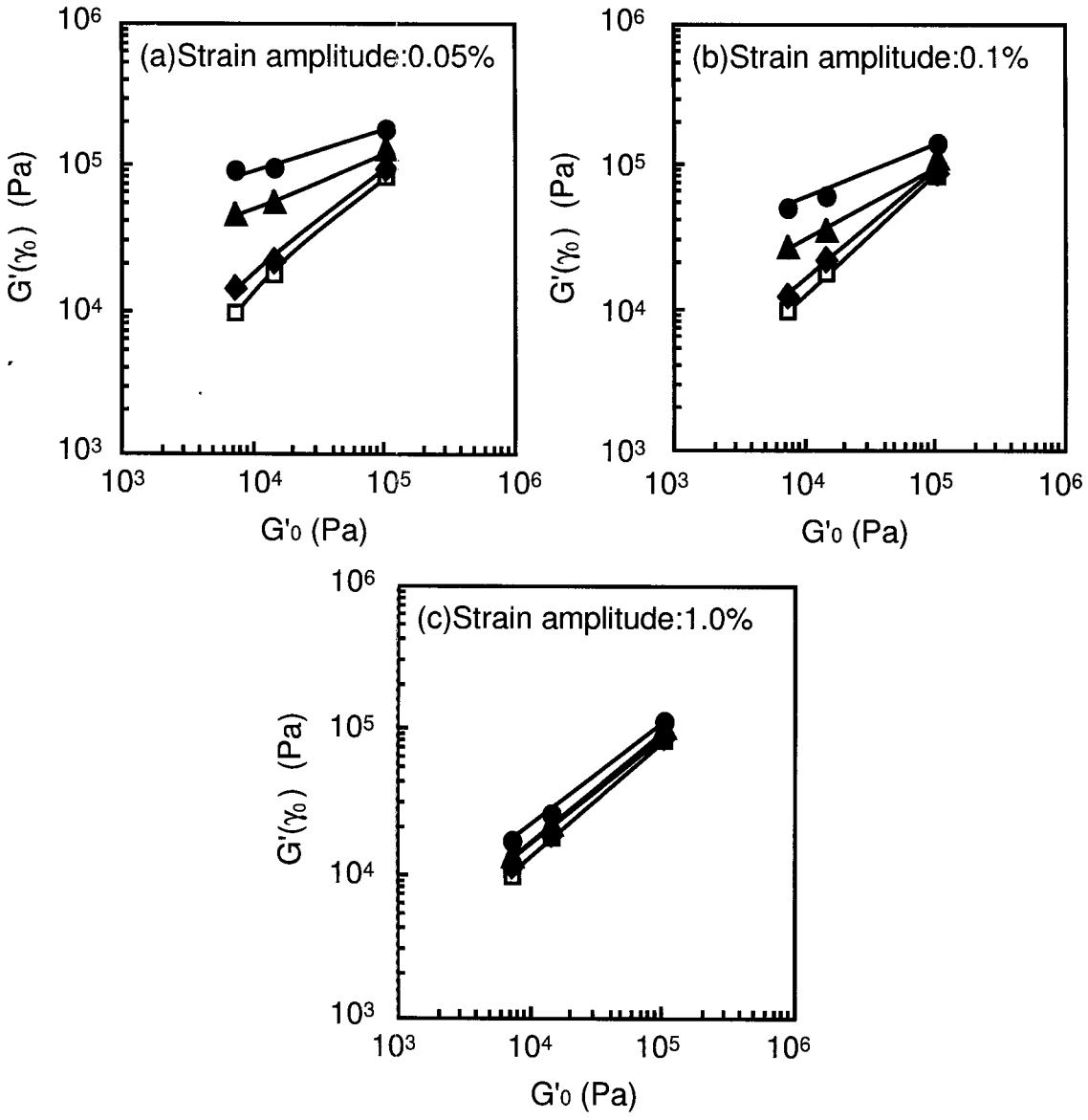

FIG. 8.9: $G^{'}(\gamma_0)$ for 50% ER elastomer as a function of original modulus of elastomer $G_0^{'}$, under dc electric fields of $0kV/mm$ (square), $0.5kV/mm$ (lozenge), $1.0kV/mm$ (triangle) and $2.0kV/mm$ (circle). The strain amplitudes γ_0 are (a) 0.05%, (b) 0.1% and (c) 1.0%.

of magnitude larger than the corresponding values for $G''(\gamma_0)$. This is not surprising since, as noted above, the electrostatic forces produce a restoring force that opposes the deformation, and furthermore the elastomer matrix is a strongly elastic material to begin with (FIG. **8.6**). FIGs. **8.9** and **8.10** are analogous to FIGs. **8.4** and **8.5**, which showed the dependence of the ERF on the oil viscosity. Both FIGs. **8.9** and **8.10** show that at small strain amplitudes (FIG. **8.9** (a), **8.10** (a)), the electric field induces large changes in the moduli, but as strain amplitude is increased these increments become smaller. Also, for a fixed strain amplitude, as the modulus of the matrix is increased the differences in moduli induced by the electric field become smaller. This behavior parallels that observed in the ERF, where we saw that the field-induced mechanical changes become smaller as the oil viscosity is raised. Similar to the ERF case, we suggest that this behavior of the ER elastomer can be simply explained by considering the competition between electrostatic and elasticity forces.

Analogous to the ERF case, let us consider the competition between the inter-particle electrostatic forces and the resistance forces due to the matrix which hinder particle movement. To be concrete, we focus on the behavior of the G' curves (FIG. **8.9**). Since we are using spherical particles of uniform size at a volume fraction of 50%, we expect the particles to form a very close packed structure. If an electric field is applied to this ER elastomer, there is expected to be a slight re-arrangement of the particle positions to a configuration with lower electrostatic energy causing a reduction in the average particle-particle gap in the field direction. Note in the case of ER elastomer however, that there are no gross structural changes such as the chain/column formation observed in ERF. As we apply larger strains to this system the particles become more displaced from this configuration and the resulting weaker electrostatic interactions between the particles cause a reduction in the increment in G' due to the electric field. This explains the amplitude dependence of the field-induced increments in G'. Note that in an ER elastomer we would expect the relative particle displacements due to the shearing to be more or less uniform through the sample thickness (since the particles have limited mobility in the elastic matrix), which is a very different situation to the more localized column rupture seen in ERF under shear. Further, if a matrix with a higher modulus is used, the larger elastic forces will more strongly hinder the initial

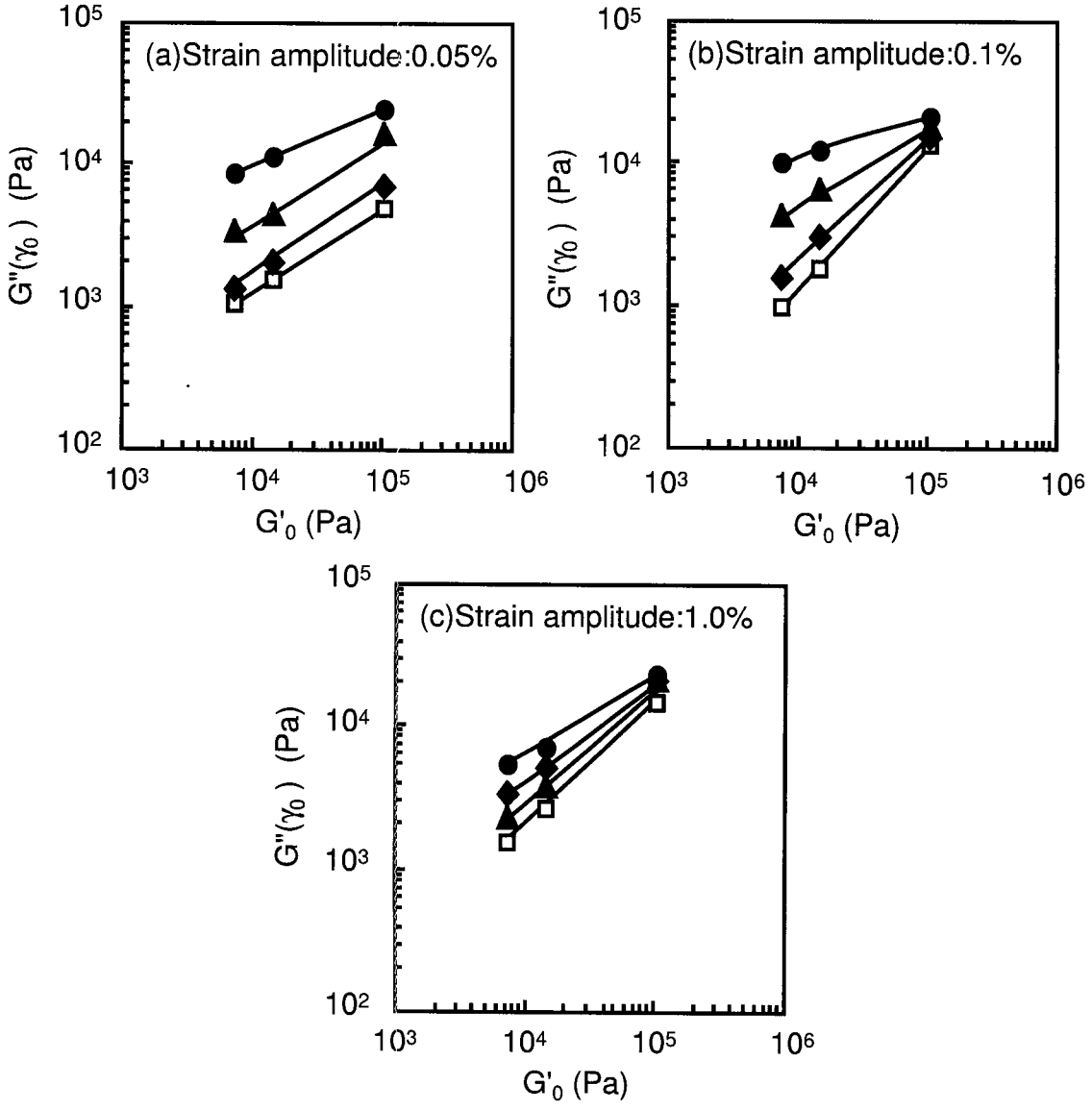

FIG. 8.10: $G''(\gamma_0)$ for 50% ER elastomer as a function of original modulus of elastomer G'_0, under dc electric fields of $0kV/mm$ (square), $0.5kV/mm$ (lozenge), $1.0kV/mm$ (triangle) and $2.0kV/mm$ (circle). The strain amplitudes γ_0 are (a) 0.05%, (b) 0.1% and (c) 1.0%.

rearrangement of the particles under an electric field, which will result in a lower field-induced increment in modulus since the inter-particle electrostatic forces rapidly decrease with increasing particle-particle gap [8]. This agrees with the dependence on elastomer modulus observed in FIG. **8.9**. A detailed calculation of these effects would be possible using the analytical solutions for the mobility of two nearly touching spherical particles in an elastic matrix [59] and the close range electrostatic interactions between particles [8], but is beyond the scope of the present work.

8.4 Conclusion

We have investigated the electric field-induced change in the dynamic mechanical response of suspensions of particles in a matrix, focusing in particular on the role of matrix viscosity (in the case of oils) or shear elastic modulus (in the case of elastomers). The use of the same type of semi-conducting particle has enabled us to isolate the effects due to the matrix viscosity or elasticity.

Our experiments with the particles dispersed in oils showed that if the electric field is less than a critical value, the yield stress under steady shear shows a strong decrease with increasing oil viscosity, while there is little variation with viscosity when large fields are applied. We were able to estimate this critical electric field through a simple calculation based on the dipole-dipole interaction model, where we focus on two adjacent particles, and consider the competition between the electrostatic force holding the particles together and the shearing force attempting to pull them apart. The measurements under oscillatory shearing showed that the electric field induces large changes in both the in-phase and 90 degree shifted component, with the dependence on the electric field becoming more pronounced as the strain amplitude is raised. Once again, we found that the model based on competing electrostatic and hydrodynamic interactions between the particles is able to account for the observed behavior. Our results confirm that the electric field-induced changes in mechanical properties (under steady or oscillatory shear) are largest when a low viscosity oil is used.

The experiments with particles dispersed in an elastomer showed that a high volume fraction of particles is needed to achieve significant changes in mechanical properties under an electric field,

with a large jump occurring when volume fraction is changed from 40% to 50% (FIG. **8.7**). Focusing on the 50% volume fraction case, we then investigated how the properties under oscillatory shearing depend on the elasticity of the elastomer used as a matrix. Parallel to the behavior observed in the oil systems, we found that the largest relative increase in mechanical properties occurred when elastomer of low elasticity is used. However, we found the electric field-induced changes became smaller as the strain amplitude was increased from 0.05% to 1%. This indicates that the most effective use of ER elastomers may be in devices where vibrations of very small amplitude need to be damped. We suggest that the observed behavior could again be explained by considering the competing effects of the shearing action (this time due to the deformation of the elastic matrix) and the electrostatic interactions.

Although our measurements were carried out in the shearing mode, it should be mentioned that the use of electrorheological materials in squeeze flow or compression mode has recently become the focus of some attention, since large changes in the mechanical properties of ERF can be achieved with a compact and simple device [70]. We would expect that the ER elastomer will also show a significant response under squeeze flow, since the same interparticle electrostatic forces would cause changes in the mechanical properties, but the effect may be modified by the compressibility of the matrix. ER elastomers under squeeze flow would appear to be an interesting avenue for future experimental work.

With the continuing strong industrial interest in the applications of electrorheological materials, an understanding of the role of the matrix in the mechanical response under electric fields is crucial to the selection of appropriate matrix materials. This chapter has attempted to clarify the effects of matrix viscosity or elasticity on the electrorheological response of particle suspensions. **The practical possibility of ER elastomer was also verified.**

Chapter 9.

Overall Conclusions

9.1 Conclusions

Recently, studies of particle dispersed composite materials have been done extensively in order to add higher functional properties such as electrical, mechanical and so on, to conventional materials. In this thesis we have carried out a study of electro-viscoelasticity of particle dispersed composite materials.

ERFs are suspensions of insulating oil and semi-conducting particles and increase viscosity when an electric field is applied. Many studies have been done since first report of this material by Winslow. And in the late of 1980's, anhydrous material that shows less temperature dependence of ER performance was discovered and much more studies have been done. The viscosity change can be controlled continuously by applied electric field and simple design of device is possible with this material, so many applications are proposed, especially applications for automobiles. However, despite the promise of these applications, ERFs have not come to be used widely even now. The main reason is the ER effect (yield stress under an electric field) is not still sufficient for these applications. Especially ER shock absorbers, one of the most attractive applications, require larger shear yield strengths than are currently available. The development of higher ER performance ERF will see its use extended to many other applications.

Considering this background, we set as one of our objectives "Improving ER performance for practical use". ER effect derives from inter-particle electrostatic force induced by electric field, and consequently, dispersed particles dominate ER effect. So we have attempted to obtain higher

ER performance by optimizing the properties of dispersed particles. However, one problem faced is that there are no efficient measuring methods that evaluate the relationship between properties of particles and their ER performance. So as another objective, we have "Establish an efficient measuring method from that we can relate properties of particle and ER performance". With a view to these objectives, we summarize in the following our conclusions from each chapter respectively.

In Chapter 1, the general features of particle dispersed ERFs are reviewed. We summarized about the typical materials, the mechanism of ER effect under an electric field and possible applications. Then we clarified current issues which should be solved for wide use of ERF and from these derived our objectives.

In Chapter 2, there is a description of the ERF materials used in this work : carbonaceous anhydrous particle and silicone oil. Then we described the measuring and analytical methods used for evaluating the properties of dispersed particles with dielectric measurement.

In Chapter 3, we have investigated the ideal structure of carbonaceous particles for ERF. We clarified the problems of currently used ERF system of homogeneous particles and design a new type of layered structure, which we attempted to synthesize. From the results of SEM and EDX measurements, we confirmed the layered structure. We also compared the difference of conductivities between central part of particle and outer part and confirmed that the conductivity of layer is lower than that of central part which was our aim. From the results of the comparison with the property of "ER effect vs current density at same electric field", we verified that ERF with layered particle showed higher ER effect than that with conventional homogeneous particle. We proposed that ERFs using layered particles may lead to an optimal ERF for devices.

In Chapter 4, we found that inter-particle conductive uniformity is an important factor and have investigated the relationship between conductive uniformity and ER effect by sets of model experiments and attempted to apply dielectric measurements on evaluating conductive uniformity. We have seen that ER performance was deteriorated by blending particles of different conductivities and we confirmed that the results of dielectric measurements were useful to evaluate inter-particle conductive uniformity of ERFs. Then we have discussed this reduction in ER effect by a qualitative

and simple model that is based on the formation of particle clusters around the relatively high conductivity particles due to the enhanced electrical forces. These results of this chapter indicate that it is essential to have uniformity in the particle electrical characteristics.

In Chapter 5, we have proposed a simple model to explain the "dip" that was shown in Chapter 4. We have done some calculations based on the model that the cluster around relatively high conductive particles prevents base particles from forming optimum configuration under deformation. At lower volume fraction of higher conductive particles, ER effect was deteriorated by the cluster, but as their volume fraction increased the ER effect would increase again to the value for 100% higher conductive particles. We have explained this effect by percolation of clusters in columns with increasing concentrations of higher conductive particles. We have seen that this effect can be quantified and can be explained by our calculation.

In Chapter 6, we have investigated the effect of adding conductive fragments on ER effect. We have seen that ER effect decreased largely with increasing concentration of carbon black. We explained the mechanism of the effect with the model of electrophoretic movement of charged carbon black under an dc electric field. We have done calculation with this model and the results showed good agreement with experimental results. These results indicate that we should be very careful with extraneous conductive impurities for high ER performance in practical fluid preparing process.

In Chapter 7, we have applied the knowledge of "The inter-particle conductive uniformity should be minimal for higher ER performance" which was obtained from previous part of this work to the practical particle preparation process of carbonization. We saw that the problem with using conventional equipment was the difficulty of achieving uniform heat treatment and so we designed a new type of rotary electric furnace that can heat particles more uniformly. With this new type of equipment, we have confirmed that the conductive uniformity of particle was more uniform than that with conventional equipment by dielectric analysis and its ER performance was greatly improved. And we also verified that scale-up of amount of preparing particle was accomplished with this equipment.

In Chapter 8, we have investigated the possibility of electrorheological elastomer by dispers-

ing particles used for ERFs into elastomer (silicone rubber). The problems of "Sedimentation of the dispersed particle" and "Fluid sealing difficulty" of ERFs are not present with this type of materials and the area of usage of electrorheological materials can be extended. We have investigated based on the hypothesis that ER response of particle dispersed elastomer under an electric field also derives from induced electric forces, same as in ERF. We focused on the balance of restriction of matrix elasticity and induced electric forces of particles. With ERFs, the ER effect (increment of storage modulus under an electric field) became lower with using oils of higher viscosity. We were able to estimate the effect of balance of these forces on ER response of ERFs with the particle dispersed elastomer. As expected with these results of ERFs, it was shown that small elasticity of matrix elastomer was effective for larger ER response. And it was shown that high concentration of particles was essential for large ER response because dispersed particles could not move and aggregate freely under an electric field in an elastomer. As a result, the practical possibility of ER elastomer was verified.

9.2 Future directions

As we described above, we have accomplished an improvement of ER performance by optimizing material (particle) properties in this work. And we have introduced dielectric measurements as an index to analyze particulate properties. Practical use of ERFs is expected with these particles obtained in this thesis more widely. We should continue this work to solve some remaining issues, as follows:

9.2.1 Issues for ERFs

Improvement of particle sedimentation issue

Sedimentation is unavoidable when using particles with materials of different specific gravities. However, some compromises can be reached in this problem. First of all, making the particles easy to re-disperse in oils with small vibration is one possible solution. Second solution is to add thixotropic property on ERF. It means ERF behaves as gel at no flow and so particles won't sediment for long period. We can achieve this thixotropic property with adding third additives into

ERFs. We are thinking that it is practical to combine these ways to control the rheological behavior at no flow in order to prevent particle sedimentation and this is currently being investigated [53].

Optimization of solvent

In this thesis, we have not mentioned about the optimization of oils. The induced interparticle forces under an electric field becomes larger and ER effect becomes larger by using oils with larger dielectric permittivity as expected from eq. (1.10). Of course we should consider the balance of electrical consumption, specific gravity, cost and so on, but we should attempt to optimize the property of oils as one of the possible solutions for still higher ER performance.

Observation of particle behavior in different conductivities

In this thesis, we have considered the effect of different conductive particle on deterioration of ER effect by preventing optimum re-arrangement in columns. But it is a mechanism base on our speculation and has not been directly confirmed. We should verify this behavior with some analytical methods. Measuring a particle size distribution under an electric field and small shear flow. If our model works, clusters around relatively higher particle should be formed and affect the distribution under steady shear flow. Another possible approach would be to carry out microscopic observation at small concentration of dispersed particles.

9.2.2 Issues for ER elastomers

Investigation of application for ER elastomers

We have verified the possibility of ER elastomer, and we see the applications of this material should be in devices with damping small amplitude, such as anti-seismic rubber, damping rubber and so on. We should incorporate this material into these devices and investigate in detail the behavior of this material under practical conditions.

Acknowledgements

I would like to gratefully acknowledge Professor Masao Sumita of T.I.T. (Tokyo Institute of Technology), the adviser of my thesis at T.I.T., for his general guidance and support. I also would like to thank Associate Professor Shigeo Asai for his helpful advice and suggestions. I would like to thank Professor T. Hashimoto, Professor A. Tanioka and Associate Professor T. Ougizawa of T. I. T. for their technical advice and suggestions.

I am also grateful to Emeritus Professor Keizo Miyasaka of T.I.T. for his appreciation and encouragement during this thesis work.

I am also grateful to Dr. K. Iida (former Director of R & D division), Mr. I. Tanuma (Department Chief), Mr. Y. Morimura (Section Chief) and Mr. T. Saito of Bridgestone Corp. who gave me an opportunity of this work, instructions, warm supports and encouragement.

I received valuable instructions and advice to this work from Dr. Y. Kurachi (Konica Corp.) and Mr. Y. Fukuyama (Tokuyama Corp.).

I gratefully appreciate my research colleagues at Bridgestone R & D division, Mr. T. Ogino, Dr. S. Endo, Dr. Y. Ishino, Mr. T. Osaki, Dr. T. Maruyama, Ms. M. Miyano and Mr. H. Tamura for their technical supports, discussions and warm friendships.

I am extremely grateful to Dr. H. See (Sydney Univ.) for his critical comments for my experiments, instructive advice, and encouragement during the course of this work. He deliberately exhibits his utmost concern on this work that boosted me to overcome the obstacles during this work.

Finally, I wish to express my deepest thanks and gratitude to my wife, Safumi, and our daughter, Sakura, for patience and encouragement throughout the course of this work. I thank our parents sincerely.

September 1999

Ryo SAKURAI

References

[1] 遠藤　茂樹, "油圧と空気圧", **25**, 46 (1994).

[2] 岡　小天, 中田　修, "固体誘電体論", (岩波書店 1960).

[3] 小口武彦, "物理学B (電磁気学)", (槙書店 1984).

[4] 東芝シリコーン株式会社, "シリコーンとその応用", (1988).

[5] Adriani, P. M. and A. P. Gast, *Phys. Fluids*, **31**, 2757 (1988).

[6] Ahlquist, C. N., *J. Appl. Phys.*, **46**, 14 (1975).

[7] Ahn, K. H. and D. J. Klingenberg, *J. Rheol.*, **38**, 713 (1994).

[8] Anderson, R. A., *Langmuir*, **10**, 2917 (1994).

[9] Bailey, J. E. and N. A. Hill, *Proc. Brit. Ceram. Soc.*, **15**, 15 (1970).

[10] Block, H., J. P. Kelly, A. Qin and T. Watson, *Langmuir*, **6**, 6 (1990).

[11] Bloodworth, R. and E. Wendt, *Polymer Preprints*, **35**, 356 (1994).

[12] Bonnecase, R. T. and J. F. Brady, *J. Chem. Phys.*, **96**, 2183 (1992).

[13] Brooks, D., R. Jullien and M. Kolb, *Colloids Surf.*, **186**, 193 (1986).

[14] Buffam, C. J. and J. E. Brignell, *Nature*, **263**, 757 (1976).

[15] Carlson, J. D., D. M. Catanzarite and K. A. St. Clair, "Electro-Rheological Fluids, Magneto-Rheological Susupensions and Associated Technology", (Edited by W. A. Bullough, World Scientific, p20, 1996).

[16] Chen, Y., A. F. Sprecher and H. Conrad, *J. Appl. Phys.*, **70**, 6796 (1991).

[17] Chen, T., R. N. Zitter and R. Tao, *Phys. Rev. Lett.*, **68**, 2555 (1992).

[18] Choi, Y., A. F. Sprecher and H. Conrad, *J. Intell. Mat. Syst. Struct.*, **1**, 91 (1990).

[19] Clercx, H. J. H. and G. Bossis, *J. Chem. Phys.*, **98**, 8284 (1993).

[20] Coble, R. L. and W. D. Kingery, *J. Am. Ceram. Soc.*, **39**, 377 (1956).

[21] Cole, K. S. and R. H. Cole, *J. Phys. Chem.*, **9**, 341 (1941).

[22] Conrad, H., M. Fisher and A. F. Sprecher, *Proc. 2nd Int. Conf. on ER Fluids*, (Edited by J. D. Carlson, A. F. Sprecher and H. Conrad, Technomic, Lancaster PA, p67, 1990).

[23] Davis, L. C., *J. Appl. Phys.*, **72**, 1334 (1992a).

[24] Davis, L. C., *Appl. Phys. Lett.*, **60**, 319 (1992b).

[25] Davis, L. C., *Phys. Rev.*, **46**, R719 (1992c).

[26] Davis, L. C., *J. Appl. Phys.*, **73**, 680 (1993).

[27] Davis, L. C., *J. Appl. Phys.*, **81**, 1985 (1997).

[28] Deinega, YuF and G. V. Vinogradov, *Rheol. Acta*, **23**, 636 (1984).

[29] Felici, N. J., *Revue Generale de l'Electricite*, **75**, 1145 (1966).

[30] Fitzer, E., K. Mueller and W. Schaefer, "Chemistry and Physics of Carbon", (Edited by P. L. Walker Jr., Vol 7, 1971).

[31] Foulc, J. N., P. Atten and N. Felici, *C. R. Acad. Sci. Paris*, **317**, 5 (1993).

[32] Gamota, D. R. and F. E. Filisco, *J. Rheol.*, **35**, 399 (1991).

[33] Gast, A. P. and C. F. Zukoski, *Adv. Colloid Interface Sci.*, **30**, 153 (1989).

[34] Gilman, J. J., *J. Appl. Phys.*, **45**, 508 (1974).

[35] Gow, C. J. and C. F. Zukoski, *J. Colloid Interface Sci.*, **136**, 175 (1990).

[36] Halsey, T. C. and W. Toor, *Phys. Rev. Lett.*, **65**, 2820 (1990).

[37] Hartsock, D. L., R. F. Novak and G. J. Chaundy, *J. Rheol.*, **35**, 1305 (1991).

[38] Hill, J. C. and T. H. van Steenkiste, *J. App. Phys.*, **70**, 1207 (1991).

[39] Hill, D., *J. Rheol.*, **40**, 449 (1996).

[40] Inoue, A., *Proc. 2nd International Conf. on Electrorheological Fluids*, (Edited by Carlson, J. D., A. F. Sprecher and H. Conrad, Technomic, Lancaster-Basel, p176, 1990).

[41] Ishino, Y., T. Maruyama, T. Ohsaki, S. Endo, T. Saito, and N. Goshima, "Anhydrous Electro-Rheological Fluid Using Carbonaceous Particulate as Dispersed Phase", *Proc. 1994 Fall National ACS Meeting: Electrorheological Materials and Fluids Symposium*, August 21-26, Washington DC, 354 (1994).

[42] Kawamata, S., N. Goshima, I. Watanabe and T. Kimura, *Proc. 2nd International Conference on Motion and Vibration control MOVIC*, Yokohama September (1994).

[43] Klass, D. L. and T. W. Martinek, *J. Appl. Phys*, **38**, 67 (1967).

[44] Klingenberg, D. J. and C. F. Zukoski, *Langmuir*, **6**, 15 (1990).

[45] Klingenberg, D. J., *J. Rheol.*, **37**, 199 (1993).

[46] Klingenberg, D. J., F. van Swol and C. F. Zukoski, *J. Chem. Phys.*, **94**, 6160 (1994).

[47] Korobko, E. V., *J. Intell. Mater. Syst. and Struct.*, **3**, 268 (1992).

[48] Khusid, B. and A. Acrivos, *Phys. Rev.*, **52**, 1669 (1995).

[49] McLeish, T. C. B., T. Jordan and M. T. Shaw, *J. Rheol.*, **35**, 427 (1991).

[50] Marshall, L., C. F. Zukoski and J. W. Goodwin, *J. Chem. Soc. Faraday Trans.* I, **85**, 2785 (1989).

[51] Martin, J. E., D. Adolf and T. C. Halsey, *J. Colloid Interface Sci.*, **167**, 437 (1994).

[52] Miki, T., T. Nagaya, H. Orihara, Y. Ishibashi and M. Doi, *Proc. 40th Symposium of the Society of Rheology of Japan*, Kobe, 254 (1992).

[53] Miyano, M. and T. Saito, *Polymer Preprints Japan*, **44**, 875 (1995).

[54] Mokeev, A. A., E. V. Korobko and L. G. Vedernikova, *J. Non-Newton Fluids*, **42**, 213 (1992).

[55] Niaura, W. S. and J. D. Rensel, presented at *The Materials Research Society 1995 Spring Meeting*, San Francisco, 17 April 1995 (unpublished).

[56] Ota, M. and T. Miyamoto, *J. Appl. Phys.*, **76**, 5528 (1994).

[57] Parthasarathy, M. and D. J. Klingenberg, *Rheol. Acta*, **34**, 417 (1995a).

[58] Parthasarathy, M. and D. J. Klingenberg, *Rheol. Acta*, **34**, 430 (1995b).

[59] Phan-Thien, N. and S. Kim, "Microstructures in elastic media: Principles and computational methods", (Oxford University Press, New York 1994).

[60] Poh, H. A. and E. H. Engelhart, *J. Phys. Chem.*, **66**, 2085 (1962).

[61] Russel, W. B., D. A. Saville and W. R. Schowalter, *Colloidal Dispersions,* Cambridge University Press, (1991), p.12.

[62] Sax, J.and J. M. Ottino, *Polym. Eng. Sci.*, **23**, 165 (1983).

[63] Scher, H. and R. Zallen, *J. Chem. Phys.*, **53**, 3759 (1970).

[64] See, H. and T. Saito, *Rheol. Acta*, **35**, 437 (1994).

[65] Shiga, T., T. Ohta, Y. Hirose, N. Satoh, A. Okada and T. Kurauchi, *Polymer Preprints Japan*, **39**, 1470 (1990).

[66] Shiga, T., Y. Hirose, A. Okada and T. Kurauchi, *Polymer Preprints Japan*, **40**, 1234 (1991).

[67] Shulman, Z. P., *Int. J. Multiphase Flow*, **12**, 935 (1986).

[68] Sprecher, A. F., J. D. Carlson and H. Conrad, *Mater. Sci. Eng.*, **95**, 187 (1987).

[69] Spriggs, R. M., *J. Am. Ceram. Soc.*, **44**, 628 (1961).

[70] Stanway, R., J. L. Sproston, M. J. Prendergast, J. R. Case and C. E. Wilne, *J. Electrostatics*, **28**, 89 (1992).

[71] Takimoto, J., *Jpn. J. Rheol.*, **26**, 207 (1998).

[72] Tao, R., J. T. Woestman and N. K. Jaggi, *J. Appl. Phys. Lett.*, **55**, 1844 (1989).

[73] Toor, W. R. and T. C. Halsey, *Phys. Rev. A*, **45**, 8617 (1992).

[74] Toor, W. R., *J. Colloid Interface Sci.*, **156**, 335 (1993).

[75] Uejima, H., *Jpn. J. Appl. Phys.*, **11**, 319 (1972).

[76] Ushijima, T., K. Takano and H. Kojima, *SAE Technical paper series* **880073** (1988).

[77] von Hippel, A. R., "Dielectrics and Waves", (John Wiley and Sons, New York, 1954).

[78] Wang, Z. Lin and R. Tao, *J. Phys. D: Appl. Phys.*, **30**, 1265 (1997).

[79] Weyenberg, T. R., J. W. Pialet and N. K. Petek, "Electro-Rheological Fluids, Magneto-Rheological Susupensions and Associated Technology", (Edited by W. A. Bullough, World Scientific, p395, 1996).

[80] Wilhelm, H. E., *Phys. Fluids*, **29**, 1441 (1986).

[81] Winslow, W. M., *J. Appl. Phys.*, **20**, 1137 (1949).

[82] Wu, C. W. and H. Conrad, *J. Apply. Phys.*, 383, (1997).

[83] Wu, C. W. and H. Conrad, *J. Apply. Phys.*, 8057, (1997).

[84] Zhang, H. and M. Widom, *Phys. Rev. E*, **51**, 2099 (1995).

[85] Zhang, Y., Y. Ma, Y. Lan, K. Lu and W. Liu, *Appl. Phys. Letters*, **73**, 1326 (1998).

[86] Zukoski, C. F., *Annu. Rev. Mater. Sci.*, **23**, 45 (1993).

List of Publications

Papers

[1] R. Sakurai, H. See and T. Saito, "The effect of blending particles with different conductivity on electrorheological properties", *J. Rheol.* **40**, 395 (1996).

[2] H. See, R. Sakurai and T. Saito, "Model of structure and conduction in an electrorheological fluid under flow", *Int. J. Modern Phys. B* **10**, 3267 (1996).

[3] R. Sakurai, H. See and T. Saito, "The effect of conductive fragments on electrorheological properties", *Jpn. J. Rheol.* **25**, 149 (1997).

[4] 櫻井　良, 斉藤　翼, 浅井茂雄, 住田　雅夫, "粒子分散系電気粘性流体の電気特性の不均一性の評価方法", 高分子論文集 **54**, 785 (1997).

[5] R. Sakurai, H. See and T. Saito, "Shear rate dependence of shear stress in blended electrorheological fluids", *Jpn. J. Rheol.* **25**, 297 (1997).

[6] 櫻井　良, 斉藤　翼, 浅井茂雄, 住田　雅夫, "電気粘性流体用粉体を用いた電気応答性弾性体の研究", *Jpn. J. Rheol.* **26**, 151 (1998).

[7] R. Sakurai, H. See and T. Saito, "Mechanism of the dip in shear stress of blended electrorheological fluids", *Jpn. J. Rheol.* **26**, 243 (1998).

[8] R. Sakurai, H. See, T. Saito and M. Sumita, "Effect of matrix viscoelasticity on the electrorheological properties of particle suspensions", *J. Non-Newtonian Fluid Mechanics* **81**, 235 (1999).

[9] R. Sakurai, H. See, T. Saito, S. Asai and M. Sumita "Suspension of layered particles : An optimum electrorheological fluid for dc application", submitted to *Rheol. Acta* (1999).

[10] H. See, R. Sakurai, T. Saito, S. Asai and M. Sumita "Mechanism of electric current behaviour through electrorheological elastomers", in preparation (1999).

Presentations

[1] 櫻井　良, 斉藤　翼, "粒子分散系電気粘性流体の電気特性の不均一性の評価方法," 第*44*回高分子学会年次大会, 横浜, (1995).

[2] H. See, R. Sakurai and T. Saito, "Model of structure and conduction in an electrorheological fluid under flow," *The 5th International Conf. on Electrorheological Fluids, Magneto-Rheological Suspensions and Associated Technology*, Sheffield, July (1995).

[3] 櫻井　良, 浅井茂雄, 住田雅夫, "粒子分散系電気粘性流体用粒子の高機能化," 日本化学会第*76*回春期年会, 横浜 (1999).

Appendix

Nomenclature

a	radius of particle
i	electric current
j	electric current density
$G^{'}$	storage modulus
$G^{"}$	loss modulus
k	Boltzmann constant
p	magnitude of electrostatic dipole
T	absolute temperature
ϵ^*	complex relative dielectric permittivity
ϵ_0	dielectric permittivity of free space
ϵ_p	relative dielectric permittivity of particle
ϵ_s	relative dielectric permittivity of solvent
ϵ_{st}	static relative dielectric permittivity
ϵ_∞	optical relative dielectric permittivity
ϕ_i	volume fraction of i component
$\dot{\gamma}$	shear rate
η_p	Bingham plastic viscosity
η_s	viscosity of solvent
σ_p	conductivity of particle
σ_s	conductivity of solvent